2024

Interactions of caffeine with anticancer drugs studied by nuclear magnetic resonance

Baylee Parish

INTERACTIONS OF CAFFEINE WITH ANTICANCER DRUGS STUDIED BY NUCLEAR MAGNETIC RESONANCE

Baylee Parish

A THESIS

Submitted in partial fulfillment of the requirements
for the degree of Master of Science
in
The Department of Chemistry
to
The Graduate School
of
The University of Alabama in Huntsville
May 2024

Approved by:
Dr. Bernhard Vogler, Committee Chair
Dr. Sharifa Love-Rutledge, Committee Member
Dr. Pam Twigg, Committee Member
Dr. Bernhard Vogler, Department Chair
Dr. Rainer Steinwandt, Dean, College of Science
Dr. Jon Hakkila, Graduate Dean

Abstract

INTERACTIONS OF CAFFEINE WITH ANTICANCER DRUGS STUDIED BY NUCLEAR MAGNETIC RESONANCE

Baylee Parish

A thesis project submitted in partial fulfillment of the requirements for the degree of Master of Science

Chemistry

The University of Alabama in Huntsville

May 2024

Caffeine can form stacking through pi-pi interactions with aromatic anticancer drugs. While caffeine can reduce toxicity of anticancer drugs, caffeine can also reduce the efficacy of anticancer drugs. Aromatic anticancer drugs, such as daunorubicin and irinotecan, work by intercalating into DNA. When caffeine binds to an anticancer drug, the new complex formed cannot easily intercalate into DNA strands. Through Nuclear Magnetic Resonance (NMR) spectroscopy, chemical shift values for pure caffeine, daunorubicin, and irinotecan, as well as, caffeine mixed with daunorubicin and irinotecan were analyzed. Different concentrations for pure compounds and mixtures were analyzed by NMR. The diffusion coefficients for daunorubicin, irinotecan, caffeine, and mixtures were determined using Diffusion Ordered Spectroscopy (DOSY). This study found caffeine caused changes in chemical shift and diffusion coefficients of daunorubicin and irinotecan when mixed with caffeine due to binding of caffeine with anticancer drugs.

Acknowledgments

I would like to thank Dr. Bernhard Vogler for allowing me to participate in this research opportunity. His knowledge and assistance allowed this research to be possible. I would also like to thank my committee members, Dr. Pamela Twigg and Dr. Sharifa Love-Rutledge, for their help and support.

My family also supported me through this process. Specifically, I would like to thank my mom and grandparents for supporting me through this endeavor. Without their love and support, I would not be where I am today.

Table of Contents

List of Figures

List of Graphs

List of Tables

List of Equations

Chapter 1. Introduction

1. 1 Cancer and Cancer Treatments

According to the World Health Organization (WHO), cancer accounted for nearly ten million deaths globally in 2020.[1] Cancer is an invasive disease that can affect any part of the body.[2] Cancer is defined as uncontrollable cell growth leading to tumor formation.[2] Cell division is an orderly process where cells divide and create new cells to replace older and damaged cells.[2] When this process does not function properly, cancerous tumors may form.[2] Tumors can fall into two different categories: benign or malignant. Benign tumors are usually noncancerous and do not always require the same treatments as cancerous tumors.[2] Malignant tumors can metastasize and spread through the body. The malignant tumors usually require treatment to slow or stop the spread of the cancerous tumors.[2]

Of the multitude of different types of cancer, breast, lung, colorectal, and prostate are the most common cancers worldwide in 2020.[1] There are five main types of cancer treatment; surgery, radiation therapy, hormone therapy, immunotherapy, and chemotherapy.[3] Chemotherapy is the cancer treatment of interest for this study. Chemotherapy utilizes certain medications to shrink or kill the cancerous cells.[3] There are many different types of chemotherapy drugs. Chemotherapy can treat multiple

different types of cancer and can be used by itself or in conjunction with other cancer treatments.[4] Depending on the type of cancer, the chemotherapy drugs can be administered to the patient in different ways, such as, orally, intramuscularly, subcutaneously, or intravenously.[5] The category of intravenous chemotherapy drugs called inhibitors is used for this study. These chemotherapy drugs work to either inhibit topoisomerase I or topoisomerase II during DNA replication.[6]

1.2 DNA Replication and Topoisomerases

During DNA replication, there are three stages.[7] During the first stage, initiation, the supercoiled DNA is unwound and separated into two strands.[7] The second stage is elongation.[7] During elongation, the separated strands of DNA are then primed for replication by different enzymes.[7,8] The last stage is termination and during this stage, the new DNA segments are assembled.[7,8] After one round of DNA replication, a new strand of DNA is formed that is comprised of half of a new strand of DNA and half of the old strand of DNA.[8] The process of DNA replication continues until two new daughter cells are formed.[8] One important group of DNA replication enzymes are topoisomerases.

Topoisomerases are needed for the unwinding of the supercoiled DNA in order for DNA replication to occur.[9,10] Topoisomerases are classified into two classes of topoisomerases: topoisomerase I and topoisomerase II.[9,10] Topoisomerase I is an enzyme that cleaves one strand of DNA to relieve the strain on the supercoiled DNA before resealing the strand. The topoisomerase I enzymes do not use cofactors for activity, instead the energy from the supercoiled DNA is used as the primary energy source.[9,10]

Topoisomerase II cleaves double-stranded DNA and uses the energy from ATP hydrolysis to propel conformational changes needed for the DNA replication reaction to occur.[9,10] Since topoisomerase is an essential enzyme in DNA replication and the growth of cells, it is an effective target for anticancer drugs and treatments.[9,10] Different anticancer drugs target specific topoisomerases. In this study, the anticancer drugs of interest are irinotecan and daunorubicin. Irinotecan targets topoisomerase I and daunorubicin targets topoisomerase II.[9]

1.3 Irinotecan

Camptothecin and irinotecan are part of a family of drugs known as DNA topoisomerase I inhibitors.[11] Camptothecin is isolated from the *Camptotheca accuminata* tree and is a pentacyclic alkaloid with anticancer properties.[11] These anticancer properties are also found in irinotecan. The anticancer drug irinotecan is used to treat a variety of different metastatic cancers, but irinotecan is used most often in the treatment of colorectal cancers.[11,12]

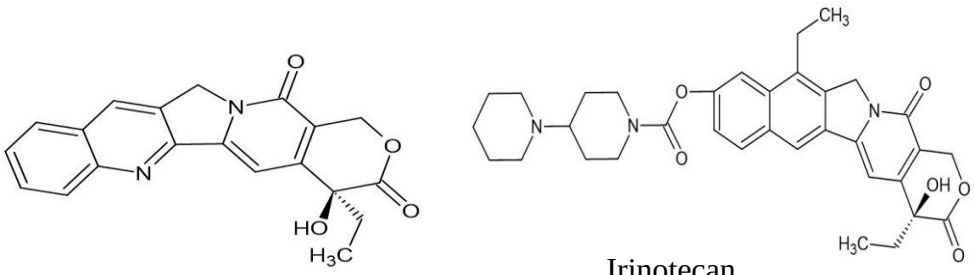

Camptothecin Irinotecan

Figure 1.1 Camptothecin structure and irinotecan structure.

The camptothecin forms a complex with the enzyme topoisomerase and DNA during DNA replication by trapping the catalytic intermediate of the topoisomerase-DNA complex.[11,13] Once the complex is formed, apoptosis or programmed cell death occurs because the enzyme is inhibited and the structure of the DNA is damaged.[11] Since camptothecin is not completely soluble in water, derivatives of camptothecin, such as irinotecan, are used to improve solubility issues.

1.4 Daunorubicin and Doxorubicin

Daunorubicin, or daunomycin as it is also called, is an anthracycline antibiotic that is red in color.[14,15] Daunorubicin is a natural product originating from the bacteria *Actinomadura roseola* and was first discovered to have antitumor capabilities in the 1960s.[14,15] While daunorubicin is used to treat multiple cancers, it is used most often for the treatment of blood cancers, such as different forms of leukemia, or breast cancer.[14]

Daunorubicin is similar to doxorubicin, another anticancer drug. Like daunorubicin, doxorubicin also became widely used during the 1960s. [16] Doxorubicin is derived from the bacteria *Streptomyces peucetius* and is an anticancer drug under the classification of an anthracycline antibiotic.[16] Structurally, daunorubicin and doxorubicin are similar. The two anticancer drugs differ by an alcohol group; doxorubicin has an extra alcohol group when compared to the structure of daunorubicin. Both daunorubicin and doxorubicin are anthracycline antibiotics that contain a dihydroxyanthraquinone ring system.[17]

Daunorubicin and doxorubicin operate as intercalators in DNA complexes. As an

intercalator, the intercalating, anticancer drug binds to the DNA through noncovalent bonds with the nucleic acid base pairs.[18] Both daunorubicin and doxorubicin are classified as topoisomerase II inhibitors.[18]

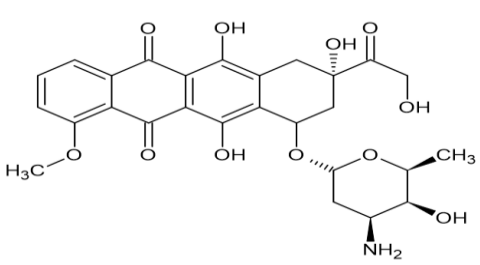

Doxorubicin (Dox)

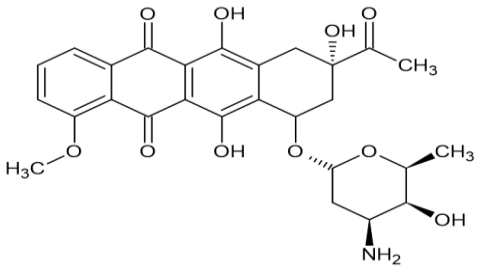

Daunorubicin (Dau)

Figure 1.2 Doxorubicin and daunorubicin structures. Doxorubicin and daunorubicin consist of a tetracyclic ring with quinine-hydroquinone groups.[19] Dox has an OH group; the OH is replaced with CH_3 in dau.

1.5 Caffeine

Caffeine (1,3,7-trimethylxanthine) is a central nervous system stimulant that is naturally occurring and was first isolated in 1820.[20,21] Caffeine is found naturally in food items, such as coffee, tea, and chocolate; it is an additive in soft drinks and energy drinks.[20] The naturally occurring, mild stimulant of caffeine is one of the most commonly used psychoactive stimulants globally.[20] The average American adult consumes approximately 135 mg of caffeine every day.[22] This amount of caffeine converts to a cup and a half of coffee. According to the United States Food and Drug Administration, a healthy adult can safely consume 400 mg of caffeine daily, or the equivalent of four cups of coffee.[22]

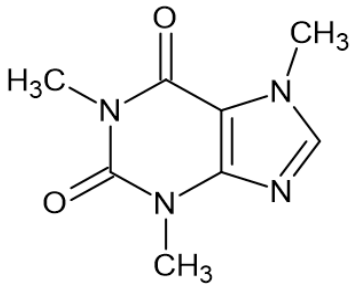

Figure 1.3 Caffeine structure.

Caffeine is a white powder that is classified as a part of the methylxanthine drug class. Methylxanthine drugs are purine-derived bronchodilators.[23] The methylxanthine drugs also have bronchodilatory and stimulatory effects.[23] This class of drugs has therapeutic value, but the therapeutic value is accompanied by numerous side effects. Like with caffeine, mild side effects of methylxanthines are nausea, vomiting, insomnia, palpitations, headaches, and tremors; more severe side effects, such as cardiac arrest and seizures, can also occur with higher concentrations of the drugs.[23]

1.6 Caffeine and Anticancer Drug Binding Interactions

In recent studies, caffeine has been shown to reduce the toxicity of intercalating agents, but caffeine also reduces the effectiveness of the aromatic anti-cancer drugs.[24] Caffeine forms a complex with aromatic anticancer drugs, such as daunorubicin. When the caffeine and aromatic anticancer drugs form a complex the free ligand concentration decreases. The decrease in free ligand concentration reduces the biological activity of the anticancer drugs.[24]

The aromatic anticancer drugs interact with DNA through intercalation. Intercalation occurs through the insertion of a planar molecule between the base pairs in DNA.[25] Caffeine, a planar molecule, can become an intercalating agent. There are two accepted theories for how caffeine interacts with DNA and anticancer drugs. In the interceptor theory, caffeine molecules bind to the anticancer drug.[26] When the caffeine binds to the anticancer drug, the anticancer drug has a more difficult time intercalating in between the base pairs of DNA molecules; the newly formed caffeine and anticancer drug complex can reduce the effectiveness of the anticancer drug. The second theory is the protector mechanism. In the protector mechanism, caffeine molecules bind to the DNA instead of the anticancer drug.[26] With the caffeine molecules bound to the DNA, the DNA is "protected" from the anticancer drugs by the caffeine. In this study, the interceptor model is the primary focus.

1.7 Proton NMR

Nuclear Magnetic Resonance (NMR) is an often-used technique in chemistry and allows for the determination of unknown structures, quantitation of mixtures of compounds, as well as the observation of how molecules interact with each other. NMR is based on the interaction of nuclei with a magnetic field. This response is not only dependent on the nucleus observed, but also the surrounding electrons that make up the bonding of multiple atoms in a chemical compound. The position of a signal in a spectrum is governed by the nature of the nucleus and the surrounding environment of electrons. Due to this phenomenon, every single isotope that is active in NMR is observed at different

frequencies relative to the magnetic field that is used. The frequency observed is relative to the gyromagnetic ratio of the particular isotope and is scaled linearly with the magnetic field. ^{1}H-NMR produces the largest frequency in a given magnet, as well as produces the largest signal relative to the concentration of the chemical of interest.[27]

When a different element is attached to a hydrogen, the chemical environment of the hydrogen is different from that of an isolated hydrogen. The full extent of the magnetic field is not felt by the hydrogen in a new chemical environment as it is with an isolated hydrogen.[28] This results in a small change in the frequency of the hydrogen. The change is measured in ppm, also referred to as chemical shift. In order to compare different measurements on different magnets, the utilization of an internal reference standard, such as tetramethylsilane (TMS) or sodium trimethylsilylpropanesulfonate (DSS), is used. When adding a known quantity of TMS or DSS, the internal reference standard can be used for the estimation of concentration.[28]

Neighboring atoms in compounds exert an additional magnetic field. This behavior gives a unique pattern of observable signals. This effect is called coupling.[26] NMR can be divided into either one-dimensional or multi-dimensional NMR spectroscopy. In multi-dimensional NMR, we can take advantage of the coupling of the nuclei with each other. As such, multi-dimensional NMR spectroscopy is beneficial for analyzing large, complex molecules that have a great deal of overlap.[29,30] Multi-dimensional NMR differs from one-dimensional NMR by adding a time component to the sequence.[29,30] One-dimensional NMR consists of a series of radiofrequency (RF) pulses followed by a Fourier Transform (FT) of the signal that gives rise to the chemical shift value in parts per million (ppm).[29,30]

Multi-dimensional NMR consists of two parts; the first part is the same as in one-dimensional NMR, while the second part varies the length of time the system evolves after the first pulse.[29,30] After a Fourier Transform, the multi-dimensional spectrum is given for the sample.

In this study, the caffeine and anticancer drug interactions are studied using proton NMR to observe small changes in chemical shift and Diffusion Order Spectroscopy (DOSY) NMR techniques. The proton chemical shift is determined, as well as, the diffusion coefficients for each of the compounds of interest for this study.

One of the more common points analyzed using NMR is the chemical shift. The chemical shift is shown as parts per million, ppm. The ppm value represents the chemical shift and gives the frequency of an atom being analyzed in comparison to an internal reference standard.[29] The frequency of the nuclear spin of an atom is related to the atom's chemical environment.[30] The internal reference appears at 0 ppm on the chemical shift table. Chemical shift is related to the differing chemical environments of the atoms. The chemical shift in a proton NMR spectrum is affected by the elements surrounding the atoms, such as electronegative atoms and unsaturated groups.[30] Some examples of electronegative groups are oxygen, nitrogen, and halogens, while examples of unsaturated groups are alkenes, aromatics, and carbonyl groups.[30] Electronegative groups cause a downfield shift, which is an increase in ppm.[30] Figure 1.4 illustrates where different organic functional groups occur based on their chemical shift.[30] The structural composition of the compound affects the magnetic field that is applied to the nuclei.[31]

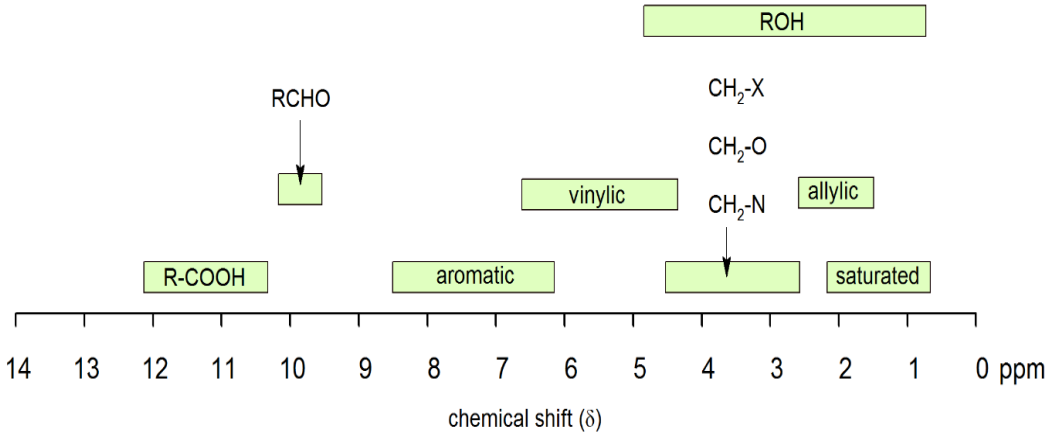

Figure 1.4 Proton NMR chemical shifts for organic functional groups.

The solvent used when preparing the solution can also influence the chemical environment and thus impact the chemical shift. Considering that most hydrogens are on the surface or the periphery of a molecule, the hydrogens are in direct contact with the solvent. The use of different solvents creates different interactions with the protons in the sample which influence the chemical shift values. Solvents in NMR are usually deuterated solvents. The use of a deuterated solvent allows for the signal of the solvent to remain low and prevents the solvent from dominating the spectrum.[31] This is governed by the fact that the observed analog signals are being digitized. Digitizers allow only for a given range of intensities. For the most part, organic molecules only have low solubilities in aqueous solvents. Since we wanted to observe the behavior of the drug in a solvent similar to biological conditions, D_2O a deuterated solvent, was used in NMR. In order to escape the aqueous environment, the organic molecules form clusters. The clusters allow the molecules to surround themselves with an organic compound which changes the chemical environment. To stay in solution, the molecules fluctuate between

the organic cluster and the dissolved in water state which leads to changes in chemical shift based on how much the molecules stay in one state versus the other state.

1.8 Diffusion-Ordered Spectroscopy (DOSY)

Another NMR technique used in this study is called Diffusion-Ordered Spectroscopy, more commonly referred to as DOSY NMR. Diffusion-Ordered Spectroscopy is a two-dimensional NMR spectroscopy method. DOSY is based on the fact that molecules have translational movement in solution.[31] The DOSY technique can be applied to the analysis of a mixture consisting of different compounds; the mixture can then be resolved based on the individual diffusion properties of each of the compounds in the mixture.[32]

In DOSY, a gradient is used to determine the position of the molecules being analyzed at a given time.[31] For DOSY to work, two different gradient pulses of opposite signs are used. First, a 90-degree radiofrequency pulse is applied to magnetize the spin into the xy-plane and the position of the molecule is labeled with the first gradient pulse (indicated as + in Figure 1.5).[31] The magnetization is inverted by a 180-degree refocusing pulse after half the time before the second gradient pulse is applied.[31] The second gradient pulse applied in the opposite direction of the first gradient pulse is used to compensate for the distortion with the first gradient pulse. Typically, a set of 15-20 spectra are run to make up one DOSY data set. If molecules do not move, a regular spectrum is observed; however, since the molecules move between the gradient pulses, the signal is broadened, resulting in smaller intensity of the new peak. Examination of

the peak height allows for the correlation of how much a compound has moved.[31] Figure 1.5 shows a simple DOSY pulse sequence, where the diffusion delay is represented as Δ, the diffusion-encoding pulse length is represented as δ, and the diffusion-encoding pulse strength is represented as g.[33]

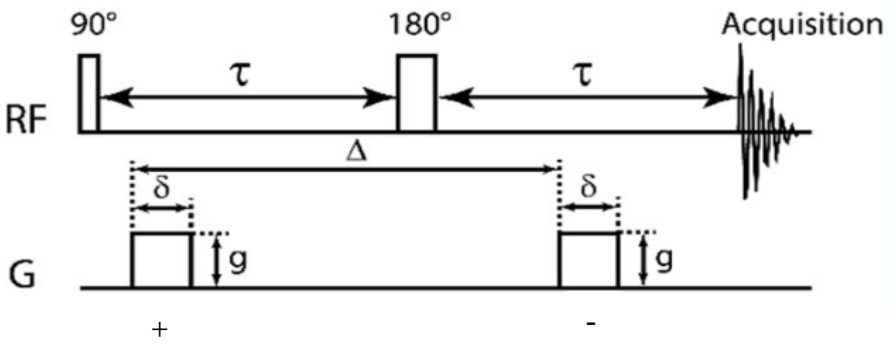

Figure 1.5 Simple DOSY pulse sequence.

Typically, a variation of gradients run over multiple spectra determines the diffusion behavior. The DOSY parameters are optimized to give the best spectrum, meaning an optimum decay of the original signal over the course of the number of spectra. The main parameters optimized for DOSY are the diffusion time, the gradient strength, and the gradient length. Increasing the diffusion time allows more time for the molecules of interest to diffuse through the sample.[34] Increasing the gradient strength (g) or gradient length (δ) allows for greater signal dephasing of the sample.[34] When a molecule diffuses, the signal is not completely refocused.[32] The greater the diffusion of the molecule, the more the intensity of the signal is lowered.[34] When optimizing the parameters, two of the parameters are kept constant while the other parameter is changed. Most commonly, the gradient strength (g) is changed while the other parameters stay constant when determining the best values for the DOSY parameters.[34]

Through the Stokes-Einstein equation, the diffusion coefficients and hydrodynamic radius are related.[35] The molecular weight of a molecule can also be related to the hydrodynamic radius and the diffusion rate. The diffusion rate decreases as the particle size increases.[36] The rate of diffusion is inversely related to the molecular weight of the molecule; this means larger molecules move smaller distances in a fixed amount of time than smaller molecules.[31] DOSY uses the diffusion coefficients of a molecule to determine the hydrodynamic radius of the molecule.[35] Figure 1.6 illustrates how the gradient pulse applied affects two molecules differently.[37] Molecule A, the larger molecule, moves a shorter distance than molecule B, the smaller molecule.

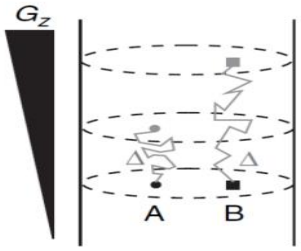

Figure 1.6 Diffusion gradient in DOSY NMR.

DOSY can be used to resolve the different components in a mixture of compounds. One of the ways the components can be differentiated is based on aggregation and π stacking that occurs in aromatics.[31,38] When the components of the mixtures are resolved, the diffusion coefficients for the components can be determined.[31] Diffusion coefficients change based on either molecular weight or aggregation due to changes in concentration. The aggregation that can occur from π stacking in aromatic

compounds create larger aggregates; these larger aggregates cause changes in the diffusion coefficients.[31] The more aggregates form from π stacking, the slower the compounds move in DOSY; this results from a decrease in the diffusion coefficient.

Diffusion coefficients can be estimated using a tool from the Manchester NMR Methodology group called a SEGWE calculator.[39] SEGWE is an acronym for the Stokes-Einstein Gierer-Wirtz estimation equation, which gives the relationship between the aggregate weight and the diffusion coefficients of the molecules. The Stokes-Einstein Gierer- Wirtz equations are shown in equations 1.1, 1.2, and 1.3. Equation 1.1 shows the Stokes-Einstein equation, where r is the hydrodynamic radius, η is the viscosity, T is the temperature, k_B is the Boltzmann constant, and f is the friction factor.[40] Equation 1.2 shows the Gierer-Wirtz equation for f, where r is the solute radius and r_s is the solvent radius.[40] Equation 1.3 is the Stokes-Einstein Gierer-Wirtz equation, where ρ_{eff} is the effective density of a small molecule, MW_s is the molecular weight of solvent, and N_A is the Avogadro number.[40]

Equation 1.1: $$D = \frac{\kappa BT}{6\pi\eta r f}$$

Equation 1.2: $$f = \left(\frac{3rs}{2r} + \frac{r}{rs}\right)^{-1}$$

Equation 1.3: $$D = \frac{kBT\left(\frac{3\alpha}{2} + \frac{1}{1+\alpha}\right)}{6\pi\eta\sqrt[3]{\frac{3MW}{4\pi\rho eff NA}}}$$, where $$\alpha = \sqrt[3]{\frac{MWs}{MW}}$$

The SEGWE calculator uses the approximate relationship to predict the diffusion coefficient of the molecule. The SEGWE calculator needs the solvent used, the

temperature, and the molecular weight of the molecule to estimate the diffusion coefficients of the molecule.[39] The SEGWE calculator also works in reverse and can predict the molecular weight of a molecule if the diffusion coefficient is known. Figure 1.7 shows the SEGWE calculator interface.[39]

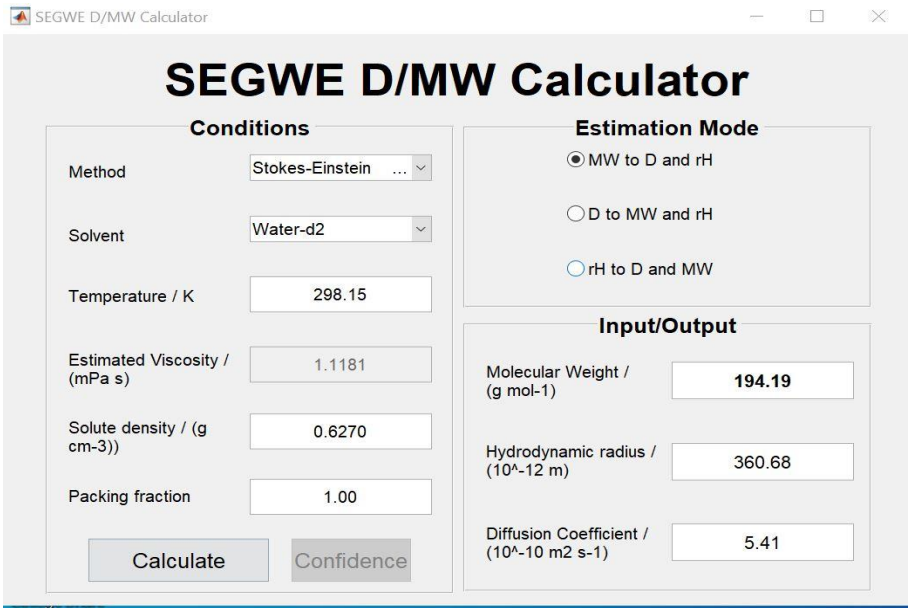

Figure 1.7 SEGWE calculator.[39]

1.9 Association Constants

In general, a chemical reaction in equilibrium can be represented as the following reaction shown in Figure 1.8.[41] The association constant, K_a, shows how likely a molecule is to bind to another molecule.

$$a\mathrm{A} + b\mathrm{B} \rightleftharpoons c\mathrm{C} + d\mathrm{D}$$

Figure 1.8 General equation for chemical equilibrium.

The K_a is determined from the equilibrium constant, K_{eq}. The K_{eq} indicates the relationship between the reactants and products in a chemical reaction at equilibrium.[31] The concentrations of the reactants and products are used to determine the K_{eq}. A K_{eq} that is less than one favors the reactants, while a K_{eq} that is greater than one favors the products.[31] Figure 1.9 shows the general chemical equation at equilibrium.

$$K_{\text{eq}} = \frac{[\text{C}]^c[\text{D}]^d}{[\text{A}]^a[\text{B}]^b}$$

Figure 1.9 Chemical equilibrium.

The association constants of a molecule can be compared to the association constant of the mixture the molecule is associated with. Standards can be compared to mixtures through the association constants. The comparison between the association constants helps to identify the π stacking interactions between the molecules.[31] When studying the π stacking interactions of a compound, the self-association of the molecules in question is compared to the association constants of a mixture.[31] The daunorubicin and irinotecan anticancer drugs do not dissolve well in the D_2O solvent. Since the anticancer drugs do not want to associate with the solvent, the anticancer drug can interact with itself instead; this gives the self-association constant for the compound. When caffeine is added to the anticancer drug compounds, the association constant can be determined.

The anticancer drug now has a choice between binding with the caffeine or binding with itself.

Chapter 2. Experimental

2.1 Preparation of Caffeine Standards

The caffeine standards were premade during previous studies.[42] The samples were prepared with D_2O and potassium phosphate buffer. The buffer concentration of 10.0 mM was chosen to result in a constant pH of around 7. The buffered potassium phosphate buffer was made with monobasic potassium phosphate (KH_2PO_4) and dibasic potassium phosphate (K_2HPO_4). A 1.0 M solution of both the monobasic potassium phosphate and the dibasic potassium phosphate was prepared in separate 100 mL volumetric flasks using 13.69 grams of monobasic potassium phosphate and 17.43 grams of dibasic potassium phosphate. In a new 100 mL volumetric flask, 38.5 mL of monobasic potassium phosphate and 61.5 mL of dibasic potassium phosphate were mixed; this ratio of monobasic potassium phosphate and dibasic potassium phosphate gives a pH of around 7. A dilution series for caffeine was prepared starting at 8.0 mM and was created to produce the following concentrations, 8.0 mM, 4.0 mM, 2.0 mM, 1.0 mM, and 0.5 mM. The actual concentrations of the caffeine standards were 8.39 mM, 4.16 mM, 1.83 mM, 0.60 mM, and 0.31 mM as determined by integration relative to 1.0 mM DSS. The concentrations were confirmed using proton NMR and MestreNova. The integrals of the peaks were used to determine the sample concentrations. The concentration is proportional to the integral area of the peak divided by the number of

nuclei that correspond to that peak. The differences between the expected concentrations and the actual concentrations were most likely due to pipetting errors.

The dilution series was prepared with 0.50 mL of the caffeine solution and 0.15 mL of the internal standard, 1.0 mM DSS, into 5 mm NMR tubes. The 5 mm NMR tubes were used for PRESAT/Proton NMR measurements. For additional measurements using DOSY NMR, 0.20 mL of each of the caffeine dilutions in the four 5 mm NMR tubes was transferred to four new 3 mm NMR tubes. When using the 5 mm NMR tubes, the series of FID's for DOSY measurements did not have the expected exponential decay shape. The distortion of the FID signal was caused by convection. Convection occurs when the liquid in the sample is warmer at the base than at the top of the sample.[43] If convection occurs with a sample, the diffusion coefficients from DOSY can be overestimated due to the extra signal attenuation in pulsed field gradient experiments.[43,44] One way to reduce the effect of convection on the sample is by using NMR tubes with narrower diameters.[43]

2.2 Preparation of Irinotecan Standards

The irinotecan standards were prepared using powdered irinotecan (hydrochloride Hydrate), D_2O, and potassium phosphate buffer. The 10.0 mM potassium phosphate buffer concentration at pH 7.0 was chosen to make the irinotecan stock solution.

A 2.0 mM stock solution of irinotecan was made using 0.0339 grams of irinotecan dissolved in D_2O and potassium phosphate buffer. Different concentrations were prepared from this stock solution for a dilution series. A dilution series for irinotecan standards was prepared at 2.0 mM and created to produce the following

concentrations: 2.0 mM, 1.0 mM, 0.5m, and 0.25 mM. The concentrations of the irinotecan standards were 1.68 mM, 1.35 mM, 0.78 mM, and 0.58 mM as determined by integration relative to 1.0 mM DSS using MestreNova. The differences between expected concentrations and actual concentrations are most likely due to pipetting errors.

After the dilution series was prepared, 0.50 mL of the irinotecan solution and 0.15 mL of the internal reference, DSS, were pipetted into 5 mm NMR tubes. PRESAT/Proton NMR measurements were performed using 5 mm NMR tubes. For DOSY NMR measurements, 0.20 mL of each of the irinotecan dilutions in the 5 mm NMR tubes were transferred to new 3 mm NMR tubes.

2.3 Preparation of Irinotecan and Caffeine Mixture Standards

Four irinotecan-caffeine mixtures were prepared. The mixtures had expected mole percentages of 80% irinotecan / 20% caffeine, 60% irinotecan / 40% caffeine, 40% irinotecan / 60% caffeine, and 20% irinotecan / 80% caffeine. The actual mole percentages were 87% irinotecan /13% caffeine, 64% irinotecan / 36% caffeine, 38% irinotecan / 62% caffeine, and 17% irinotecan / 83% caffeine as determined using MestreNova. After the mixtures were prepared, 0.50 mL of the mixture and 0.15 mL of the internal standard, 1.0 mM DSS, were pipetted into 5 mm NMR tubes. The actual concentrations of irinotecan in irinotecan-caffeine mixtures are verified with MestreNova.

The concentration of the buffered caffeine and the buffered irinotecan stock solutions were both 2.0 mM. The expected concentrations of irinotecan in irinotecan-

caffeine mixtures were 1.60 mM, 1.20 mM, 0.80 mM, and 0.40 mM; however, the actual concentrations for irinotecan in irinotecan-caffeine mixtures were 2.14 mM, 1.68 mM, 0.97 mM, and 0.42 mM as determined by integration relative to 1.0 mM DSS using MestreNova. The expected concentrations of caffeine in irinotecan-caffeine mixtures were 0.40 mM, 0.80 mM, 1.20 mM, and 1.60 mM. The actual concentrations of caffeine in irinotecan-caffeine mixtures were 0.31 mM, 0.93 mM, 1.56 mM, and 2.04 mM as determined by MestreNova. The differences between the expected concentrations and the actual concentrations are most likely due to pipetting errors. PRESAT/Proton NMR measurements were performed using 5 mm NMR tubes. For DOSY NMR measurements, 0.20 mL of each of the prepared mixtures in the 5 mm NMR tubes were transferred to new 3 mm NMR tubes.

2.4 Preparation of Daunorubicin Standards

The daunorubicin standards were prepared without buffer because of solubility issues when the buffer is added. A 2.0 mM stock solution of daunorubicin was made with 0.0282 grams of pure daunorubicin dissolved in D_2O. The daunorubicin solutions were lyophilized and redissolved in D_2O for optimal solubility. A dilution series for daunorubicin was prepared starting at 2.0 mM and created to produce the following concentrations: 2.0 mM, 1.0 mM, 0.5 mM, and 0.25 mM. The concentrations of daunorubicin were 1.95 mM, 1.43 mM, 0.49 mM, and 0.20 mM as determined by integration relative to 1.0 mM DSS. The actual concentrations were determined using the NMR editing and evaluating software MestreNova. The differences between the

expected concentrations and the actual concentrations are most likely due to pipetting errors.

After the dilution series was prepared, 0.50 mL of the daunorubicin solution and 0.15 mL of the internal reference, 1.0 mM DSS, were pipetted into 5 mm NMR tubes. PRESAT/Proton NMR measurements were performed using 5 mm NMR tubes. For DOSY NMR measurements, 0.20 mL of each of the daunorubicin dilutions in the 5 mm NMR tubes were transferred to new 3 mm NMR tubes.

2.5 Preparation of Daunorubicin and Caffeine Mixture Standards

Four daunorubicin-caffeine mixtures are prepared. The mixtures had expected mole percentages of 80% daunorubicin / 20% caffeine, 60% daunorubicin / 40% caffeine, 40% daunorubicin / 60% caffeine, and 20% daunorubicin / 80% caffeine. The actual mole percentages were 95% daunorubicin / 5% caffeine, 70% daunorubicin / 30% caffeine, 35% daunorubicin / 65% caffeine, and 10% daunorubicin / 90% caffeine as determined using MestreNova.

The concentrations of the buffered caffeine and the non-buffered daunorubicin stock solutions were 2.0 mM. The expected concentrations of daunorubicin in the daunorubicin-caffeine mixture were 1.60 mM, 1.20 mM, 0.80 mM, and 0.40 mM; however, the actual concentrations for daunorubicin in daunorubicin-caffeine mixtures were 2.89 mM, 1.76 mM, 0.88 mM, and 0.25 mM as determined by integration relative to 1.0 mM of DSS using MestreNova. The expected concentrations of caffeine in the daunorubicin-caffeine mixtures are 0.40 mM, 0.80 mM, 1.20 mM, and 1.60 mM. The

actual concentrations of caffeine in the daunorubicin-caffeine mixtures were 0.15 mM, 0.75 mM, 1.62 mM, and 2.20 mM as determined using MestreNova. The differences between the expected concentrations and the actual concentrations are most likely due to pipetting errors. After the mixtures were prepared, 0.50 mL of the mixture and 0.15 mL of the internal standard, 1.0 mM DSS, were pipetted into 5 mm NMR tubes. PRESAT/Proton NMR measurements were performed using 5 mm NMR tubes. For DOSY NMR measurements, 0.20 mL of each of the prepared mixtures in the 5 mm NMR tubes were transferred to new 3 mm NMR tubes.

2.6 PRESAT Specifications

The D_2O solvent minimizes a large water signal in the NMR spectrum. The anticancer drugs and caffeine samples, the NMR tubes, and the surrounding environment contain small amounts of water. Even though the interaction with water involved is relatively small, when working with millimolar concentrations, minute amounts of water can greatly distort the NMR spectrum. The NMR water suppression technique PRESAT is used to overcome the large water peak. PRESAT reduces the intensity of the water peak.[45]

Shown below in Figures 2.1, 2.2, and 2.3 are the procedures and specifications for the Varian 500 MHz machine using Open VNMRJ 4.2. The PRESAT was run at 25°C with 64 scans, 6.0 seconds for acquisition time, and 10.0 seconds for relaxation delay. The water peaks in the spectrum are chosen during PRESAT to suppress the water peak.

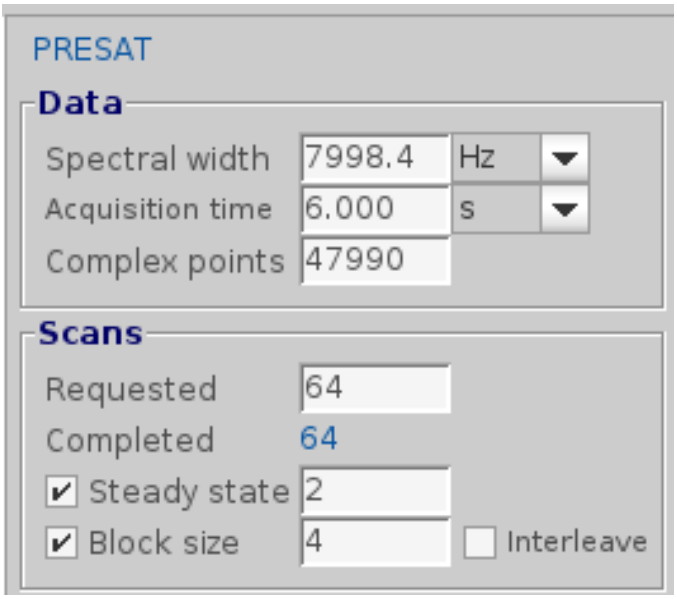

Figure 2.1 PRESAT procedures and specifications.

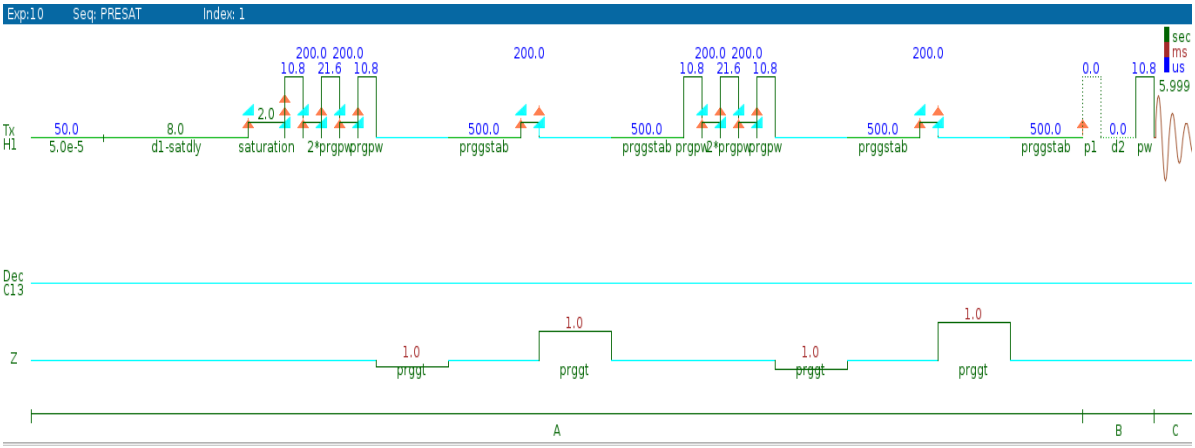

Figure 2.2 Pulse sequence for PRESAT.

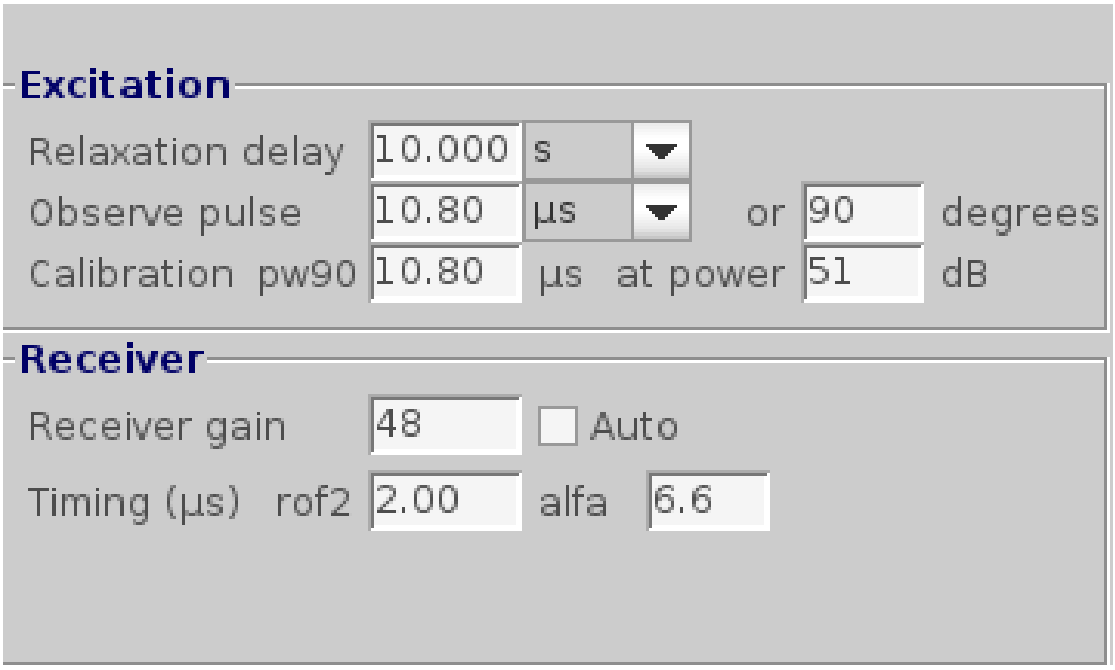

Figure 2.3 PRESAT pulses.

2.7 DOSY Specifications

Shown below in Figures 2.4 and 2.5 are the procedures and specifications from the Varian 500 MHz machine. The DOSY is run at 25°C with 32 scans to 256 scans, 4.0 seconds for acquisition time, and 2.0 seconds for relaxation delay. Before running the oneshot DOSY, the parameters are optimized. First, proton/PRESAT scans are run. After the PRESAT scans, the actual diffusion delay (del), the total diffusion-encoding pulse strength (gt1), and the diffusion-encoding pulse strength (gzlvl1) are set up. In the beginning, gt1 is set to 0.002 and del is set to 0.05 for small molecules. The gzlvl1 goes from a strength of 500 as the minimum to 25,000 as the maximum. After entering the initial values, the values are optimized for the type of sample being used. A test DOSY is run with the initial values, and the result is two spectra. For the values to be optimized,

the second spectrum should be 10% of the first spectrum in order to give the proper gradient array for the experiment.[46] If the second spectrum is greater than 10% of the first spectrum, gt1 can be increased up to a maximum of 0.04. If the second spectrum is less than 10% of the first spectrum, gt1 can be decreased. Once the second spectrum is 10% of the first spectrum, the parameters are optimized and the values should be recorded. This process is repeated and the optimized DOSY parameters are determined for each of the different samples. Even though the gradient array and parameters are the same for the oneshot DOSY scans, the number of scans is varied. The lower the concentration of the sample, the higher the number of scans needed to improve the signal-to-noise ratio; more scans will provide the spectrum with less noise.[47] The number of scans is varied from 32 scans to 256 scans.

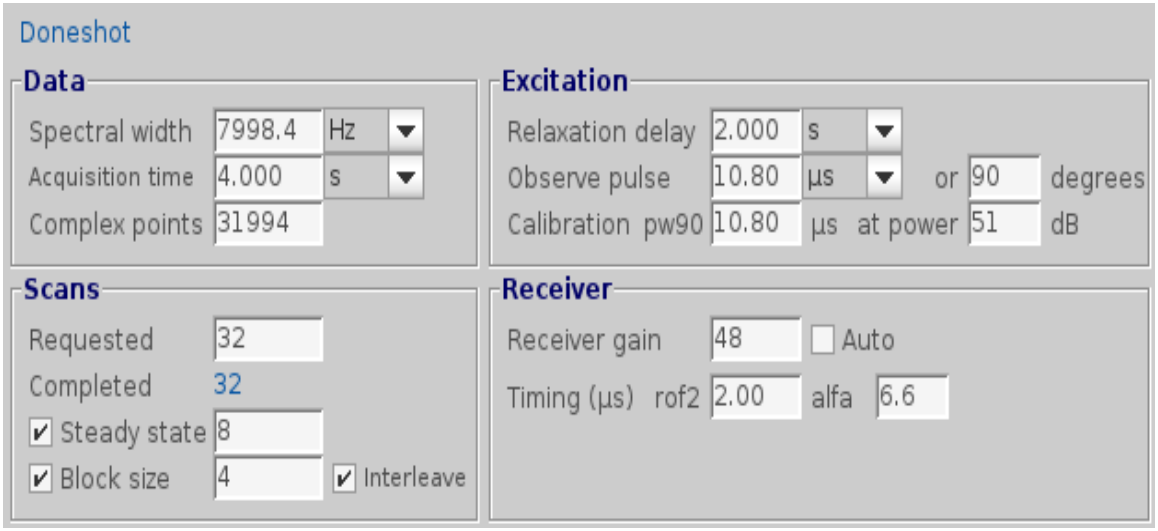

Figure 2.4 DOSY procedures and specifications.

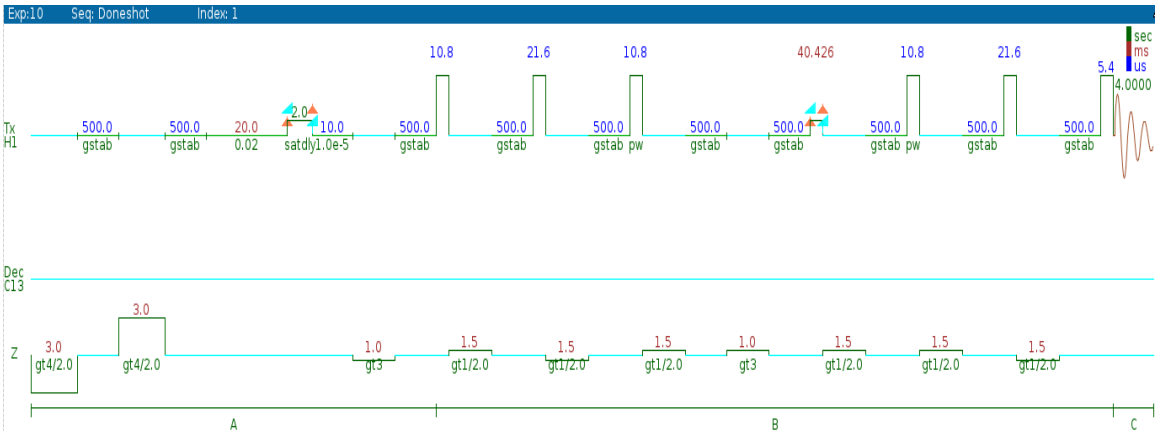

Figure 2.5 Pulse sequence for DOSY.

2.8 NMR Processing Software

Different NMR analysis tools are used to process the NMR data obtained from the Varian 500 MHz machine using Open VNMRJ 4.2. The main NMR analysis tool used is the General NMR Analysis Toolbox (GNAT) from the Manchester NMR Methodology Group. The GNAT software can be downloaded from the following website: https://www.nmr.chemistry.manchester.ac.uk/?q=node/430. The GNAT software is utilized to establish the chemical shift data, as well as, diffusion coefficient data from pure anticancer drugs and caffeine individually from anticancer drug/caffeine mixtures.

The NMR processing software MestreNova is used to confirm the concentrations of each of the samples. First, the reference signal of DSS is set to 0 ppm.[31] Once the reference signal is set to 0 ppm, each of the peaks in the spectrum is analyzed using the multiplet analysis tool. Using the quantitation section of MestreNova, the concentration is determined as shown in Figure 2.6.[31] MestreNova compares the peak integrals of the molecule of interest relative to the internal standard, 1.0 mM DSS.[48]

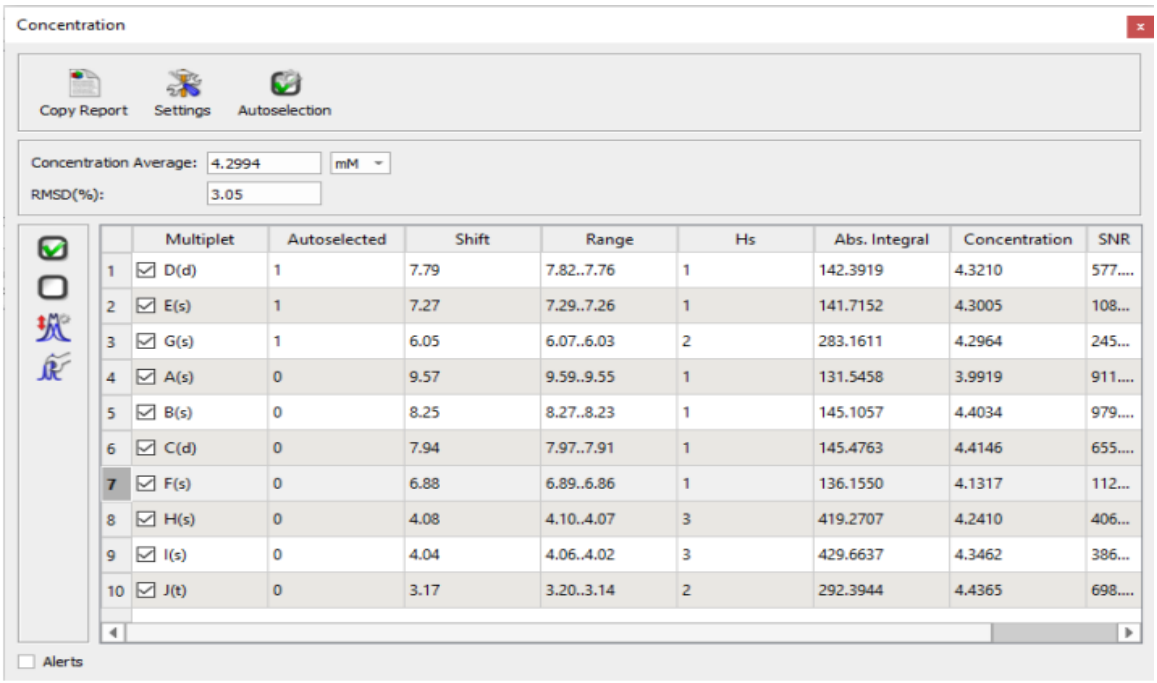

	Multiplet	Autoselected	Shift	Range	Hs	Abs. Integral	Concentration	SNR
1	D(d)	1	7.79	7.82..7.76	1	142.3919	4.3210	577....
2	E(s)	1	7.27	7.29..7.26	1	141.7152	4.3005	108...
3	G(s)	1	6.05	6.07..6.03	2	283.1611	4.2964	245...
4	A(s)	0	9.57	9.59..9.55	1	131.5458	3.9919	911....
5	B(s)	0	8.25	8.27..8.23	1	145.1057	4.4034	979....
6	C(d)	0	7.94	7.97..7.91	1	145.4763	4.4146	655....
7	F(s)	0	6.88	6.89..6.86	1	136.1550	4.1317	112...
8	H(s)	0	4.08	4.10..4.07	3	419.2707	4.2410	406...
9	I(s)	0	4.04	4.06..4.02	3	429.6637	4.3462	386...
10	J(t)	0	3.17	3.20..3.14	2	292.3944	4.4365	698....

Figure 2.6 Example of quantitation of concentration in MestreNova.[31]

Next, the reference concentration is set to 1.0 mM and the nuclide reference is entered as nine; this is because there are nine identical protons in DSS.[31] Figure 2.7 shows the setting of the reference concentration and the reference nuclides.[31]

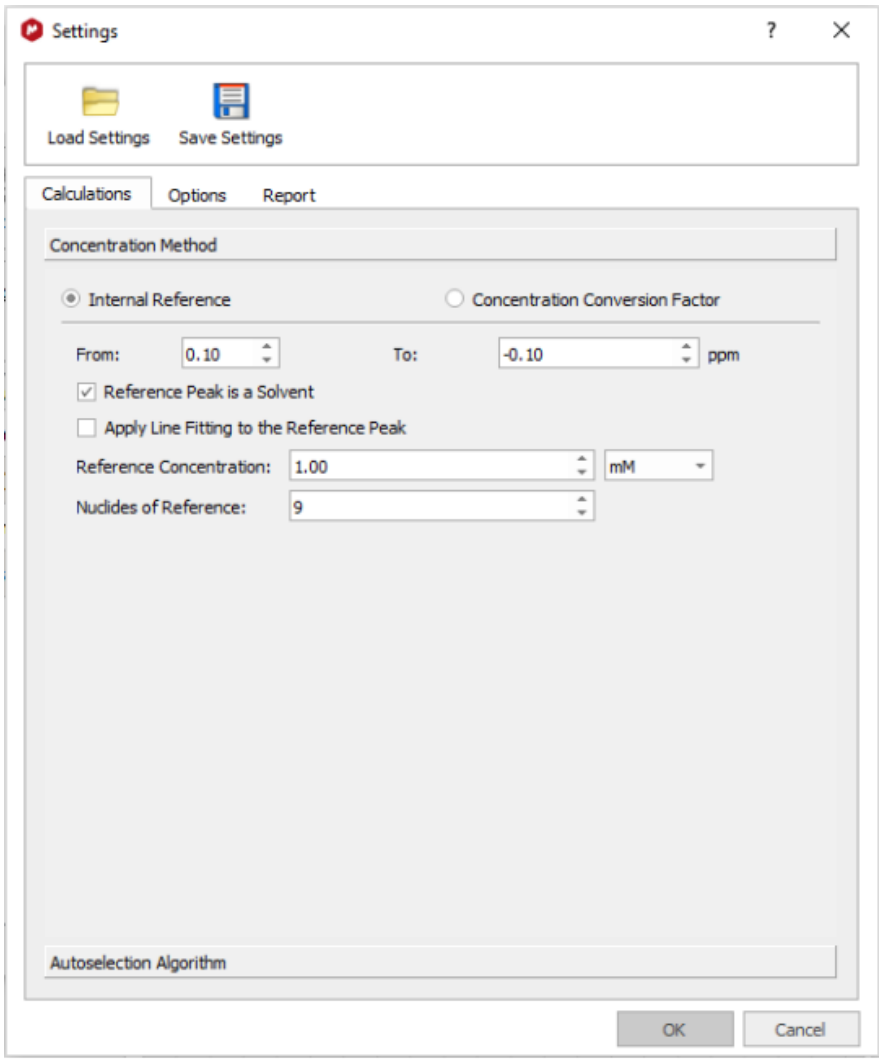

Figure 2.7 MestreNova setting of reference concentration and nuclides.[31]

Once the references are set, the number of hydrogens present for each position in the molecule of interest is entered and the concentration of the sample is determined. Figure 2.8 shows the final steps to determine the concentration of each of the samples.[31] The process is repeated for each of the samples.

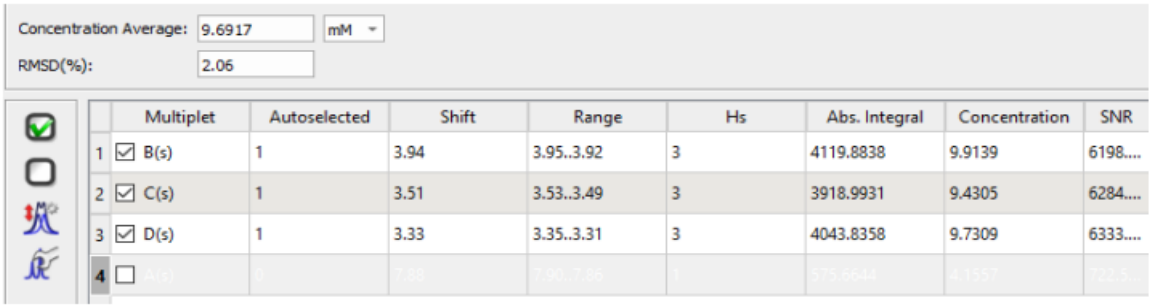

Figure 2.8 Determination of final concentration using MestreNova.

For each of the data sets, performed in triplicate, the standard deviation (STDEV) is determined. The standard deviation measures the distribution of a set of data relative to the average of the data set.[49] The higher the STDEV, the more the data is spread out from the mean.[49] The STDEV formula is shown in Equation 2.1, where x is the data points, a is the average of the data points, and n is the number of data points.[49] The STDEV is added as error bars to the graphs.

Equation 2.1: $\text{STDEV} = \sqrt{\frac{\sum(x-a)^2}{n-1}}$

2.9 Determination of $K_{association}$ (K_a)

The K_a is determined for self-association of caffeine and the anticancer drugs and the binding of caffeine anticancer drug mixtures. The Rose-Drago equation, which was originally developed for UV data, is shown in Equation 2.2.[50,51] In the original Rose-Drago equation, ε_c is the extinction coefficient of the complex, ε_A is the extinction coefficient of the free ligand, A_o is the initial concentration of the acceptor, B_o is the initial concentration of the donor, and $\beta = K(A_o + B_o)+1$.[50] It is assumed the acceptor and the donor molecules react and come together to form a complex.[52]

The proton peak positions are used to determine the K_a using a modified version of the Rose-Drago equation as shown in Equation 2.3.[42,53] In the modified Rose-Drago equation y0 is the maximum calculated proton peak position, y1 is the minimum calculated proton peak position, K is the association constant, and x is the concentration.

Equation 2.2: $a - ao = \frac{\varepsilon c - \varepsilon a(\beta - (\beta^2 - 4K^2 AoBo)^{0.5}}{2K}$

Equation 2.3: $Calculated\ peak = y0 + (y1 - y0) * K * x(\frac{2}{1 + (4K*x+1)^{0.5}})^2$

In Table 2.1, the experimental peak positions are highlighted in red, the calculated proton peak positions calculated with Equation 2.2 are highlighted in black, and the concentrations are highlighted in blue. For the example in Table 2.1, the concentrations and proton peak positions for caffeine are used.

Table 2.1 Example of experimental (red) and calculated (black) peak positions and concentration (blue) for caffeine.

Concentration	Experimental				Calculated			
	1	2	3	4	1	2	3	4
8.39 mM	3.3136	3.4921	3.9224	7.8713	3.31	3.49	3.92	7.87
4.16 mM	3.3276	3.5082	3.9323	7.8761	3.33	3.51	3.93	7.88
1.83 mM	3.3345	3.5161	3.9369	7.8778	3.34	3.52	3.94	7.88
0.60 mM	3.3386	3.5209	3.9398	7.8792	3.34	3.52	3.94	7.88
0.31 mM	3.3417	3.5244	3.9423	7.8811	3.34	3.52	3.94	7.88

Using the information from Table 2.1, y0, and y1, the K_a and root mean squared error (RMSE) are determined using Excel and Solver as shown in Table 2.2. The root sum square error between the calculated peak positions and experimental peak positions is calculated with Equation 2.4 where n is the number of data points.[54]

Equation 2.4: $RMSE = \sqrt{\sum \frac{(Calculated - Experimental)^2}{n}}$

The y0 value is a number above the highest experimental proton peak position, while the y1 value is a number below the lowest experimental proton peak position. Solver needs starting values that are at the upper (y0) and lower (y1) end of the range of the calculated peaks as shown in Table 2.2 in order to determine K_a and the error.[42]

Table 2.2 Examples of y0, y1, K_a, and error using Excel and Solver for caffeine.

y0	**y1**	**K_a**	**Error**
3.3417	2.8538	7.7087	0.0016
3.5244	2.8752	6.5414	0.0019
3.9423	3.6750	10.2576	0.0014
7.8811	7.8294	33.3673	0.0013

Solver is an Excel program used for analysis.[55] Solver determines the optimal value, either maximum or minimum, for a scenario based on the constraints placed on the scenario.[55] In this experiment, y0 and y1 are the constraints and Solver is trying to determine the optimal K_a by varying the constraints.[55] The y0, y1, and K_a cells are varied in order to make the error as close to zero as possible.[42] Solver uses fifty iterations to make the error cell as close to zero as possible.[42] Once Solver finishes the iterations, the K_a for caffeine, daunorubicin, irinotecan, caffeine-daunorubicin, and caffeine-irinotecan were determined.

Chapter 3. Results

3.1 Caffeine Standards Analysis

The caffeine standards and each of the anticancer drugs were studied individually to determine changes in chemical shift values compared to changes in concentration. The chemical shifts for the dilution series for caffeine standards, irinotecan standards, and daunorubicin standards were determined individually for the three compounds. The anticancer drugs were analyzed in mixtures with caffeine. The anticancer drug caffeine mixtures were also analyzed for chemical shifts. The diffusion coefficients for caffeine, anticancer drugs, and caffeine-anticancer drug mixtures were determined, as well. The diffusion coefficients were determined using GNAT and SEGWE software.

3.1.1 Caffeine Proton Positions

The proton positions (δ) determined from proton/PRESAT NMR at 25°C with 5 mm NMR tubes were run in three trials and reported in Tables 3.1. The average proton peak positions were reported in Table 3.4 with the standard deviation (STDEV). The PRESAT was performed due to the high water content of the solvent. The peak assignments for caffeine were shown in Figure 3.1 and adapted from a study by Webb, et al.[55] These peak assignments will continue to be used in this study. Figure 3.2 shows the

NMR spectrum for pure caffeine processed using the MestreNova NMR processing software.

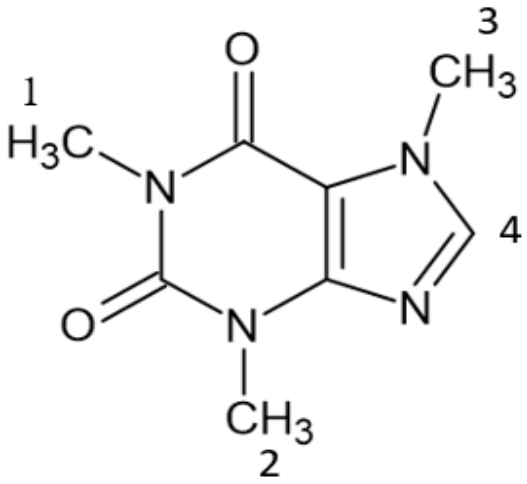

Figure 3.1 Caffeine chemical structure with proton assignment.

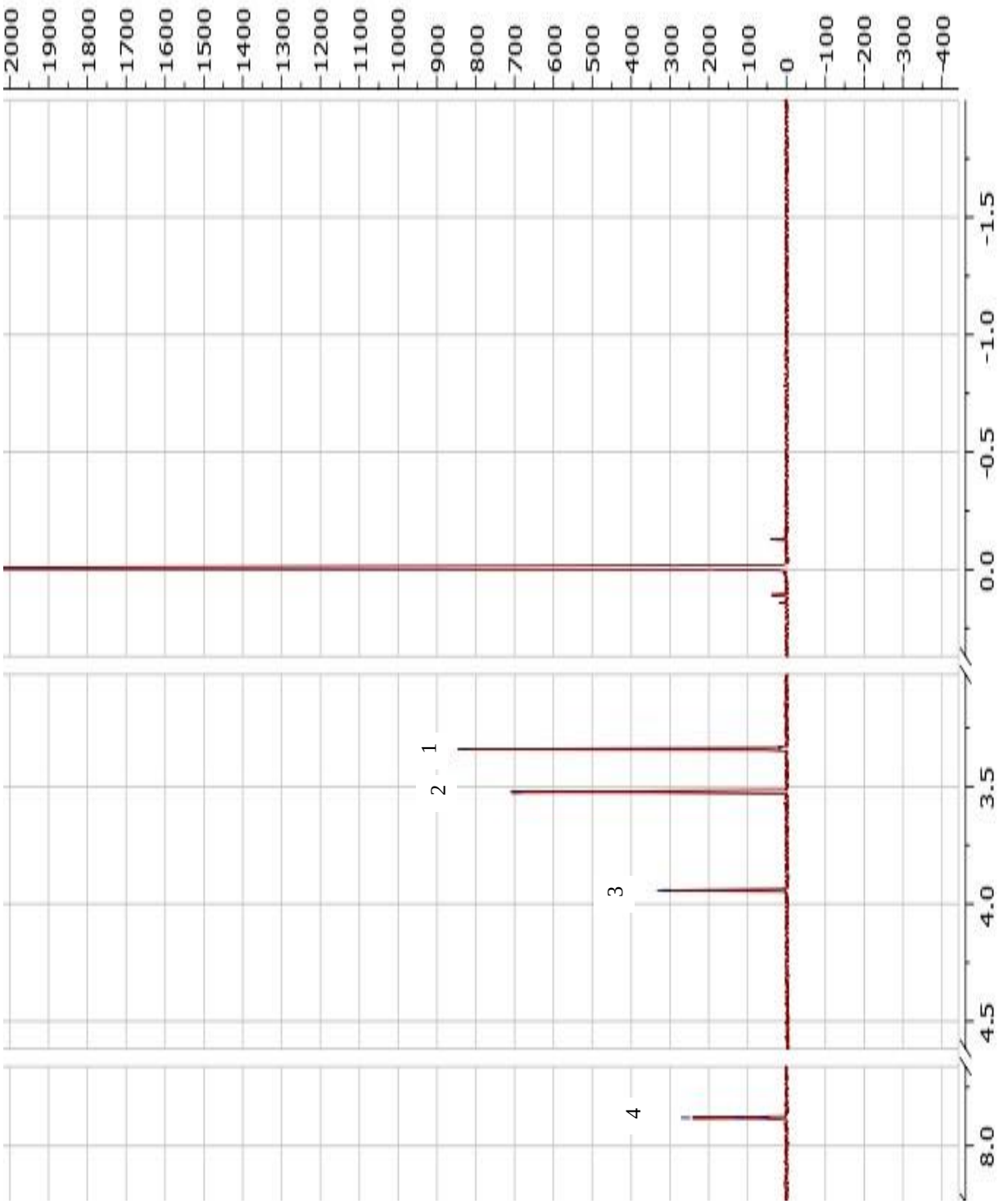

Figure 3.2 Caffeine proton NMR spectrum.

Table 3.1 Caffeine proton peak positions in parts per million (ppm) trial one.

Concentrations (mM)	Peak Positions (δ, ppm)			
	1	**2**	**3**	**4**
8.39 mM	3.3264	3.5003	3.9308	7.8832
4.16 mM	3.3374	3.5180	3.9424	7.8868
1.83 mM	3.3446	3.5263	3.9470	7.8881
0.60 mM	3.3420	3.5302	3.9489	7.8876
0.31 mM	3.3494	3.5317	3.9498	7.8881

Table 3.2 Caffeine proton peak positions in parts per million (ppm) trial two.

Concentrations (mM)	Peak Positions (δ, ppm)			
	1	**2**	**3**	**4**
8.39 mM	3.3337	3.5134	3.9395	7.8844
4.16 mM	3.3407	3.5216	3.9443	7.8865
1.83 mM	3.3374	3.5180	3.9424	7.8867
0.60 mM	3.3483	3.5304	3.9493	7.8883
0.31 mM	3.3500	3.5326	3.9502	7.8891

Table 3.3 Caffeine proton peak positions in parts per million (ppm) trial three.

Concentrations (mM)	Peak Positions (δ, ppm)			
	1	**2**	**3**	**4**
8.39 mM	3.3259	3.5045	3.9346	7.8840
4.16 mM	3.3405	3.5213	3.9439	7.8866
1.83 mM	3.3520	3.5337	3.9538	7.8942
0.60 mM	3.3420	3.5302	3.9489	7.8876
0.31 mM	3.3560	3.5383	3.9564	7.8947

Table 3.4 Average caffeine proton peak positions in parts per million (ppm) with plus or minus standard deviation.

Concentrations (mM)	Peak Positions (δ, ppm)			
	1	**2**	**3**	**4**
8.39 mM	3.3287±0.0044	3.5061±0.0067	3.9350±0.0044	7.8839±0.0006
4.16 mM	3.3395±0.0000	3.5203±0.0012	3.9435±0.0010	7.8866±0.0002
1.83 mM	3.3447±0.0073	3.5260±0.0079	3.9477±0.0057	7.8897±0.0040
0.60 mM	3.3441±0.0036	3.5303±0.0001	3.9490±0.0023	7.8878±0.0004
0.31 mM	3.3518±0.0037	3.5342±0.0036	3.9521±0.0037	7.8906±0.0036

Table 3.5 Change in average proton peak position for caffeine with plus or minus standard deviation.

Concentration (mM)	**Change in Peak Positions (Δδ, ppm)**			
	1	**2**	**3**	**4**
0.31 mM-8.39 mM	0.0280±0.0069	0.0320±0.0078	0.0020±0.0058	0.0100±0.0034
0.31 mM-4.16 mM	0.0140±0.0031	0.0160±0.0030	0.0010±0.0035	0.0050±0.0036
0.31 mM-1.85 mM	0.0070±0.0048	0.0080±0.0056	0.0020±0.0030	0.0030±0.0013
0.31 mM-0.60 mM	0.0030±0.0062	0.0030±0.0036	0.0040±0.0038	0.0020±0.0037

Caffeine has four proton peaks. The proton peaks for caffeine numbered one through three correspond to the methyl groups in the caffeine compound. Peak four corresponds to the aromatic proton on the five-membered ring. The location in the five-membered ring and the proximity to a nitrogen account for the downfield shift away from the three methyl proton peaks. Graph 3.1 corresponds to the proton peaks of caffeine with STDEV error bars. Table 3.5 shows the changes in proton peak positions (Δδ) with the STDEV between the change in proton peak position for caffeine trials one-three. The Δδ are the lowest concentration chemical shifts subtracted from the chemical shifts of the other concentrations. The non-aromatic proton peaks show a larger increase in ppm from the highest concentration of caffeine to the second-highest concentration of caffeine. The remaining concentrations have smaller changes in comparison and appear more linear in a graph. The aromatic protons show the same relationship. The largest change in ppm occurs between the two highest concentrations.

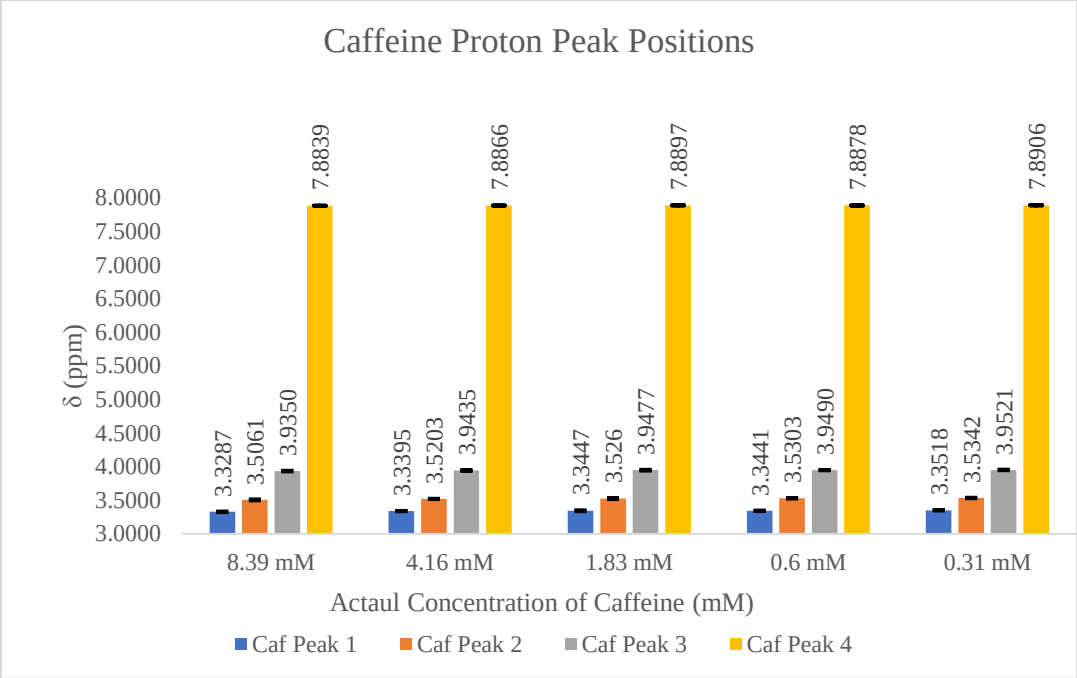

Graph 3.1 Average caffeine proton positions with STDEV error bars.

Graph 3.2 displays the changes in proton peak position between the lowest and highest concentrations as well as the changes between the lowest concentration peak positions and the peak positions of each of the other concentrations with STDEV error bars. The changes in the chemical shift in caffeine peak three have a different slope from the other caffeine peaks. Caffeine peak three is the closest proton to the water peak in solution. The water suppression performed on the NMR spectrum leads to a distortion in the proton closest to the water peak. Graph 3.2 indicates there is a correlation between the concentration of a solution and the chemical shift values of the proton peaks in the solution. As the concentration decreases, the chemical shift values for the concentrations increase.

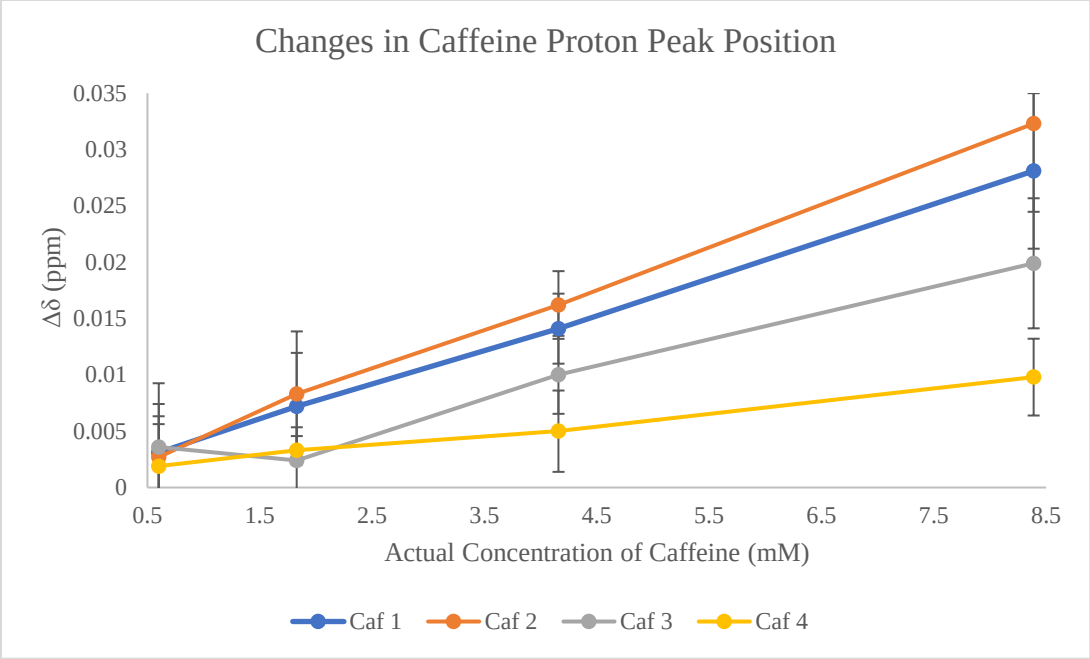

Graph 3.2 Changes in average caffeine proton peak positions with STDEV error bars.

3.1.2 K_a of Caffeine Standard Solutions

The K_a for the caffeine dilution series is determined using a modified version of the Rose-Drago equation and Solver function of Excel as outlined in Chapter 2. Table 3.6 outlines the y0 (minimum calculated position), y1 (maximum calculated position), K_a, and error calculated for caffeine using Solver. Table 3.7 reports the STDEV between the calculated data derived from Solver. Graphs 3.3-3.6 show the experimental K_a with STDEV for each proton in caffeine. The calculated K_a of caffeine is 1.01 mM^{-1}–3.61 mM^{-1}.

Table 3.6 Caffeine y0, y1, K_a, and error.

Peak Positions	y0	y1	K_a	error
1	3.34928	1.97885	1.8363	0.004961
2	3.53337	0.26856	1.0142	0.002600
3	3.95159	3.37519	3.6134	0.001804
4	7.88997	7.58934	2.5059	0.002199

Table 3.7 Standard deviation (STDEV) between the average calculated proton peak positions for caffeine and trials one-three.

Concentrations (mM)	**Peak Positions (δ, ppm)**			
	1	**2**	**3**	**4**
8.39 mM	0.00094	0.00278	0.00356	0.00273
4.16 mM	0.00033	0.00021	0.00250	0.00238
1.83 mM	0.00330	0.00283	0.00160	0.00024
0.60 mM	0.00417	0.00019	0.00068	0.00153
0.31 mM	0.00127	0.00297	0.00151	0.00045

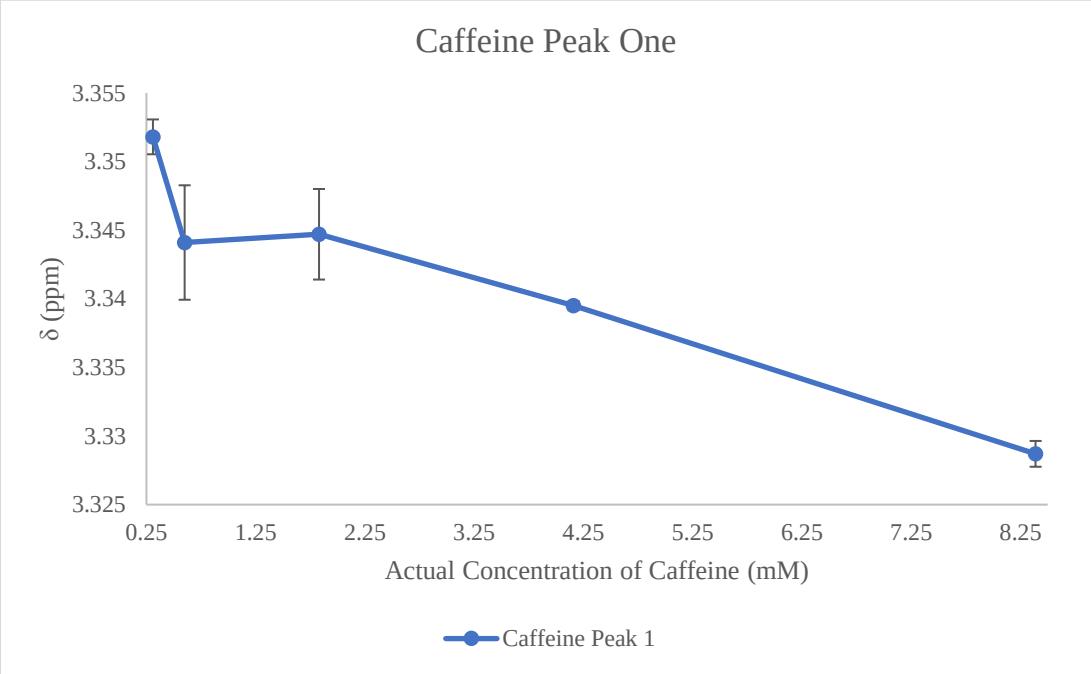

Graph 3.3 Average calculated proton peak positions for caffeine peak one with STDEV error bars. Refer to tables 3.1-3.4 for caffeine peak trials one-three and the average proton peak positions.

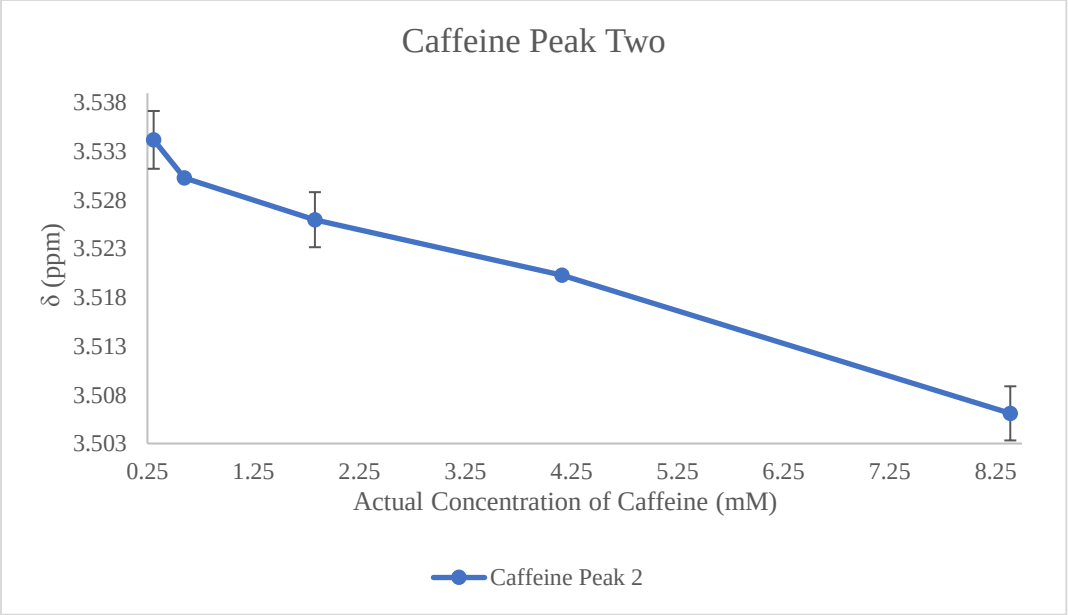

Graph 3.4 Average calculated proton peak positions for caffeine peak two with STDEV error bars. Refer to tables 3.1-3.4 for caffeine peak trials one-three and the average proton peak positions.

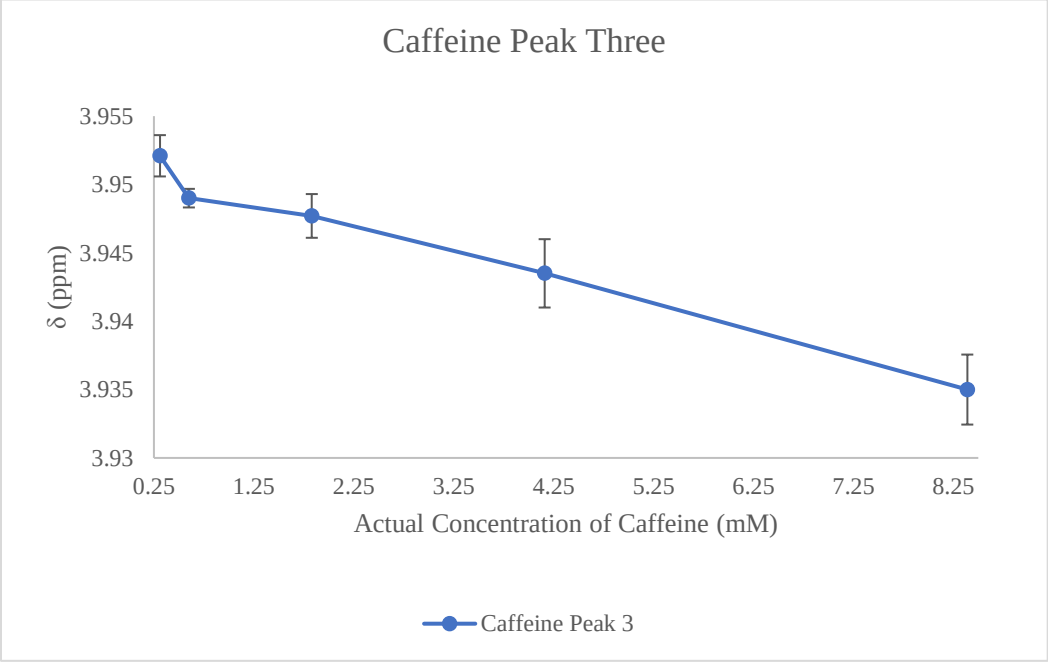

Graph 3.5 Average calculated proton peak positions for caffeine peak three with STDEV error bars. Refer to tables 3.1-3.4 for caffeine peak trials one-three and the average proton peak positions.

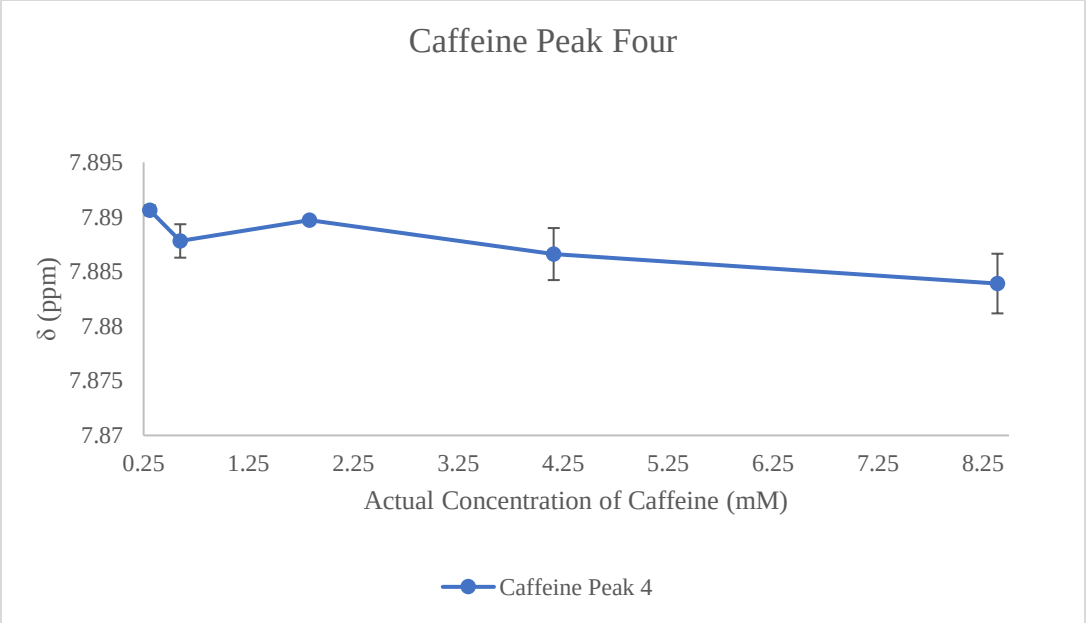

Graph 3.6 Average calculated proton peak positions for caffeine peak four with STDEV error bars. Refer to tables 3.1-3.4 for caffeine peak trials one-three and the average proton peak positions.

3.1.3 Diffusion Coefficients of Caffeine Standard Solutions

The diffusion coefficients (D) for each concentration of caffeine in the dilution series are determined using 3 mm NMR tubes. The 3 mm NMR tubes are used for DOSY because they reduce the effect of convection on the spectrum. Table 3.8 gives the diffusion coefficients for trials one-three, the average diffusion coefficients, and the standard deviation (STDEV) between the three trials for the determined concentrations from MestreNova of caffeine. Graph 3.7 shows the average diffusion coefficients for caffeine plotted against the concentrations with STDEV error bars. The diffusion coefficients are obtained with GNAT software. There is not a clear connection between the concentration and diffusion coefficients of caffeine. The molecular weight of caffeine is 194.19 g mol^{-1}. Using the SEGWE calculator and the molecular weight of caffeine, the predicted diffusion coefficient for caffeine is 5.44 x 10^{-10} m^2 s^{-1}. Table 3.11

shows the average aggregate weight from each concentration of caffeine predicted from the diffusion coefficient using SEGWE. The predicted aggregate weight and the molecular weight of caffeine is compared to determine the number of aggregates that are formed at each concentration of caffeine. The lower the diffusion coefficient, the higher the predicted aggregate weight and number of aggregates formed. When comparing the aggregate weights for the concentrations of caffeine, the highest number of aggregates forms at 1.83 mM and the lowest number of aggregates forms at 0.60 mM.

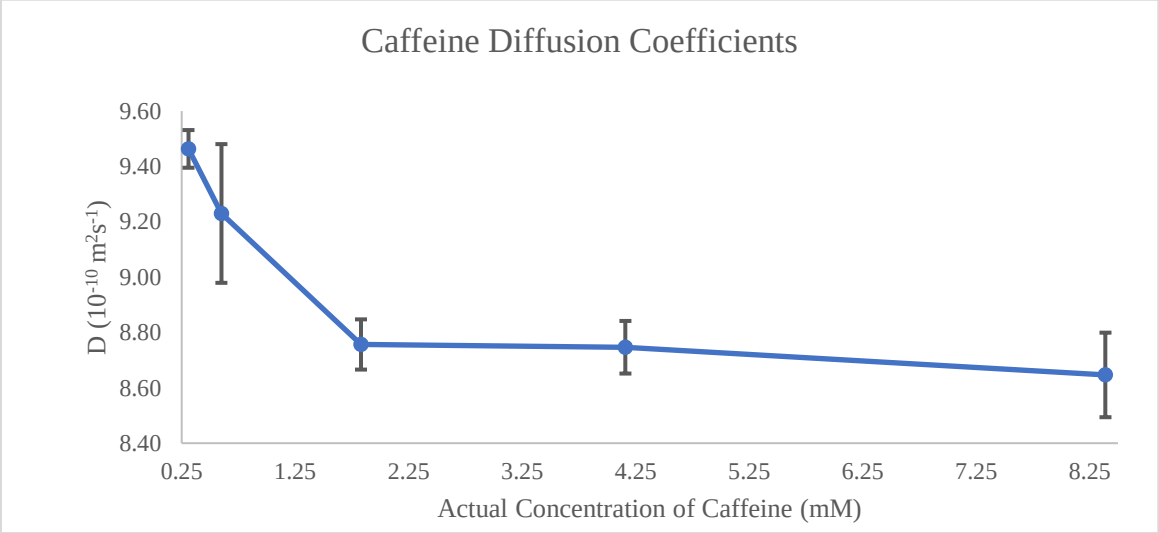

Graph 3.7 Average caffeine diffusion coefficients from 3 mm NMR tubes with STDEV error bars.

Table 3.8 Diffusion coefficients for caffeine in 10^{-10} m^2 s^{-1} from 3 mm NMR tubes, trials one-three, average diffusion coefficients, and STDEV.

Concentrations	**Diffusion Coefficients (10^{-10} m^2/s)**				
	Trial One	**Trial Two**	**Trial Three**	**Average**	**STDEV**
8.39 mM	8.48	8.78	8.68	8.65	0.15
4.16 mM	8.84	8.75	8.65	8.75	0.10
1.83 mM	8.69	8.86	8.72	8.76	0.09
0.60 mM	8.99	9.21	9.49	9.23	0.25
0.31 mM	9.54	9.41	9.44	9.46	0.07

Table 3.9 Average aggregate weight (g mol^{-1}) and number for caffeine from SEGWE.

Concentrations	Aggregate Weight (g mol^{-1})	Aggregate Number
8.39 mM	107.99	0.556
4.16 mM	105.37	0.543
1.83 mM	105.12	0.543
0.60 mM	94.10	0.485
0.31 mM	89.34	0.460

3.2 Daunorubicin Standards Analysis

The daunorubicin dilution series standards are studied individually to determine the changes in chemical shift values compared to changes in concentration. The chemical shifts for daunorubicin-caffeine mixtures are also analyzed. The diffusion coefficients for daunorubicin and daunorubicin-caffeine mixtures are determined using GNAT and SEGWE software.

3.2.1 Daunorubicin Proton Positions

The proton positions determined from proton/PRESAT NMR at 25°C with 5 mm NMR tubes are run in three trials and reported in Tables 3.10-3.12. The average proton peak positions are reported in Table 3.13 along with the STDEV between the trials. Table 3.14 reports the changes in average peak position for each of the concentrations of daunorubicin with the STDEV between the change in proton peak position for daunorubicin trials one-three. The changes in peak position are the lowest concentration chemical shift subtracted from the chemical shifts from each of the other concentrations. PRESAT is performed because of the high water content of the solvent solution system.

The peak assignments used for daunorubicin are shown in Figure 3.3 and are adapted from a study by Florczak, et al.[56] These peak assignments will continue to be used in this study. Figure 3.4 shows the proton spectrum for pure daunorubicin.

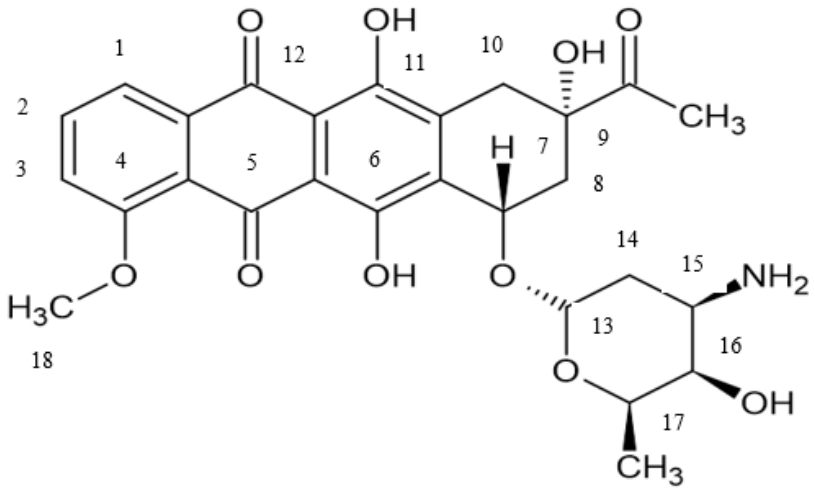

Figure 3.3 Daunorubicin chemical structure with proton assignments.

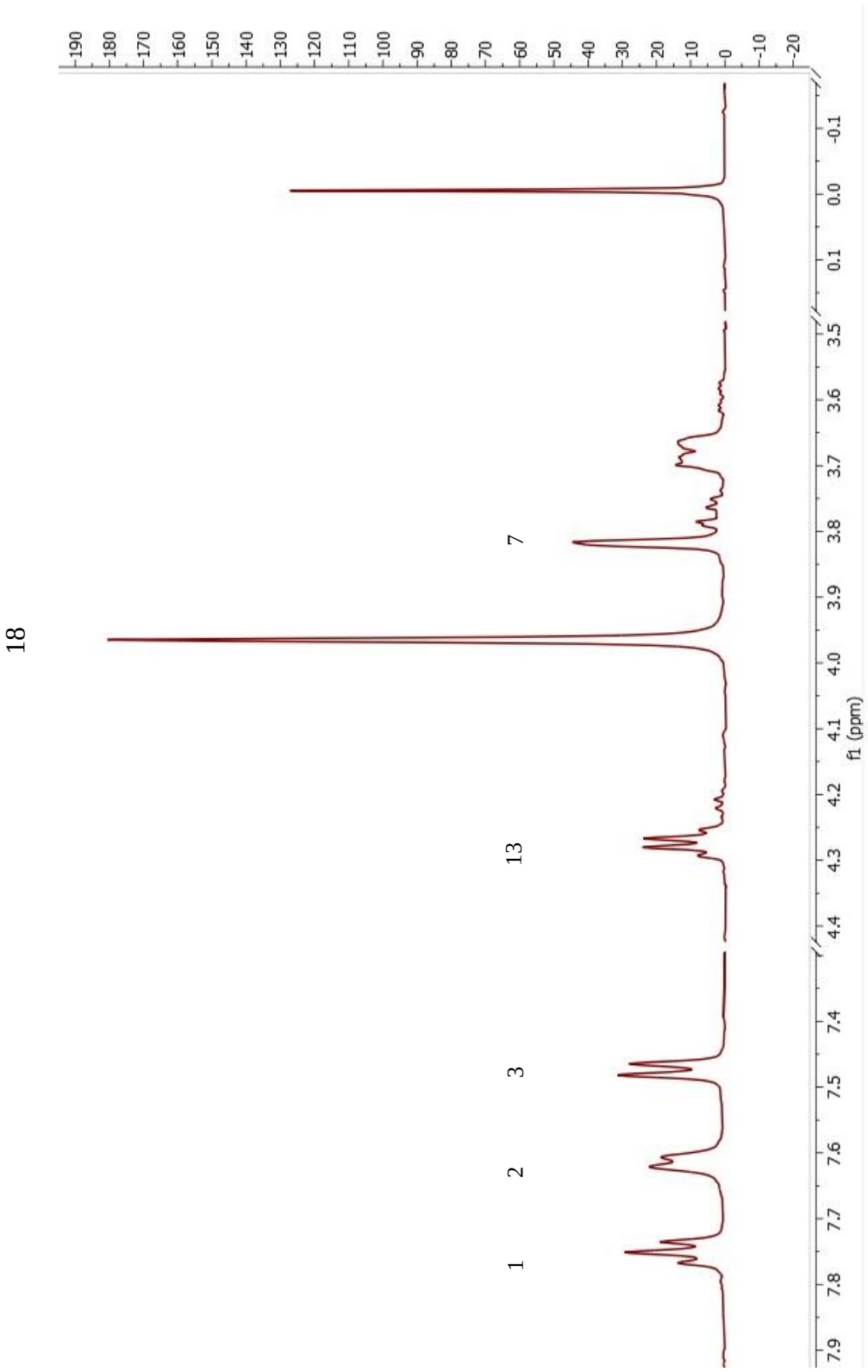

Figure 3.4 Daunorubicin proton NMR spectrum.

Table 3.10 Daunorubicin proton peak positions in parts per million (ppm) trial one.

Concentration (mM)	Peak Positions (δ, ppm)				
	1	**2**	**3**	**18**	**7**
1.95 mM	7.7513	7.4673	7.4731	4.2705	3.9769
1.43 mM	7.7789	7.5257	7.5139	4.2832	3.9980
0.49 mM	7.8100	7.5609	7.5608	4.2920	4.0216
0.20 mM	7.8299	7.5768	7.5767	4.2998	4.0328

Table 3.11 Daunorubicin proton peak positions in parts per million (ppm) trial two.

Concentration (mM)	Peak Positions (δ, ppm)				
	1	**2**	**3**	**18**	**7**
1.95 mM	7.7511	7.4675	7.4733	4.2704	3.9768
1.43 mM	7.7791	7.5255	7.5139	4.2834	3.9983
0.49 mM	7.8104	7.5608	7.5608	4.2921	4.0219
0.20 mM	7.8298	7.5769	7.5769	4.2994	4.0329

Table 3.12 Daunorubicin proton peak positions in parts per million (ppm) trial three.

Concentration (mM)	Peak Positions (δ, ppm)				
	1	**2**	**3**	**18**	**7**
1.95 mM	7.7512	7.4674	7.4732	4.2702	3.9769
1.43 mM	7.7790	7.5257	7.5138	4.2834	3.9982
0.49 mM	7.8104	7.5609	7.5610	4.2924	4.0218
0.20 mM	7.8230	7.5770	7.5770	4.2994	4.0329

Table 3.13 Average daunorubicin proton peak positions in parts per million (ppm) with STDEV.

Concentration (mM)	Peak Positions (δ, ppm)				
	1	**2**	**3**	**18**	**7**
1.95 mM	7.7512±0.0001	7.4674±0.0001	7.4732±0.0001	4.2704±0.0002	3.9769±0.0001
1.43 mM	7.7790±0.0001	7.5256±0.0001	7.5139±0.0001	4.2833±0.0001	3.9982±0.0000
0.49 mM	7.8103±0.0002	7.5609±0.0001	7.5609±0.0001	4.2922±0.0002	4.0218±0.0002
0.20 mM	7.8299±0.0001	7.5769±0.0001	7.5769±0.0002	4.2995±0.0002	4.0329±0.0001

Table 3.14 Change in average proton peak positions for daunorubicin with STDEV.

Concentration (mM)	Change in Peak Positions (Δδ, ppm)				
	1	**2**	**3**	**1 8**	**7**
0.20mM-1.95mM	0.0560±0.0010	0.0291±0.0002	0.1037±0.0001	0.1095±0.0002	0.0787±0.0010
0.20mM-1.4mM	0.0347±0.0002	0.0162±0.0001	0.0630±0.0002	0.0513±0.0004	0.0509±0.0010
0.20mM-0.49mM	0.0111±0.0003	0.0073±0.0010	0.0160±0.0002	0.0160±0.0004	0.0196±0.0010

Graph 3.8 shows the peak positions for daunorubicin with STDEV error bars. Unlike the caffeine non-aromatic proton peak positions, the proton peak positions for daunorubicin appear to have a more linear relationship. Graph 3.9 shows the changes in proton peak position between the lowest and highest concentrations as well as the changes between the lowest concentration's peak positions and the other concentration's peak positions with STDEV error bars. Graph 3.9 indicates there is a correlation between the concentration of a solution and the chemical shift values of the proton peaks in the solution.

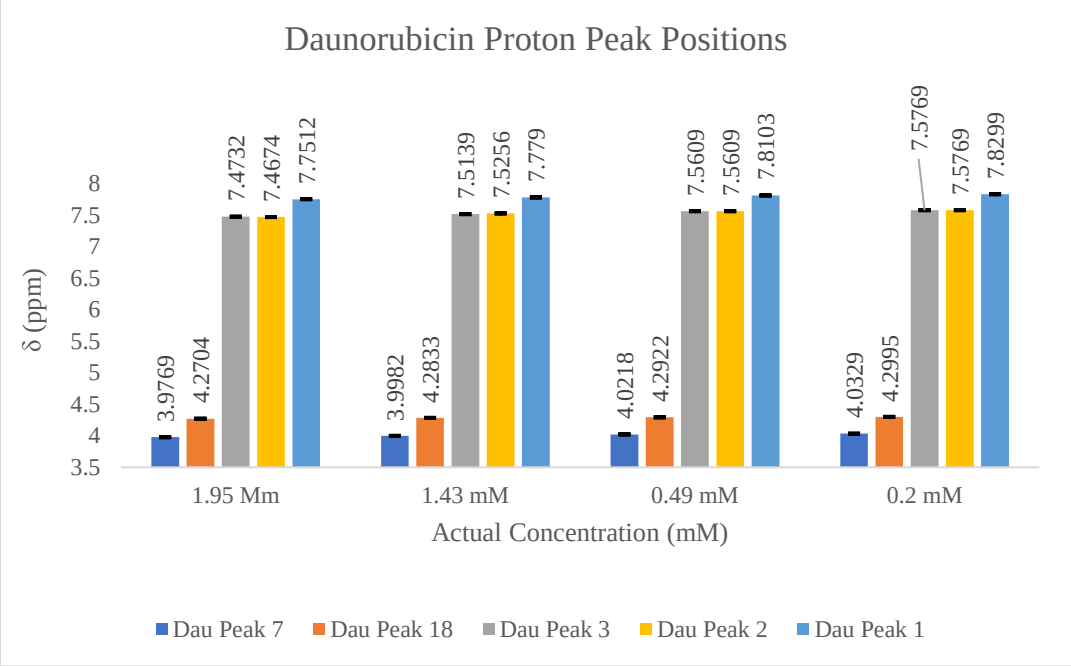

Graph 3.8 Average daunorubicin proton peak positions with STDEV error bars.

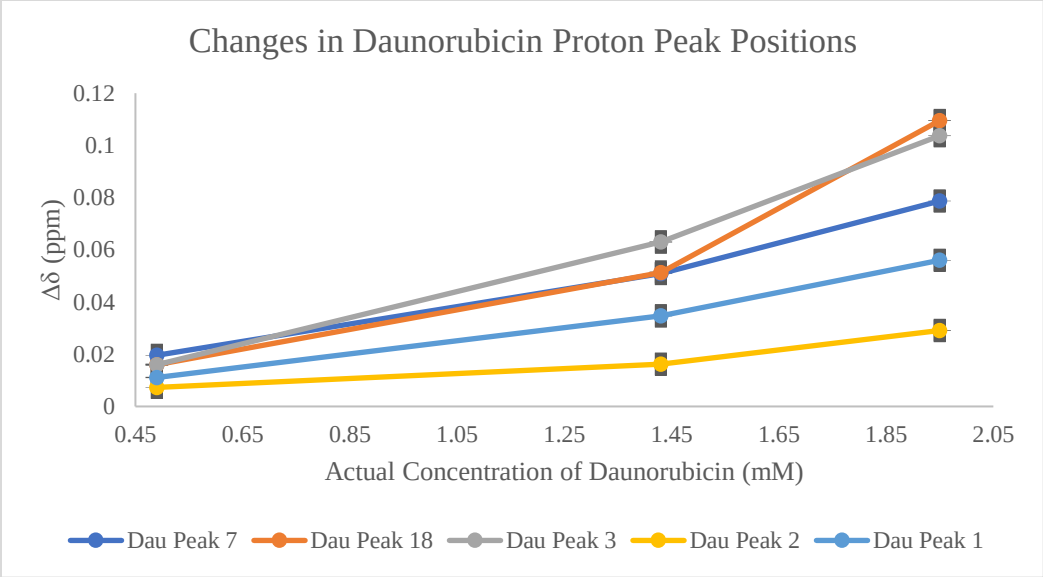

Graph 3.9 Changes in average daunorubicin peak positions with STDEV bars.

3.2.2 K_a of Daunorubicin Standard Solutions

The K_a for the daunorubicin dilution series is determined using the modified version of the Rose-Drago equation and the Solver function of Excel as outlined in Chapter 2. Table 3.15 outlines the y0, y1, K_a, and error calculated for caffeine using Solver. Table 3.16 reports the STDEV between the calculated data derived from Solver. Graphs 3.10-3.14 show the calculated K_a data with STDEV for each proton in daunorubicin. The calculated K_a range of daunorubicin is between 3.52 mM^{-1} and 16.81 mM^{-1}.

Table 3.15 Daunorubicin y0, y1, K_a, and error.

Peak Positions	y0	y1	K_a	error
7	4.0383	0.0000000	7.728391	0.004494
18	4.3015	0.0000000	3.524034	0.004328
3	7.5854	0.0000000	6.165277	0.007363
2	7.8712	0.0000000	16.80604	0.025427
1	7.8616	0.0000000	7.408965	0.010473

Table 3.16 Standard deviation (STDEV) between average experimental proton peak positions for daunorubicin and trials one-three.

Concentration (mM)	**Peak Positions (δ, ppm)**				
	7	**18**	**3**	**2**	**1**
1.95 mM	0.00219	0.00028	0.00537	0.00990	0.00290
1.43 mM	0.00580	0.00233	0.00396	0.01450	0.00587
0.49 mM	0.00127	0.00156	0.00064	0.00785	0.00007
0.20 mM	0.00205	0.00035	0.00219	0.00035	0.00127

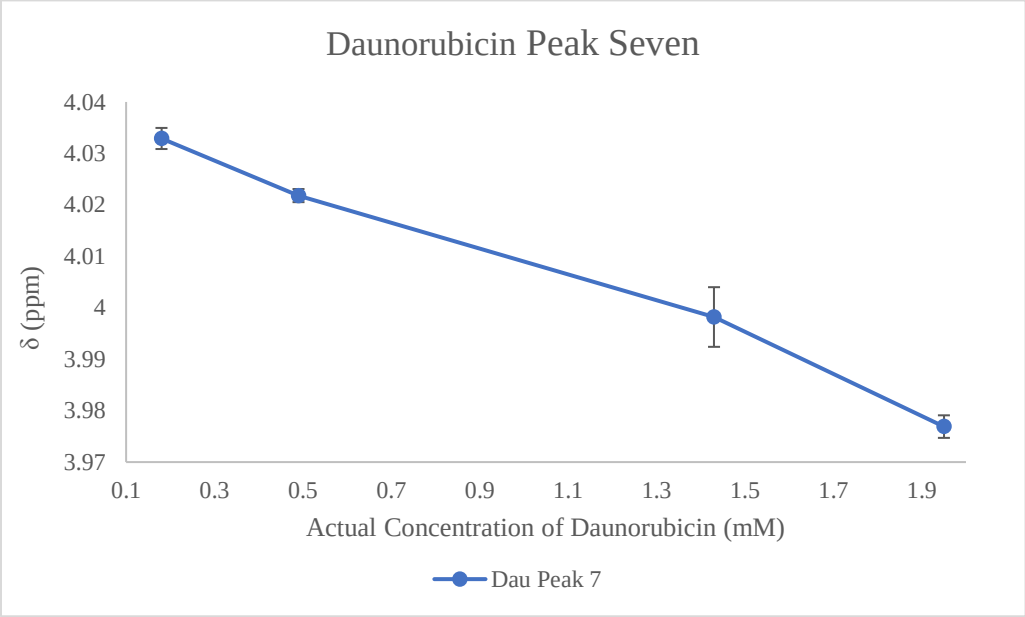

Graph 3.10 Average calculated proton peak positions for daunorubicin peak seven with STDEV error bars. Refer to tables 3.10-3.12 for daunorubicin peak trials one-three and the average proton peak positions.

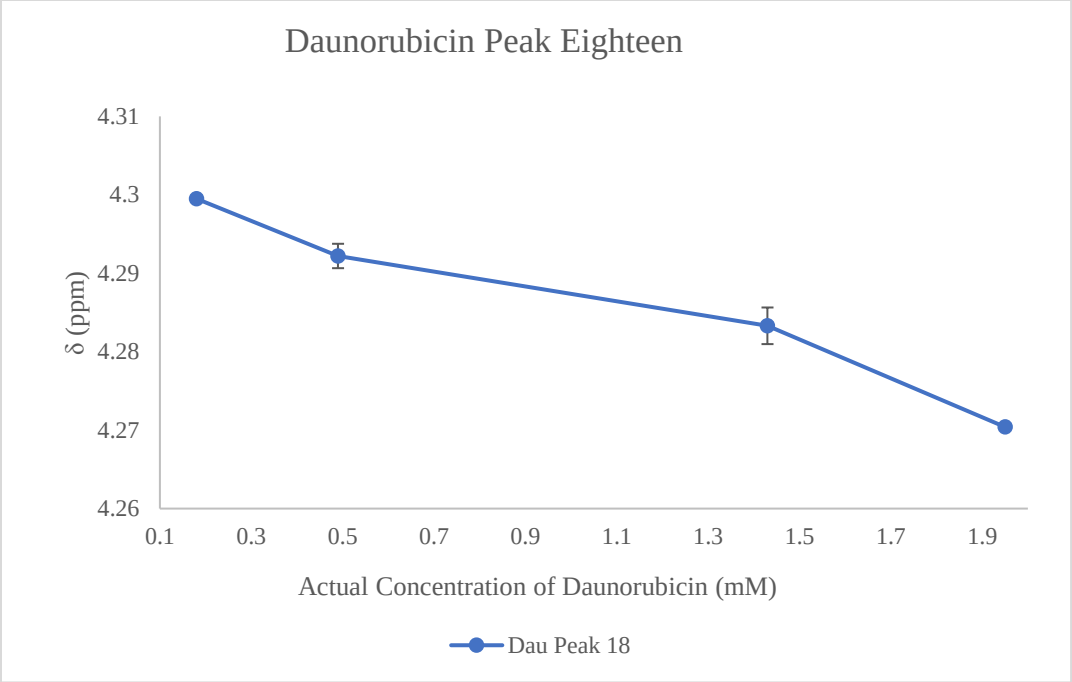

Graph 3.11 Average calculated proton peak positions for daunorubicin peak eighteen with STDEV error bars. Refer to tables 3.10-3.12 for daunorubicin peak trials one-three and the average proton peak positions.

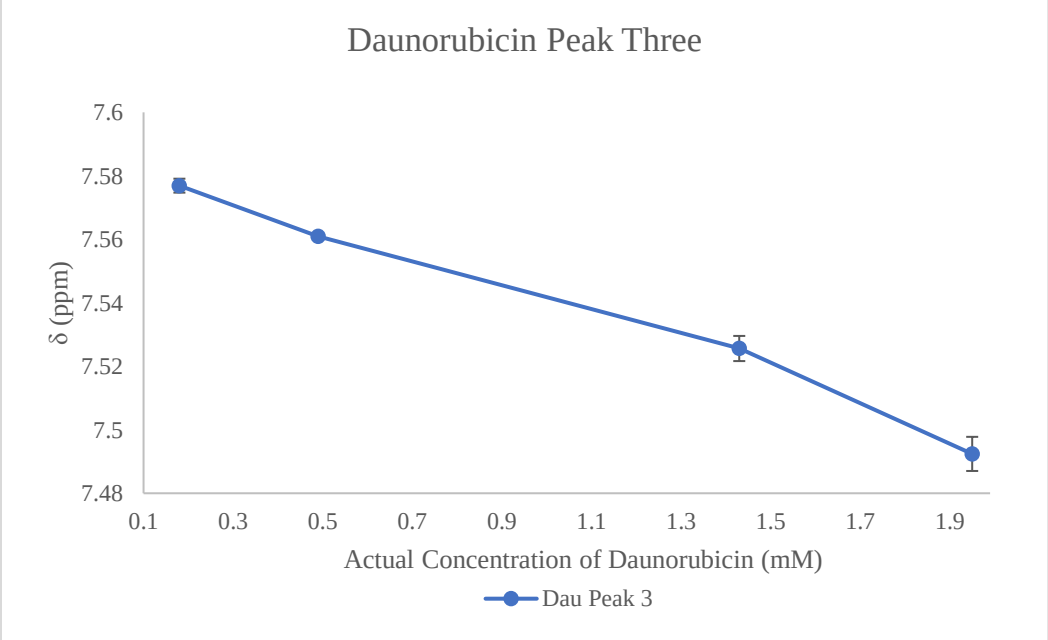

Graph 3.12 Average calculated proton peak positions for daunorubicin peak three with STDEV error bars. Refer to tables 3.10-3.12 for daunorubicin peak trials one-three and the average proton peak positions.

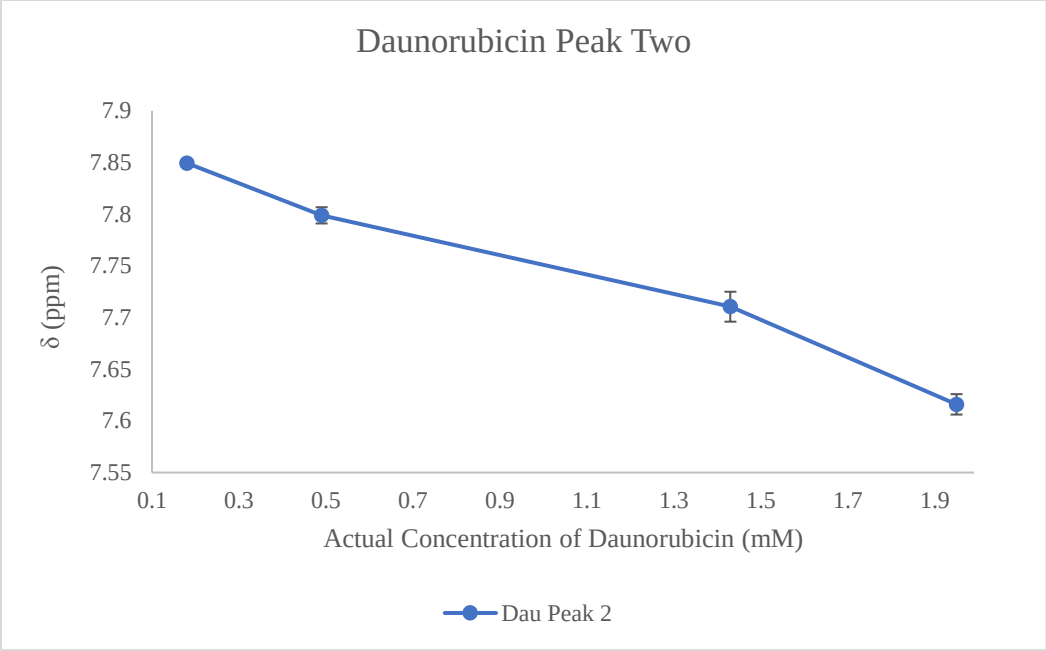

Graph 3.13 Average calculated proton peak positions for daunorubicin peak two with STDEV error bars. Refer to tables 3.10-3.12 for daunorubicin peak trials one-three and the average proton peak positions.

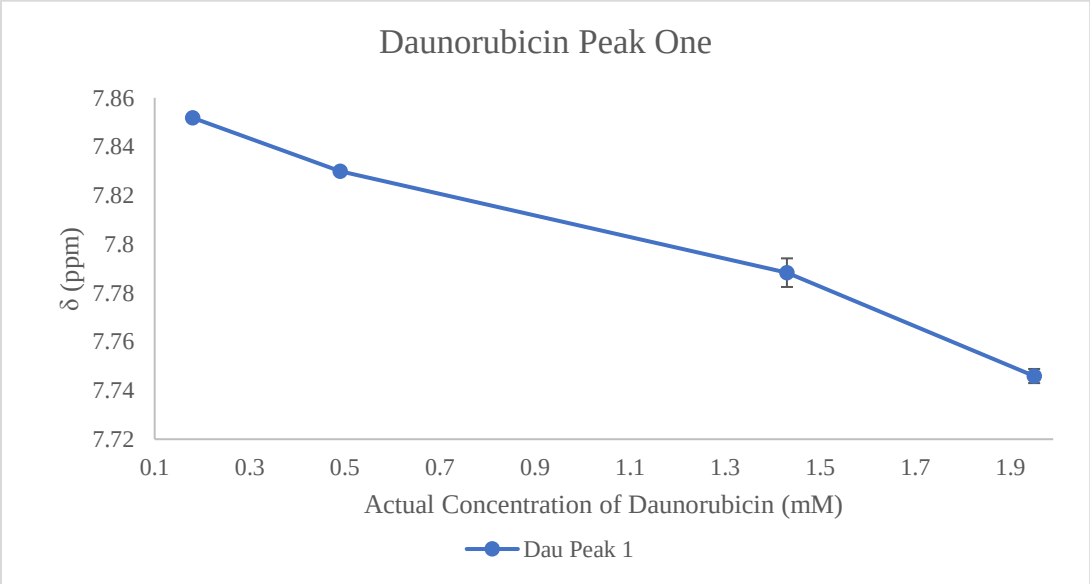

Graph 3.14 Average calculated proton peak positions for daunorubicin peak one with STDEV error bars. Refer to tables 3.10-3.12 for daunorubicin peak trials one-three and the average proton peak positions.

3.2.3 Diffusion Coefficients of Daunorubicin Standard Solutions

The diffusion coefficients for each concentration, determined from the dilution series, of daunorubicin in the dilution series are determined using 3 mm NMR tubes. The 3 mm NMR tubes are used for DOSY because they reduce the effect of convection on the spectrum. Table 3.17 outlines the diffusion coefficients for trials one-three, the average diffusion coefficients, and STDEV between the three trials for daunorubicin. Graph 3.15 illustrates the average diffusion coefficients for daunorubicin versus the concentration with STDEV error bars. The diffusion coefficients are obtained using the GNAT software. The diffusion coefficients appear to increase with decreasing concentrations apart from the diffusion coefficient between concentrations 0.49 mM and 0.20 mM. Between the 0.49 mM and 0.20 mM concentrations, there is a slight increase in the diffusion coefficients. The change in diffusion coefficients between 0.49 mM and 0.20 mM could be due to a mix-up in the solutions.

The molecular weight of daunorubicin is 564.0 g mol^{-1}. Using the SEGWE calculator and the molecular weight of daunorubicin, the predicted diffusion coefficient of daunorubicin is approximately 3.80 x 10^{-10} m^2 s^{-1}. Table 3.18 shows the aggregate weight from each concentration of daunorubicin predicted from the diffusion coefficients using SEGWE. The predicted aggregate weight and the molecular weight of daunorubicin are compared to determine the number of aggregates that are formed at each concentration of daunorubicin. The lower the diffusion coefficient, the higher the predicted aggregate weight and number of aggregates formed. When comparing the

aggregate weights for the actual concentrations of daunorubicin, the highest number of aggregates forms at 1.95 mM and the lowest number of aggregates forms at 0.20 mM.

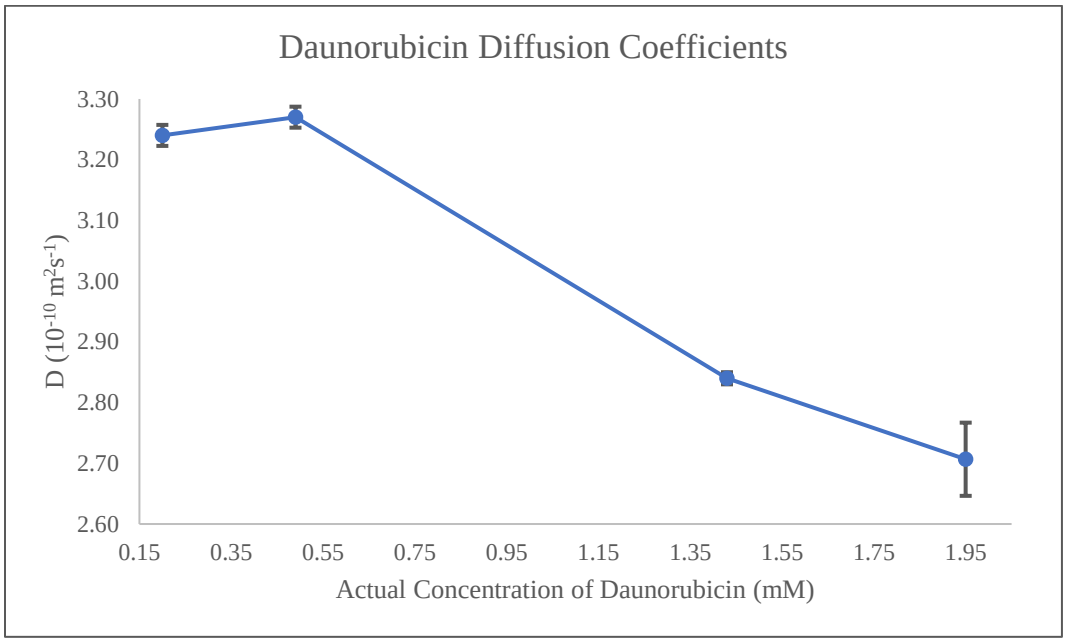

Graph 3.15 Average daunorubicin diffusion coefficients from 3 mm NMR tubes with STDEV error bars.

Table 3.17 Diffusion coefficients for daunorubicin in 10^{-10} m^2 s^{-1} in 3 mm NMR tubes.

Concentrations	**Diffusion Coefficients (10^{-10} m^2/s)**				
	Trial One	**Trial Two**	**Trial Three**	**Average**	**STDEV**
1.95 mM	2.70	2.65	2.77	2.71	0.06
1.43 mM	2.83	2.85	2.84	2.84	0.01
0.49 mM	3.28	3.28	3.25	3.47	0.02
0.20 mM	3.22	3.25	3.25	3.24	0.02

Table 3.18 Average aggregate Weight (g mol^{-1}) and number for dau from SEGWE.

Concentrations	**Aggregate Weight (g mol^{-1})**	**Aggregate Number**
1.95 mM	1679.58	2.98
1.43 mM	1488.30	2.64
0.49 mM	895.48	1.59
0.20 mM	1063.78	1.89

3.3 Irinotecan Standards Analysis

The irinotecan dilution series standards are studied individually to determine the changes in chemical shift values compared to changes in concentration. The proton spectra are run in triplicate using 5 mm NMR tubes. The chemical shifts for irinotecan-caffeine mixtures are also analyzed. The diffusion coefficients for both irinotecan and the irinotecan-caffeine mixtures are determined using GNAT and SEGWE software.

3.3.1 Irinotecan Proton Positions

The proton positions are determined from proton/PRESAT NMR at 25°C and reported in Tables 3.19-3.21. The average proton peak position is reported in Table 3.22 with STDEV between the three trials. The changes in proton peak positions between the lowest concentration and each of the other concentrations are shown in Table 3.23 along with the STDEV between the change in proton peak position for irinotecan trials one-three. The changes in proton peak position are the lowest concentration chemical shift subtracted from the chemical shifts from each of the other concentrations. The peak assignments for irinotecan are shown in Figure 3.5 and adapted from a study by Anbarasan, et al.[57] These peak assignments will continue to be used throughout this study. Figure 3.6 shows the proton NMR spectrum for pure irinotecan.

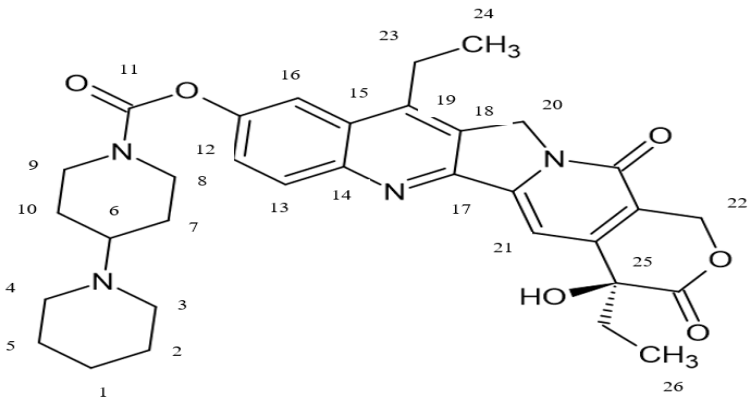

Figure 3.5 Irinotecan chemical structure with proton assignments.

Table 3.19 Irinotecan proton peak positions in parts per million (ppm) trial one.

Concentrations (mM)	**Peak Positions (δ, ppm)**				
	6	**9**	**11**	**15**	**12**
1.68 mM	3.5560	4.2610	7.2840	7.3930	7.7550
1.35 mM	3.5580	4.2690	7.3180	7.4240	7.7670
0.78 mM	3.5600	4.2800	7.4000	7.4280	7.8820
0.58 mM	3.5620	4.2860	7.4280	7.4880	7.8970

Table 3.20 Irinotecan proton peak positions in parts per million (ppm) trial two.

Concentrations (mM)	**Peak Positions (δ, ppm)**				
	6	**9**	**11**	**15**	**12**
1.68 mM	3.5563	4.2604	7.2839	7.3925	7.7547
1.35 mM	3.5581	4.2690	7.3183	7.4244	7.7674
0.78 mM	3.5597	4.2798	7.4000	7.4276	7.8822
0.58 mM	3.5623	4.2861	7.4277	7.4877	7.8966

Table 3.21 Irinotecan proton peak positions in parts per million (ppm) trial three.

Concentrations (mM)	**Peak Positions (δ, ppm)**				
	6	**9**	**11**	**15**	**12**
1.68 mM	3.5560	4.2610	7.2839	7.3928	7.7548
1.35 mM	3.5580	4.2690	7.3184	7.4243	7.7675
0.78 mM	3.5600	4.2800	7.4001	7.4277	7.8823
0.58 mM	3.5620	4.2860	7.4275	7.4878	7.8964

Table 3.22 Irinotecan average proton peak positions in parts per million (ppm).

Concentrations (mM)	Peak Positions (δ, ppm)				
	6	**9**	**11**	**15**	**12**
1.68 mM	3.5563±0.0001	4.2605±0.0001	7.2839±0.0001	7.3927±0.0002	7.7548±0.0001
1.35 mM	3.5581±0.0000	4.2691±0.0001	7.3183±0.0001	7.4243±0.0001	7.7674±0.0001
0.78 mM	3.5597±0.0001	4.2799±0.0000	7.4001±0.0001	7.4276±0.0001	7.8822±0.0002
0.58 mM	3.5623±0.0002	4.2860±0.0001	7.4276±0.0001	7.4877±0.0001	7.8964±0.0001

Table 3.23 Changes in average proton peak positions for irinotecan.

Concentrations (mM)	Changes in Peak Positions (Δδ, ppm)				
	6	**9**	**11**	**15**	**12**
0.58mM-1.68mM	0.0060±0.0001	0.0255±0.0002	0.1437±0.0001	0.0950±0.0001	0.1416±0.0073
0.58mM-1.35mM	0.0042±0.0000	0.0169±0.0002	0.1093±0.0002	0.0634±0.0001	0.1290±0.0002
0.58mM-0.78mM	0.0026±0.0003	0.0101±0.0001	0.0275±0.0002	0.0601±0.0002	0.0142±0.0002

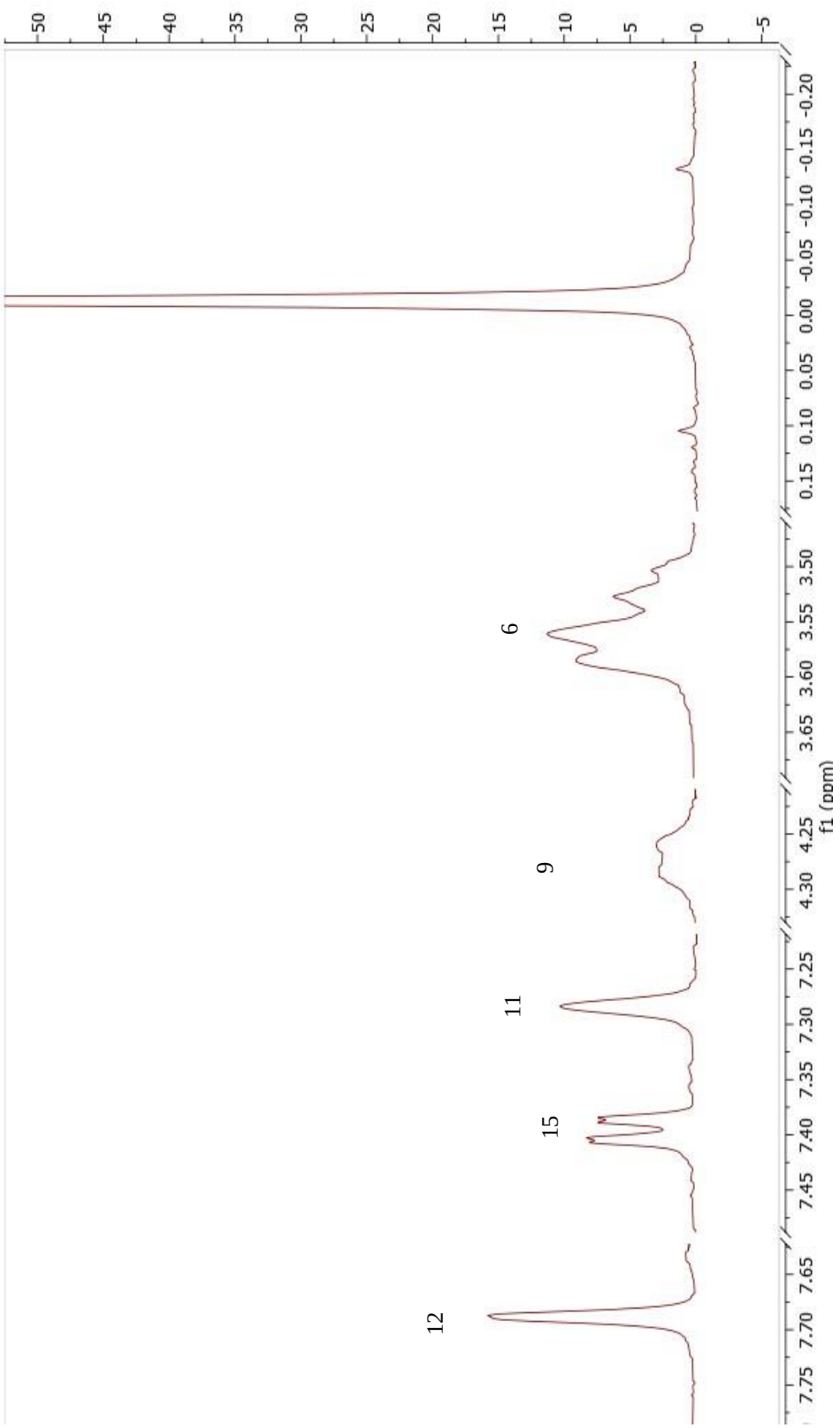

Figure 3.6 Irinotecan proton NMR spectrum.

Graph 3.16 shows the peak positions for irinotecan with STDEV error bars. Unlike the caffeine non-aromatic proton peak positions, the proton peak positions for irinotecan appear to have a linear relationship. Graph 3.17 shows the changes in proton peak position between the highest concentration and the lowest concentration as well as the proton peak positions of the lowest concentrations and the proton peak positions of each of the other concentrations with STDEV error bars. The changes in the peak position graph indicate there is a correlation between the concentration of the solution and the chemical shift values of the proton peaks. The graph does show the higher concentration, 1.68 mM, of irinotecan has smaller changes in peak positions as compared to the lowest concentration, 0.58 mM, of irinotecan. The smaller changes in peak positions in comparison to daunorubicin show irinotecan does not self-associate as easily as daunorubicin.

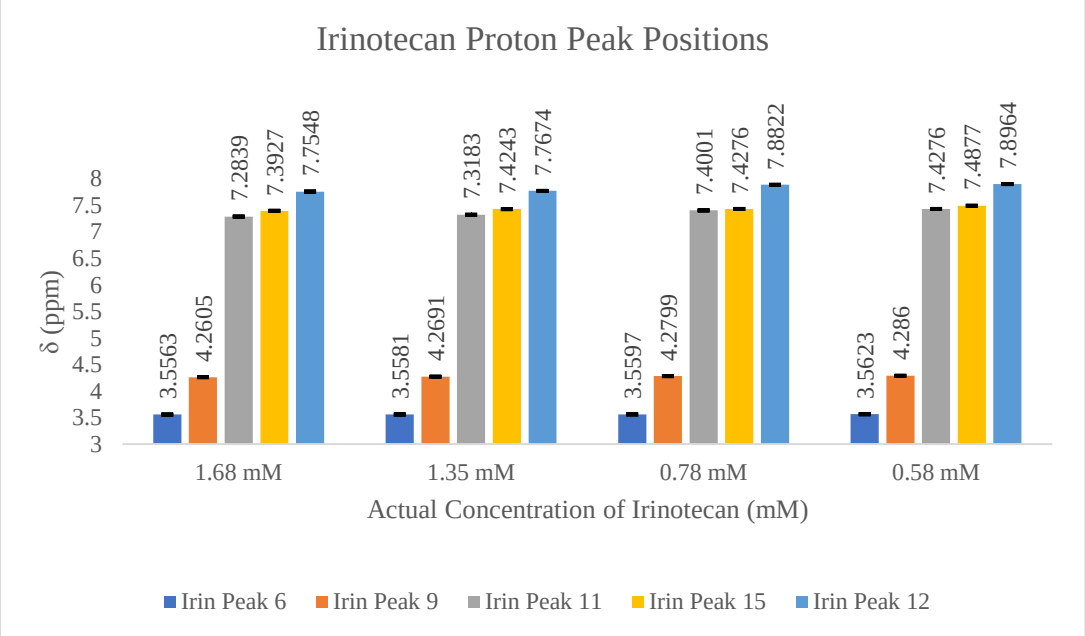

Graph 3.16 Irinotecan average proton peak positions with STDEV error bars.

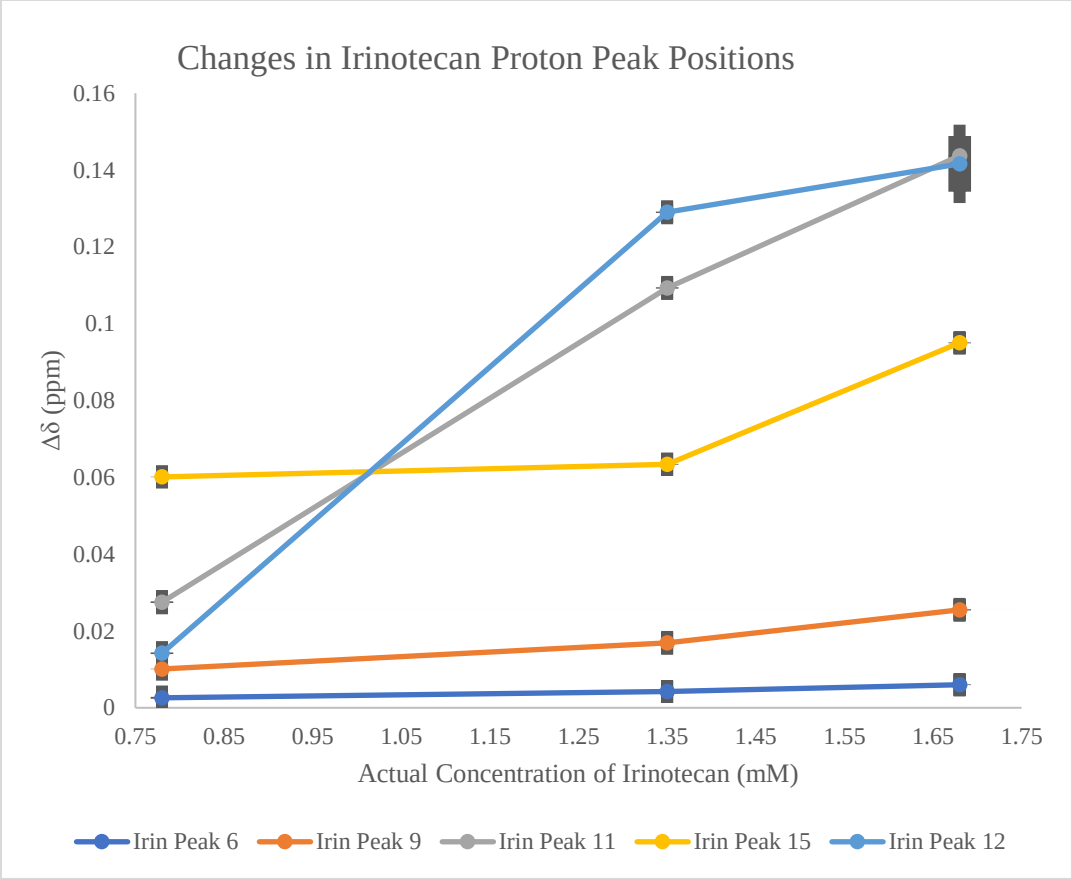

Graph 3.17 Changes in average peak position for irinotecan with STDEV error bars.

3.3.2 K_a of Irinotecan Standard Solutions

The K_a for the irinotecan dilution series is determined using the modified version of the Rose-Drago equation and the Solver function of Excel as outlined in Chapter 2. Table 3.24 outlines the y0, y1, K_a, and error calculated for irinotecan using Solver, while Table 3.25 reports the STDEV for calculated data points from SOLVER. Graphs 3.18-3.22 show the calculated K_a data with the STDEV for each proton of interest in irinotecan The calculated K_a range of irinotecan is between 1.49 mM^{-1} and 23.32 mM^{-1}.

Table 3.24 Irinotecan y0, y1, K_a, and error.

Peak Positions	y0	y1	K_a	error
6	3.5933	0.0000	5.0076	0.0168
9	4.2825	0.0000	1.4913	0.0086
11	7.5118	0.0000	15.673	0.0678
15	7.8212	0.0000	25.319	0.1655
12	7.9810	0.0000	19.677	0.0728

Table 3.25 Standard deviation (STDEV) between average calculated proton peak positions for irinotecan and trials one-three.

Concentrations (mM)	Peak Positions (δ, ppm)				
	6	9	11	15	12
1.68 mM	0.00566	0.00035	0.02150	0.07114	0.02567
1.35 mM	0.00219	0.00276	0.03521	0.08973	0.03932
0.78 mM	0.00545	0.00424	0.02291	0.00176	0.01966
0.58 mM	0.00714	0.00290	0.00679	0.01506	0.00474

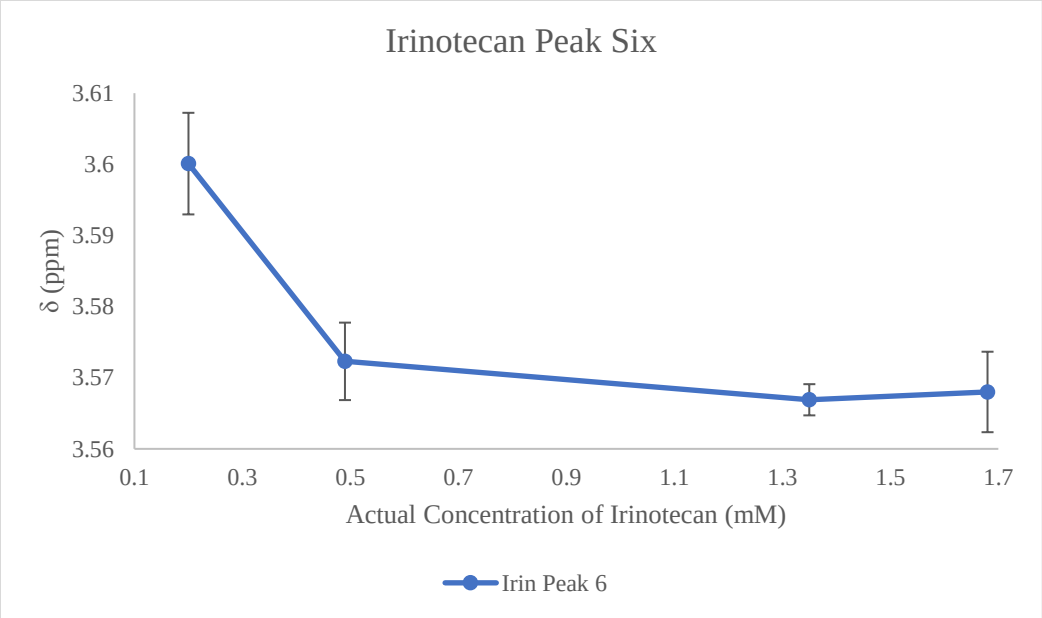

Graph 3.18 Average calculated proton peak positions for irinotecan peak six with STDEV error bars. Refer to tables 3.19-3.22 for irinotecan peak trials one-three and average proton peak positions.

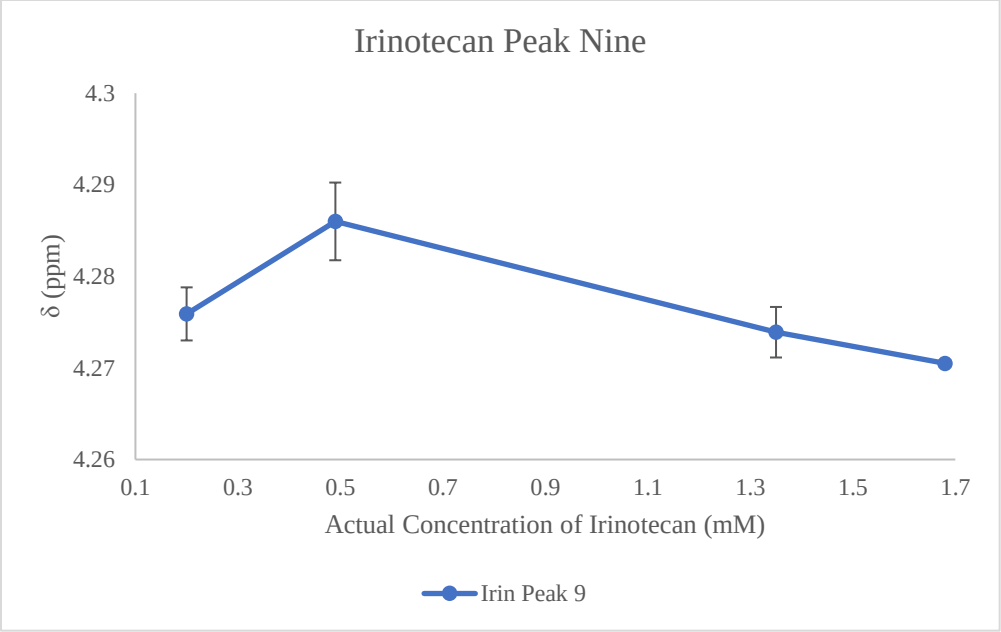

Graph 3.19 Average calculated proton peak positions for irinotecan peak nine with STDEV error bars. Refer to tables 3.19-3.22 for irinotecan peak trials one-three and average proton peak positions.

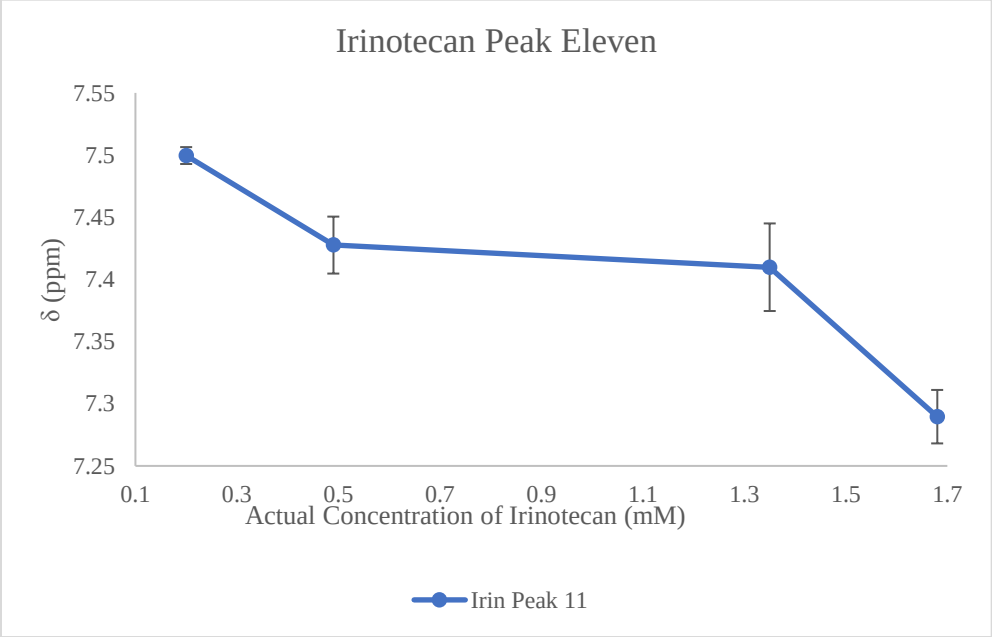

Graph 3.20 Average calculated proton peak positions for irinotecan peak eleven with STDEV error bars. Refer to tables 3.19-3.22 for irinotecan peak trials one-three and average proton peak positions.

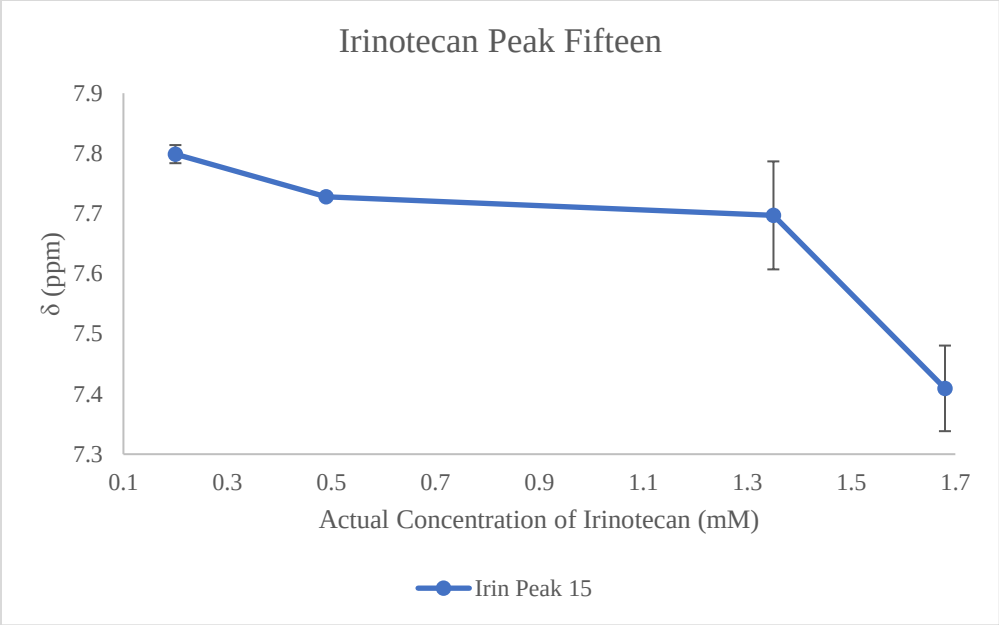

Graph 3.21 Average calculated proton peak positions for irinotecan peak fifteen with STDEV error bars. Refer to tables 3.19-3.22 for irinotecan peak trials one-three and average proton peak positions.

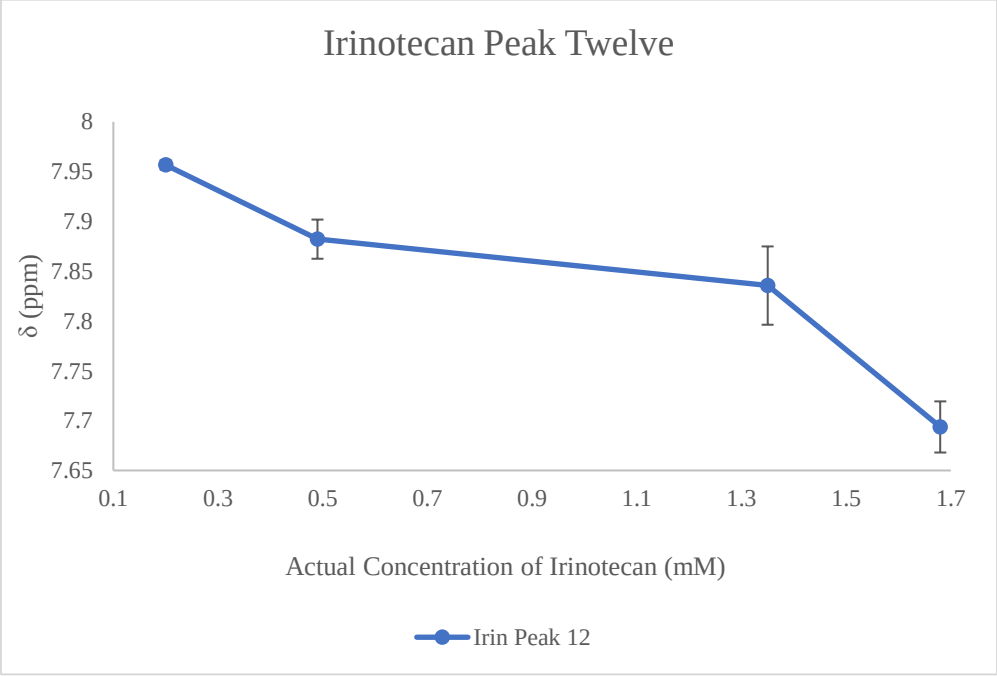

Graph 3.22 Average calculated proton peak positions for irinotecan peak twelve with STDEV error bars. Refer to tables 3.19-3.22 for irinotecan peak trials one-three and average proton peak positions.

3.3.3 Diffusion Coefficients of Irinotecan Standard Solutions

The diffusion coefficients for each concentration of irinotecan in the dilution series are determined using 3 mm NMR tubes. The 3 mm NMR tubes are used for DOSY because they reduce the effect of convection on the spectrum. Table 3.26 outlines the diffusion coefficients for trials one-three, the average diffusion coefficient, and STDEV between the three trials for irinotecan. Graph 3.23 shows the average diffusion coefficients for irinotecan versus the concentrations with STDEV error bars. The diffusion coefficients are obtained using the GNAT software. The diffusion coefficients appear to increase with decreasing concentration. The molecular weight of the drug irinotecan is 677.20 g mol^{-1}. Using the SEGWE calculator and the molecular weight of irinotecan, the predicted diffusion coefficient of irinotecan is 3.57×10^{-10} m^2 s^{-1}. Table 3.27 shows the aggregate weight from each concentration of irinotecan predicted from the diffusion coefficients using SEGWE. The predicted aggregate weight and the molecular weight of irinotecan are compared to determine the number of aggregates that are formed at each concentration of irinotecan. The lower the diffusion coefficient, the higher the predicted aggregate weight and number of aggregates formed. When comparing the aggregate weights for the concentrations of irinotecan, the highest number of aggregates forms at 1.35 mM and the lowest number of aggregates forms at 0.58 mM.

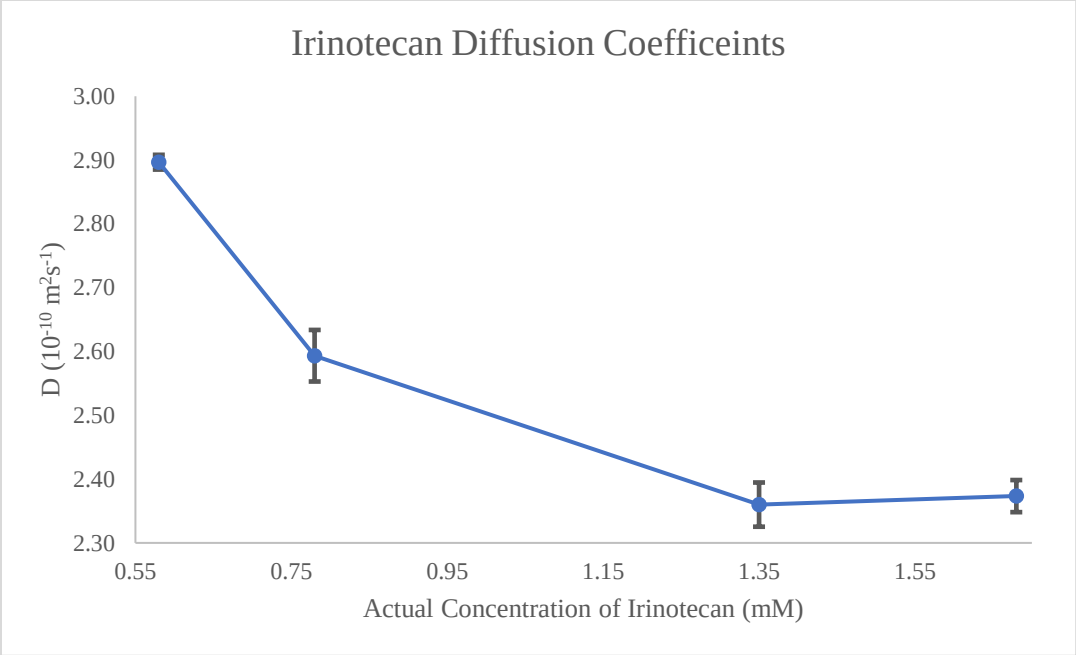

Graph 3.23 Average irinotecan diffusion coefficients from 3 mm NMR tubes with STDEV error bars.

Table 3.26 Diffusion coefficients for irinotecan in 10^{-10} m^2 s^{-1} from 3 mm NMR tubes for trials one-three, the average diffusion coefficients, and STDEV.

Concentrations	**Diffusion Coefficients (10^{-10} m^2/s)**				
	Trial One	**Trial Two**	**Trial Three**	**Average**	**STDEV**
1.68 mM	2.40	2.35	2.37	2.37	0.03
1.35 mM	2.40	2.34	2.34	2.36	0.03
0.78 mM	2.63	2.60	2.55	2.59	0.04
0.58 mM	2.89	2.89	2.91	2.90	0.01

Table 3.27 Average aggregate weight (g mol^{-1}) and number for irinotecan from SEGWE.

Concentrations	**Aggregate Weight (g mol^{-1})**	**Aggregate Number**
1.68 mM	2383.64	3.52
1.35 mM	2410.34	3.56
0.78 mM	1889.17	2.79
0.58 mM	1410.49	2.08

3.4 Caffeine and Anticancer Drug Mixtures

After analyzing caffeine, daunorubicin, and irinotecan individually, the two anticancer drugs are analyzed in a mixture with caffeine. The chemical shift data and the diffusion coefficients are determined for the mixtures. The mixtures are created with varying percentages of the caffeine and the anticancer drug in the solution mixture. While the percentages of the caffeine and anticancer drugs varied with each mixture, the overall concentration of the caffeine remains constant at 2.0 mM. GNAT software is used to analyze the chemical shift data, and GNAT and the SEGWE calculator are used to analyze the diffusion coefficient data.

3.4.1 Caffeine-Daunorubicin Mixtures Proton Positions

Four daunorubicin and caffeine mixtures are prepared. The concentrations of caffeine and daunorubicin remain constant for each of the daunorubicin and caffeine mixtures. The expected versus actual percentages and concentrations for daunorubicin and caffeine are reported in Table 3.28. The actual concentrations are determined using MestreNova.

Table 3.28 Expected versus actual percentages (percent %) and concentrations (Con. mM) for daunorubicin (dau) and caffeine (caf).

Expected Percent (%)	Actual Percent (%)	Expected Con. (mM)	Actual Con. (mM)
80 Dau / 20 Caf	95 Dau / 5 Caf	1.60 Dau / 0.40 Caf	2.89 Dau / 0.15 Caf
60 Dau / 40 Caf	70 Dau / 30 Caf	1.20 Dau / 0.80 Caf	1.76 Dau / 0.75 Caf
40 Dau / 60 Caf	35 Dau / 65 Caf	0.80 Dau / 1.20 Caf	0.88 Dau / 1.62 Caf
20 Dau / 80 Caf	10 Dau / 90 Caf	0.40 Dau / 1.60 Caf	0.25 Dau / 2.20 Caf

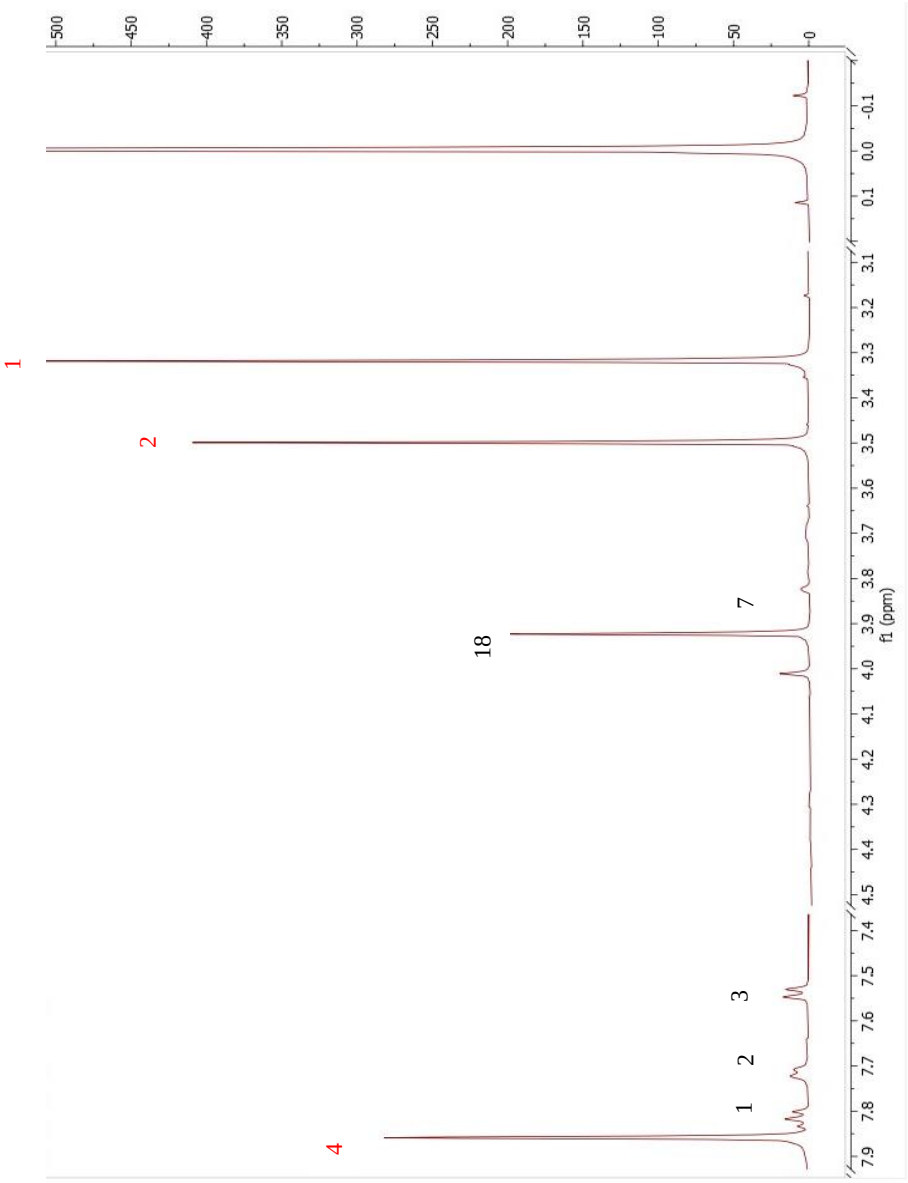

Figure 3.7 Daunorubicin-caffeine mixture proton NMR spectrum (black daunorubicin and red caffeine).

Figure 3.7 shows the proton NMR spectrum for the daunorubicin-caffeine mixture. The proton spectra are run in triplicate with 5 mm NMR tubes. Tables 3.29-3.31 show the peak positions for daunorubicin and the aromatic proton of caffeine in the

daunorubicin-caffeine mixture. Table 3.32 shows the average proton peak positions with STDEV for the three trials. Table 3.33 also shows the changes in average peak position between the lowest and highest concentrations of daunorubicin in the daunorubicin-caffeine mixtures with the STDEV between the change in proton peak position for daunorubicin in the daunorubicin-caffeine mixture in trials one-three. The changes are determined by subtracting the lowest chemical shift concentration from each of the other chemical shift concentrations. Peaks seven and thirteen represent the non-aromatic protons of daunorubicin, while peaks one, two, and three represent the aromatic protons of daunorubicin. Peak four is the aromatic proton of caffeine.

Table 3.29 Daunorubicin-caffeine proton peak positions in parts per million (ppm) trial one. Caffeine peak highlighted in red.

Concentrations of Dau (%)	**Proton Peaks (δ, ppm)**					
	7	**18**	**3**	**2**	**1**	**4**
95% Dau	3.2400	3.9230	7.4430	7.5270	7.7219	7.8090
70% Dau	3.2642	3.9450	7.4775	7.5540	7.7560	7.8068
35% Dau	3.2954	3.9700	7.5080	7.6513	7.8173	7.8350
10% Dau	3.3185	3.9910	7.5386	7.6640	7.8370	7.8393

Table 3.30 Daunorubicin-caffeine proton peak positions in parts per million (ppm) trial two. Caffeine peak highlighted in red.

Concentrations of Dau (%)	**Proton Peaks (δ, ppm)**					
	7	**18**	**3**	**2**	**1**	**4**
95% Dau	3.2402	3.9228	7.4440	7.5260	7.7218	7.8080
70% Dau	3.2641	3.9453	7.4773	7.5520	7.7558	7.8068
35% Dau	3.2954	3.9693	7.5090	7.6515	7.8175	7.8370
10% Dau	3.3186	3.9911	7.5386	7.6610	7.8340	7.8391

Table 3.31 Daunorubicin-caffeine proton peak positions in parts per million (ppm) trial three. Caffeine peak highlighted in red.

Concentrations of Dau (%)	Proton Peaks (δ, ppm)					
	7	**18**	**3**	**2**	**1**	**4**
95% Dau	3.2401	3.9229	7.4435	7.5270	7.7219	7.8080
70% Dau	3.2640	3.9453	7.4774	7.5530	7.7559	7.8069
35% Dau	3.2955	3.9694	7.5080	7.6514	7.8174	7.8360
10% Dau	3.3185	3.9913	7.5387	7.6620	7.8360	7.8392

Table 3.32 Average daunorubicin-caffeine proton peak positions in parts per million (ppm) with STDEV. Caffeine peak highlighted in red.

Concentrations of Dau (%)	Proton Peaks (δ, ppm)					
	7	**18**	**3**	**2**	**1**	**4**
95% Dau	3.2401±0.0001	3.9229±0.0001	7.4440±0.0005	7.5270±0.0006	7.7219±0.0006	7.8080±0.0006
70% Dau	3.2641±0.0000	3.9453±0.0001	7.4774±0.0001	7.5530±0.0010	7.7559±0.0001	7.8068±0.0006
35% Dau	3.2953±0.0001	3.9694±0.0001	7.5080±0.0006	7.6514±0.0001	7.8174±0.0001	7.8360±0.0010
10% Dau	3.3185±0.0001	3.9912±0.0001	7.5386±0.0006	7.6620±0.0015	7.8360±0.0015	7.8392±0.0001

Table 3.33 Average changes in proton peak position for daunorubicin in dau-caf mixtures with STDEV. Caffeine peak highlighted in red.

Concentrations of Dau (%)	Proton Peaks (Δδ, ppm)					
	7	**18**	**3**	**2**	**1**	**4**
10%-95%	0.0784±0.0001	0.0683±0.0002	0.0946±0.0005	0.1350±0.0012	0.1141±0.0015	0.0312±0.0005
10%-70%	0.0544±0.0000	0.0459±0.0002	0.0612±0.0001	0.1090±0.0006	0.0801±0.0014	0.0324±0.0001
10%-35%	0.0232±0.0001	0.0218±0.0002	0.0306±0.0006	0.0106±0.0016	0.0186±0.0016	0.0032±0.0011

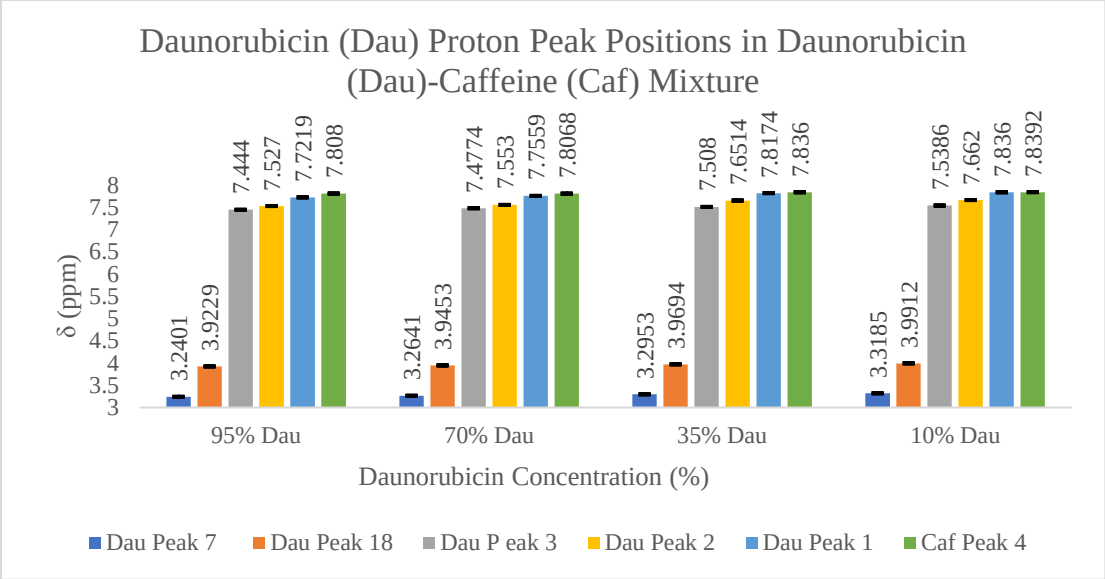

Graph 3.24 Daunorubicin-caffeine proton peak positions with STDEV error bars

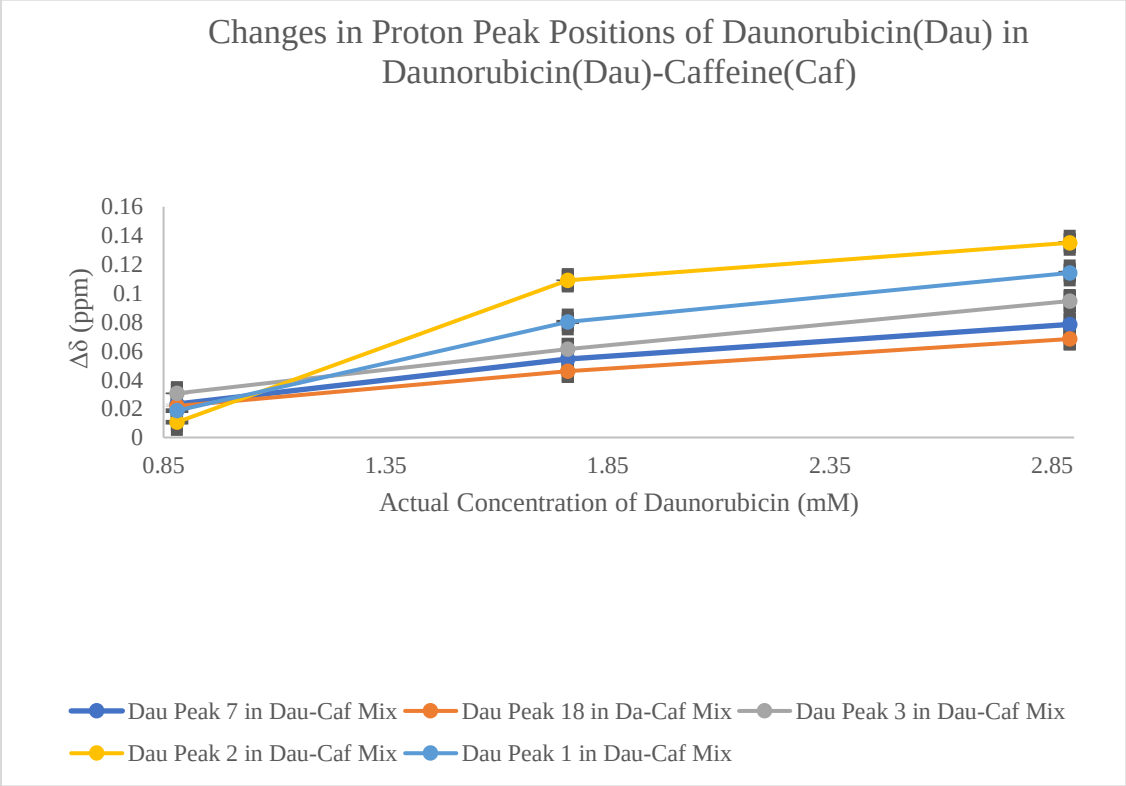

Graph 3.25 Changes in peak position of dau peaks in dau-caf STDEV error bars.

In Graph 3.24, the daunorubicin peak chemical shift values are compared to the different concentrations of the mixtures of daunorubicin-caffeine, pure 1.95 mM daunorubicin, and pure 8.39 mM caffeine. The aromatic protons in daunorubicin and caffeine increase with decreasing amounts of daunorubicin. Graph 3.25 shows the changes in proton peak position between the lowest chemical shift value concentration of daunorubicin and the lowest chemical shift value concentration of daunorubicin as well as the proton peak positions between the lowest concentration and each of the other concentrations. The changes in Graph 3.25 indicate there is a correlation between the concentration and the chemical shift values of the proton peaks.

3.4.2 K_a of Caffeine-Daunorubicin Mixtures

The K_a for the caffeine-daunorubicin mixture is determined using the modified version of the Rose-Drago equation and Solver function of Excel as outlined in Chapter 2. Table 3.34 outlines the y0, y1, K_a, and error calculated for the caffeine-daunorubicin mixture, while Table 3.35 reports the STDEV between the calculated daunorubicin proton peak positions in the daunorubicin-caffeine mixture. Graphs 3.26-3.30 show the calculated K_a data with STDEV for each proton of interest. The calculated K_a of the caffeine-daunorubicin mixture is between 20.45 mM^{-1} and 67.55 mM^{-1}.

Table 3.34 Daunorubicin-caffeine y0, y1, K_a, and error.

Peak Positions	y0	y1	K_a	error
7	3.3185	1.8229	20.4549	0.0227
18	3.9912	2.8675	23.9753	0.8629
3	7.5386	6.7301	50.4713	0.0382
2	7.6908	6.4983	67.5549	0.0961
1	7.8549	6.6152	47.7940	0.0806

Table 3.35 Standard deviation (STDEV) between average calculated proton peak positions for daunorubicin in the daunorubicin-caffeine mix and trials one-three.

Concentrations of Dau (%)	Proton Peaks (δ, ppm)				
	7	**18**	**3**	**2**	**1**
95% Dau	0.00000	0.03536	0.00212	0.03182	0.04243
70% Dau	0.01414	0.09405	0.01768	0.01061	0.02121
35% Dau	0.00212	0.00141	0.00636	0.01980	0.01626
10% Dau	0.00919	0.05798	0.01697	0.05445	0.03041

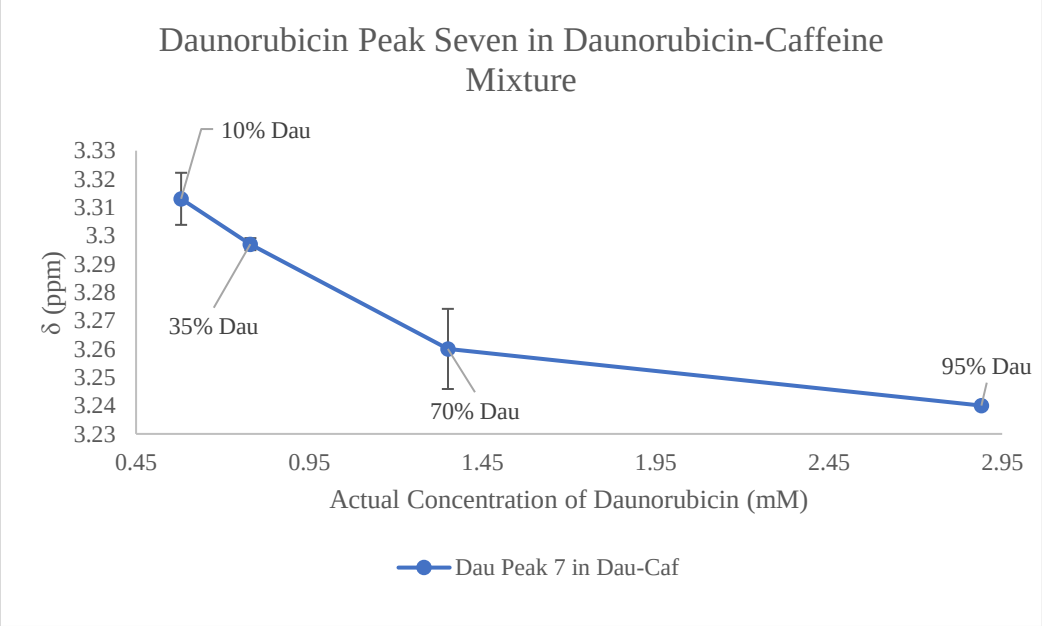

Graph 3.26 Average calculated proton peak positions for daunorubicin peak seven in the daunorubicin-caffeine mix with STDEV error bars. Refer to tables 3.29-3.32 for daunorubicin peak trials one-three and the average proton peak positions.

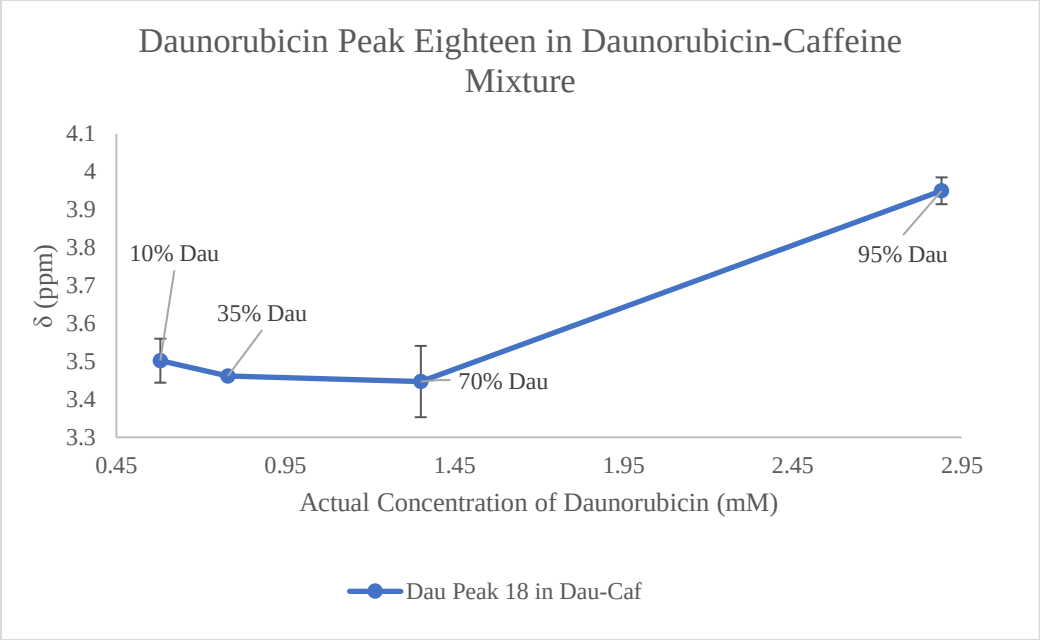

Graph 3.27 Average calculated proton peak positions for daunorubicin peak eighteen in the daunorubicin-caffeine mix with STDEV error bars. Refer to tables 3.29-3.32 for daunorubicin peak trials one-three and the average proton peak positions.

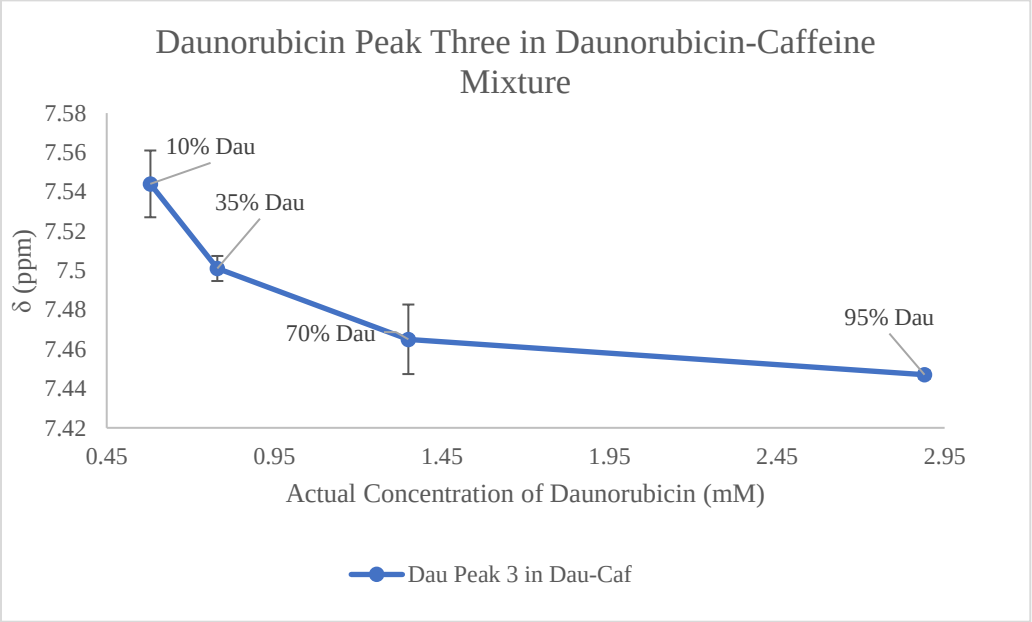

Graph 3.28 Average calculated proton peak positions for daunorubicin peak three in the daunorubicin-caffeine mix with STDEV error bars. Refer to tables 3.29-3.32 for daunorubicin peak trials one-three and the average proton peak positions.

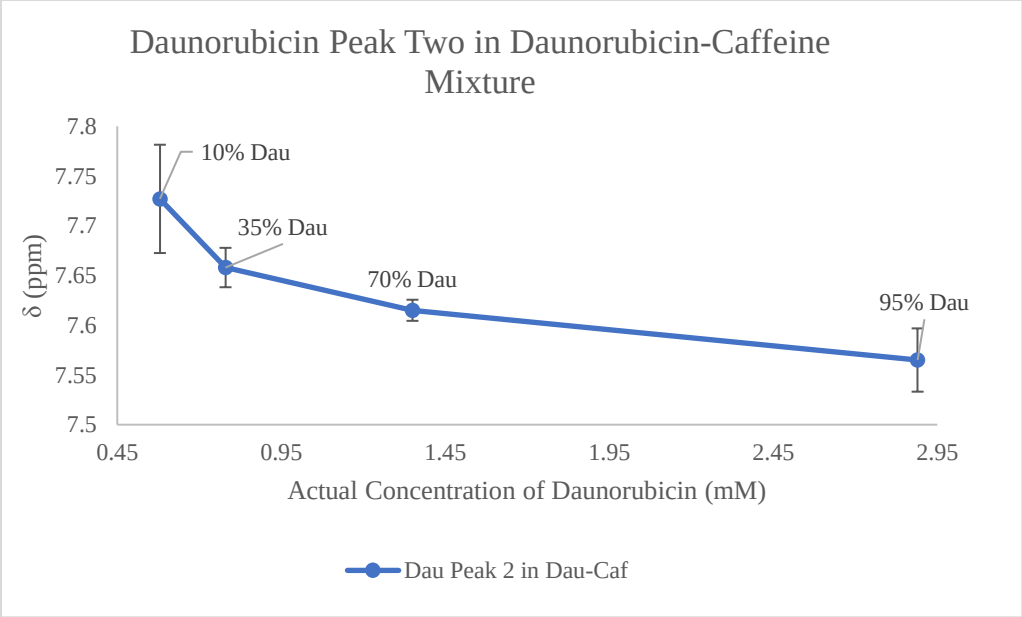

Graph 3.29 Average calculated proton peak positions for daunorubicin peak two in the daunorubicin-caffeine mix with STDEV error bars. Refer to tables 3.29-3.32 for daunorubicin peak trials one-three and the average proton peak positions.

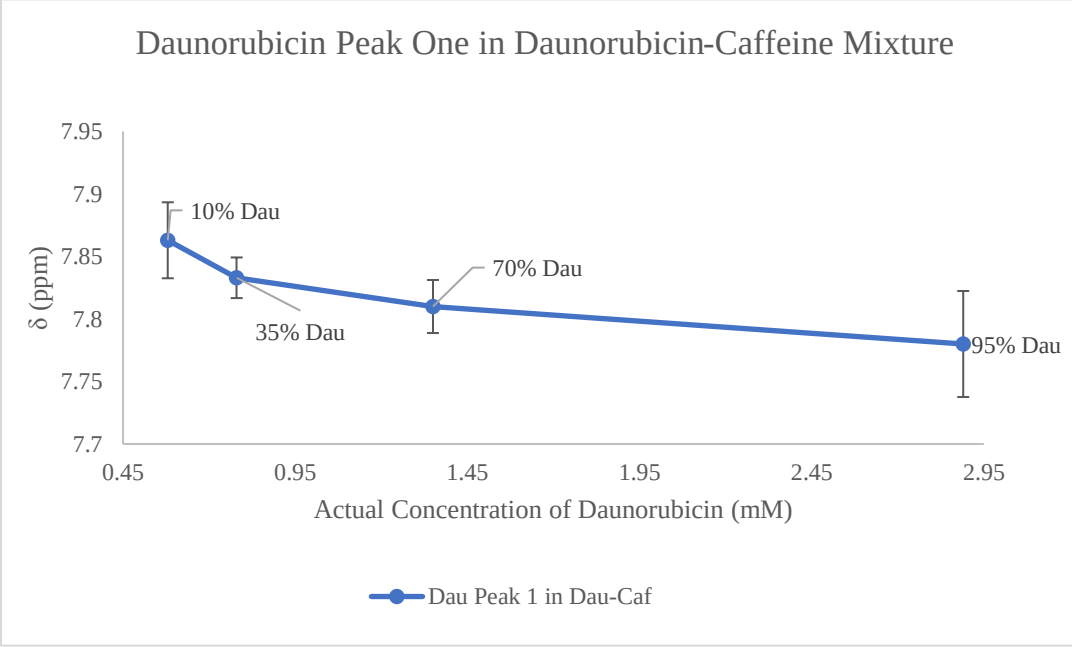

Graph 3.30 Average experimental proton peak positions for daunorubicin peak one in the daunorubicin-caffeine mix with STDEV error bars. Refer to tables 3.29-3.32 for daunorubicin peak trials one-three and the average proton peak positions.

3.4.3 Caffeine-Daunorubicin Mixtures Diffusion Coefficients

The diffusion coefficients for daunorubicin in each of the daunorubicin-caffeine mixtures are determined using 3 mm NMR tubes. The 3 mm NMR tubes are used for DOSY because they reduce the effect of convection on the spectrum. Table 3.36 outlines the diffusion coefficient information for daunorubicin in the daunorubicin-caffeine mixture for trials one-three, the average diffusion coefficient, and the STDEV between trials one-three. Graph 3.31 shows the average diffusion coefficients for daunorubicin in the daunorubicin-caffeine mixture plotted versus the concentration of daunorubicin in the daunorubicin-caffeine mixture with STDEV error bars. The diffusion coefficients are obtained using the GNAT software. The diffusion coefficients appear to increase with decreasing concentrations of daunorubicin and increasing concentrations of caffeine. The combined molecular weight of daunorubicin and caffeine is 758.19 g mol^{-1}. Table 3.37 shows the aggregate weight from each concentration of daunorubicin in the daunorubicin-caffeine mixture predicted from the diffusion coefficients using SEGWE. The predicted aggregate weight and the molecular weight of daunorubicin and caffeine are compared to determine the number of aggregates that are formed at each concentration of the daunorubicin and caffeine mixture. The lower the diffusion coefficient, the higher the predicted aggregate weight and number of aggregates formed. When comparing the aggregate weights for daunorubicin concentrations of the caffeine and daunorubicin mixtures, the highest number of aggregates formed at 95% daunorubicin and 5% caffeine and the lowest number of aggregates formed at 10% daunorubicin and 90% caffeine.

Table 3.37 outlines the diffusion coefficient information for caffeine in the daunorubicin-caffeine mixture for trials one-three, the average diffusion coefficient, and the STDEV between trials one-three. Graph 3.32 shows the average diffusion coefficients for caffeine in the daunorubicin-caffeine mixture plotted versus the concentration of daunorubicin in the daunorubicin-caffeine mixture with STDEV error bars. The diffusion coefficients are obtained using the GNAT software. The diffusion coefficients appear to decrease with increasing concentrations of caffeine and decreasing concentrations of daunorubicin. Table 3.38 shows the aggregate weight from each concentration of caffeine in the daunorubicin-caffeine mixture predicted from the diffusion coefficients using SEGWE. When comparing the aggregate weights for caffeine concentrations of the caffeine and daunorubicin mixtures, the highest number of aggregates formed at 90% caffeine and 10% daunorubicin, and the lowest number of aggregates formed at 5% caffeine and 95% daunorubicin.

Table 3.36 Diffusion coefficients for daunorubicin in dau-caf mixtures in 10^{-10} m^2 s^{-1} from 3mm NMR tubes for trials one-three, the average diffusion coefficient, and STDEV.

Concentrations	**Diffusion Coefficients (10^{-10} m^2/s)**				
	Trial One	**Trial Two**	**Trial Three**	**Average**	**STDEV**
95% Dau	2.51	2.53	2.47	2.50	0.03
70% Dau	2.95	2.93	2.90	2.93	0.03
35% Dau	4.40	4.48	4.52	4.47	0.06
10% Dau	8.15	8.15	8.09	8.13	0.03

Table 3.37 Average aggregate weight (g mol^{-1}) and number for dau in dau-caf mix from SEGWE.

Concentrations	**Aggregate Weight (g mol^{-1})**	**Aggregate Number**
95% Dau	2071.88	2.73
70% Dau	1373.77	1.81
35% Dau	481.67	0.64
10% Dau	123.36	0.16

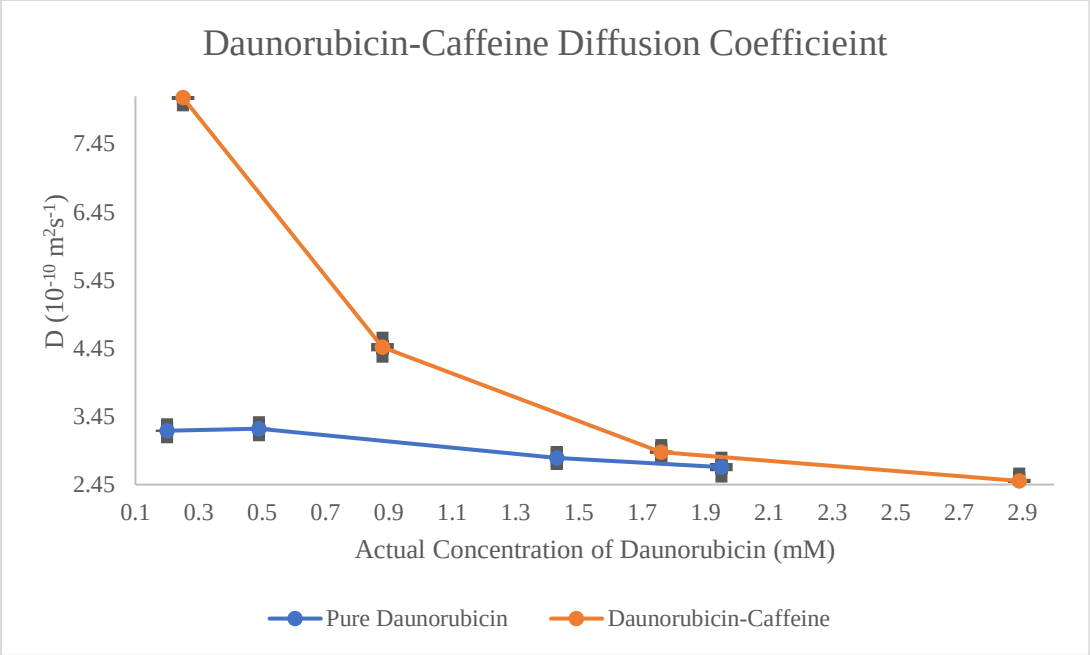

Graph 3.31 Average daunorubicin diffusion coefficients in daunorubicin-caffeine mixture from 3 mm NMR tubes with STDEV error bars versus pure daunorubicin diffusion coefficients.

Table 3.38 Diffusion coefficients for caffeine in dau-caf mixtures in 10^{-10} m^2 s^{-1} from 3 mm NMR tubes for trials one-three, the average diffusion coefficient, and STDEV.

Concentrations	**Diffusion Coefficients (10^{-10} m^2/s)**				
	Trial One	**Trial Two**	**Trial Three**	**Average**	**STDEV**
5% Caf	9.09	9.12	9.15	9.12	0.03
30% Caf	4.17	4.17	4.16	4.17	0.01
65% Caf	3.47	3.40	3.45	3.44	0.04
90% Caf	3.06	3.05	3.10	3.07	0.03

Table 3.39 Average aggregate weight (g mol^{-1}) and number for caf in dau-caf mix from SEGWE.

Concentrations	**Aggregate Weight (g mol^{-1})**	**Aggregate Number**
5% Caf	96.51	0.13
30% Caf	569.55	0.75
65% Caf	915.13	1.21
90% Caf	1219.47	1.61

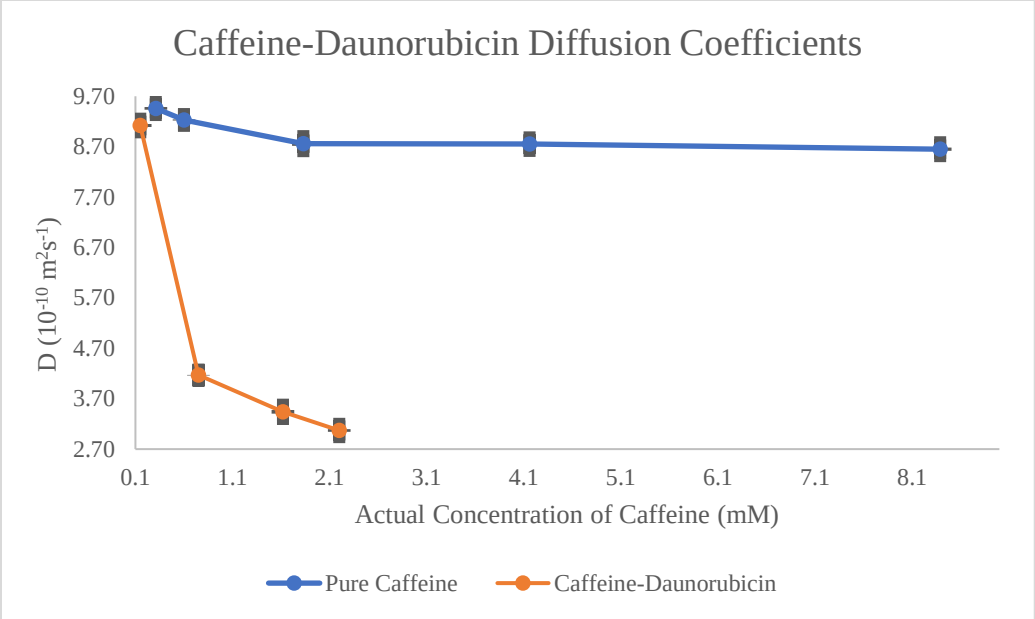

Graph 3.32 Average caffeine diffusion coefficients in daunorubicin-caffeine mixture from 3 mm NMR tubes versus pure caffeine diffusion coefficients.

3.4.4 Caffeine-Irinotecan Mixtures Proton Positions

Four irinotecan and caffeine mixtures are prepared. The concentrations for caffeine and irinotecan remain constant for each of the irinotecan and caffeine mixtures. The expected versus the actual percentages and concentrations of irinotecan and caffeine are reported in Table 3.40. The actual concentrations are determined using MestreNova as shown in Chapter 2.

Table 3.40 Expected versus actual percentages (percent %) and concentrations (Con. mM) for irinotecan (irin) and caffeine (caf).

Expected Percent (%)	Actual Percent (%)	Expected Con. (mM)	Actual Con. (mM)
80 Irin / 20 Caf	87 Irin /13 Caf	1.60 Irin / 0.40 Caf	2.14 Irin / 0.31 Caf
60 Irin / 40 Caf	64 Irin / 36 Caf	1.20 Irin / 0.80 Caf	1.68 Irin / 0.93 Caf
40 Irin / 60 Caf	38 Irin / 62 Caf	0.80 Irin / 1.20 Caf	0.97 Irin / 1.56 Caf
20 Irin / 80 Caf	17 Irin / 83 Caf	0.40 Irin / 1.60 Caf	0.42 Irin / 2.04 Caf

Figure 3.8 shows the proton NMR spectrum for the irinotecan-caffeine mixture. The proton spectra are run in triplicate with 5 mm NMR tubes. Tables 3.41-3.43 show the peak positions for irinotecan and caffeine in the irinotecan-caffeine mixture. Table 3.44 shows the average proton peak positions with the STDEV for the three trials, and Table 3.45 also shows the changes in average peak position between the lowest and highest concentrations of irinotecan in the irinotecan-caffeine mixtures with the STDEV. The changes are determined by subtracting the lowest chemical shift concentration from each of the other chemical shift concentrations.

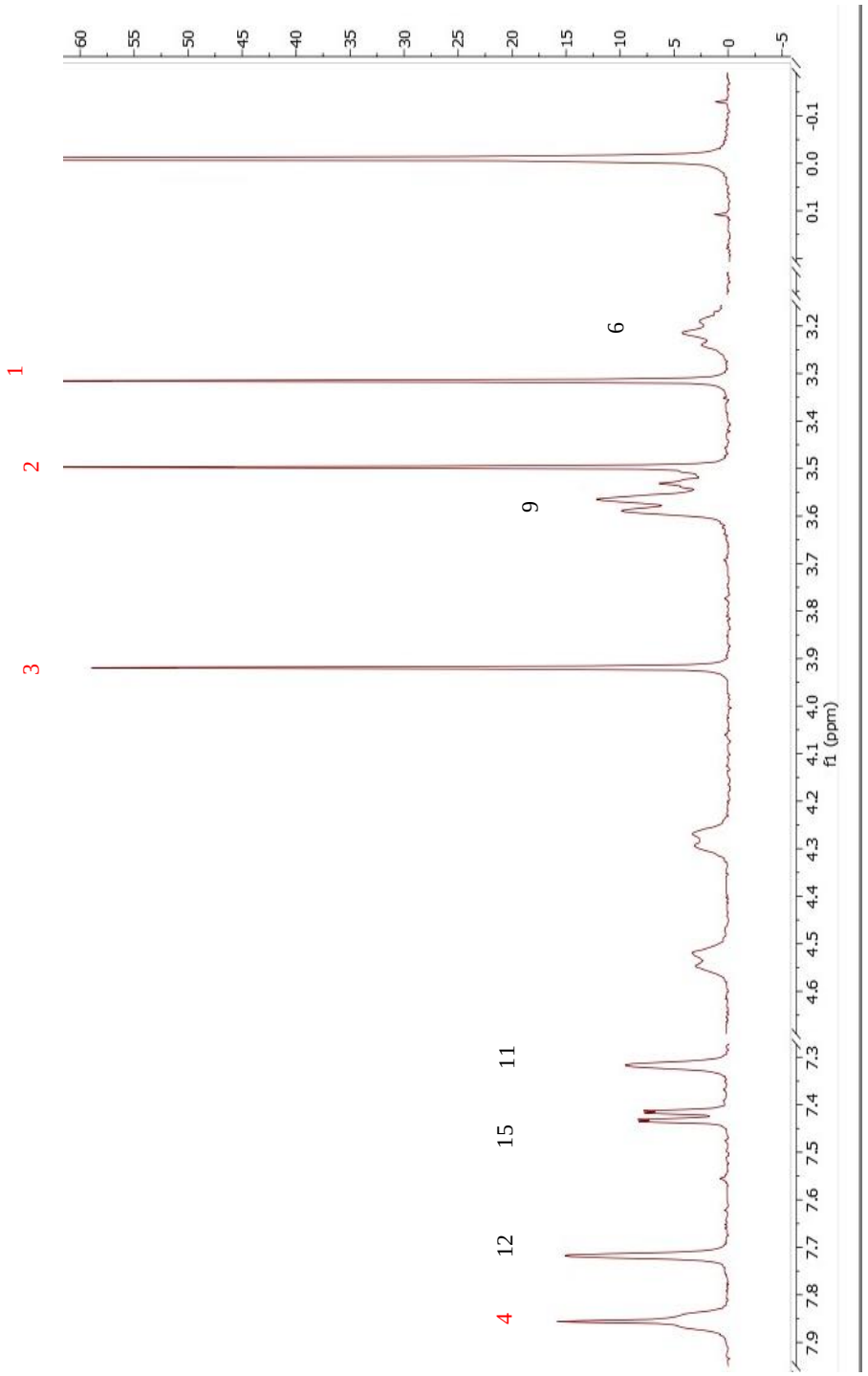

Figure 3.8 Irinotecan-caffeine mixture proton NMR spectrum (black for irinotecan and red for caffeine).

Table 3.41 Irinotecan-caffeine proton peak positions in parts per million (ppm) trial one. Caffeine peak highlighted in red.

Concentrations of Irin (%)	Peak Positions (δ, ppm)					
	6	**9**	**11**	**15**	**12**	**4**
87% Irin	3.3077	3.4890	7.2732	7.3856	7.6820	7.8255
64% Irin	3.3159	3.4971	7.3175	7.4240	7.7190	7.8562
38% Irin	3.3229	3.5040	7.3690	7.4670	7.7608	7.8630
17% Irin	3.3323	3.5138	7.4542	7.5315	7.8722	8.0050

Table 3.42 Irinotecan-caffeine proton peak positions in parts per million (ppm) trial two. Caffeine peak highlighted in red.

Concentrations of Irin (%)	Peak Positions (δ, ppm)					
	6	**9**	**11**	**15**	**12**	**4**
87% Irin	3.3079	3.4887	7.2732	7.3855	7.6820	7.8257
64% Irin	3.3159	3.4972	7.3174	7.4242	7.7180	7.8563
38% Irin	3.3229	3.5042	7.3692	7.4670	7.7607	7.8631
17% Irin	3.3323	3.5137	7.4542	7.5314	7.8721	8.0040

Table 3.43 Irinotecan-caffeine proton peak positions in parts per million (ppm) trial three. Caffeine peak highlighted in red.

Concentrations of Irin (%)	Peak Positions (δ, ppm)					
	6	**9**	**11**	**15**	**12**	**4**
87% Irin	3.3078	3.4889	7.2733	7.3857	7.6810	7.8256
64% Irin	3.3158	3.4971	7.3173	7.4241	7.7180	7.8562
38% Irin	3.3227	3.5041	7.3691	7.4660	7.7609	7.8631
17% Irin	3.3321	3.5137	7.4540	7.5314	7.8721	8.0040

Table 3.44 Irinotecan-caffeine average proton peak positions in parts per million (ppm) with STDEV. Caffeine peak highlighted in red.

Concentrations of Irin (%)	Peak Positions (δ, ppm)					
	6	**9**	**11**	**15**	**12**	**4**
87%	3.3078±0.0001	3.4889±0.0002	7.2733±0.0001	7.3857±0.0001	7.6810±0.0006	7.8256±0.0001
64%	3.3158±0.0000	3.4971±0.0002	7.3173±0.0001	7.4241±0.0010	7.7180±0.0006	7.8562±0.0001
38%	3.3227±0.0001	3.5041±0.0001	7.3691±0.0001	7.4660±0.0006	7.7609±0.0001	7.8631±0.0001
17%	3.3321±0.0001	3.5137±0.0001	7.4540±0.0001	7.5314±0.0001	7.8721±0.0001	8.0040±0.0006

Table 3.45 Changes in average proton peak position for irinotecan in irin-caf mixtures with STDEV. Caffeine peak highlighted in red.

Concentrations of Irin (%)	Proton Peaks (Δδ, ppm)				
	6	**9**	**11**	**15**	**12**
17%-10%	0.0244±0.0002	0.0248±0.0001	0.1809±0.0002	0.1454±0.0001	0.1901±0.0001
17%-64%	0.0163±0.0000	0.0166±0.0001	0.1367±0.0001	0.1074±0.0002	0.1541±0.0002
17%-38%	0.0094±0.0000	0.0096±0.0002	0.0850±0.0002	0.0644±0.0006	0.1130±0.0006

Graph 3.33 represents the irinotecan proton peak chemical shift values compared to the different concentrations of the irinotecan-caffeine mixtures, pure 1.68 mM irinotecan, and pure 8.39 mM caffeine. Graph 3.34 displays the changes in proton peak positions between the lowest concentrations of irinotecan and the highest concentrations of irinotecan as well as the proton peak position between the lowest concentration of irinotecan and each of the other concentrations of irinotecan. There is a correlation between the concentration of a solution and the chemical shift values of the proton peaks as shown in Graph 3.34.

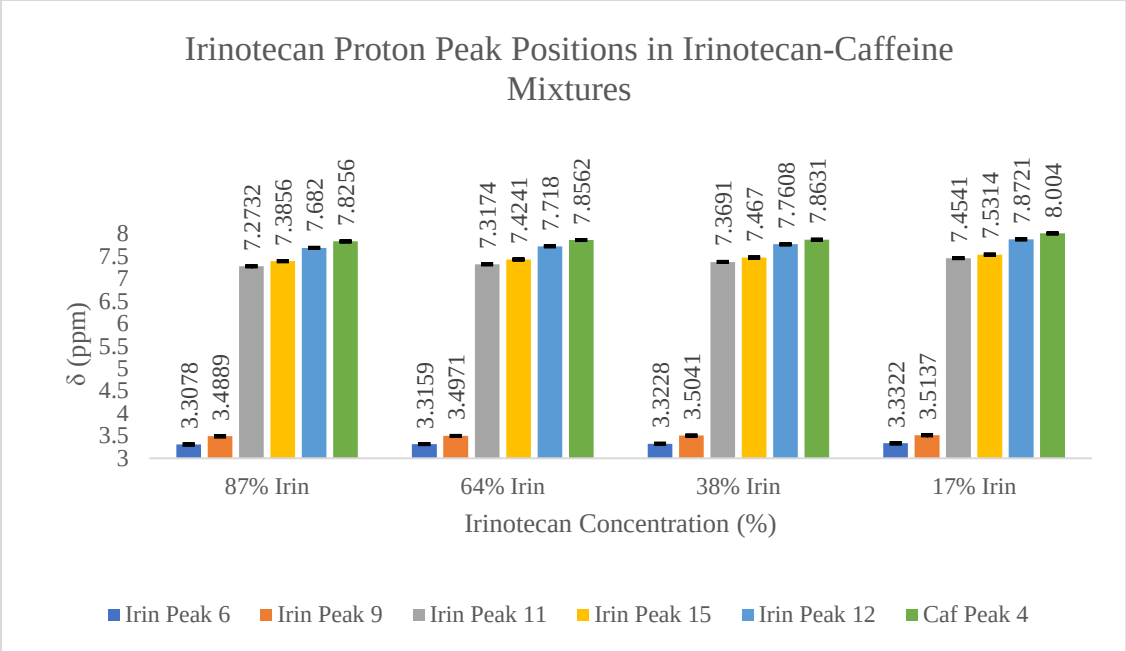

Graph 3.33 Irinotecan-caffeine proton peak positions with STDEV error bars.

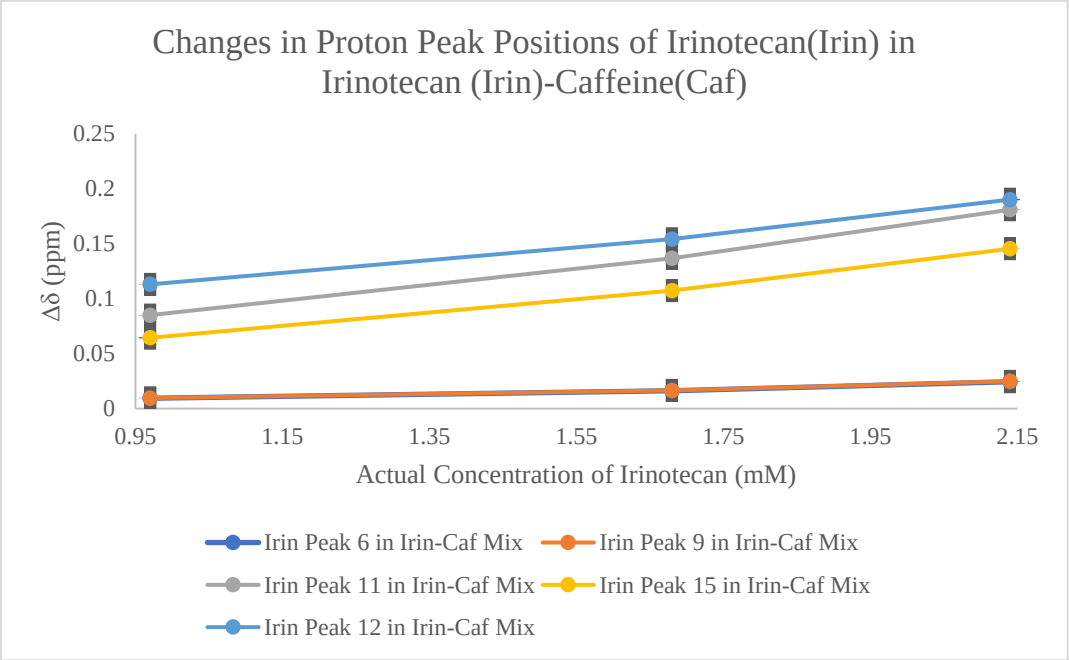

Graph 3.34 Changes in proton peak positions for irinotecan in irinotecan-caffeine.

3.4.5 K_a of Caffeine-Irinotecan Mixtures

The K_a for the caffeine-irinotecan mixture is determined using the modified version of the Rose-Drago equation and the Solver function of Excel as outlined in Chapter 2. Table 3.46 outlines the y0, y1, K_a, and error calculated for the caffeine-irinotecan mixture using Solver, while Table 3.47 reports the STDEV between the calculated data points from Solver. Graphs 3.35-3.39 show the calculated K_a data with STDEV for each proton of interest. The calculated K_a of the caffeine-irinotecan mixture is between 5.04 mM^{-1} and 52.86 mM^{-1}.

Table 3.46 Irinotecan-caffeine y0, y1, K_a, and error.

Peak Positions	y0	y1	K_a	error
6	3.348926	0.000000	6.831173	0.004863
9	3.528079	0.000000	5.038163	0.002870
11	8.014805	0.000000	52.86286	0.057845
15	7.899576	0.000000	21.36697	0.102849
12	7.753487	0.312706	8.361699	0.250388

Table 3.47 Standard deviation (STDEV) between average calculated proton peak positions for irinotecan in the irinotecan-caffeine mix and trials one-three.

Concentrations of Irin (%)	Peak Positions (δ, ppm)				
	6	9	11	15	12
87% Irin	0.00021	0.00081	0.00080	0.06272	0.09801
64% Irin	0.00025	0.00056	0.01731	0.05798	0.02121
38% Irin	0.00281	0.00120	0.03311	0.04257	0.04582
17% Irin	0.00182	0.00095	0.01662	0.02765	0.09122

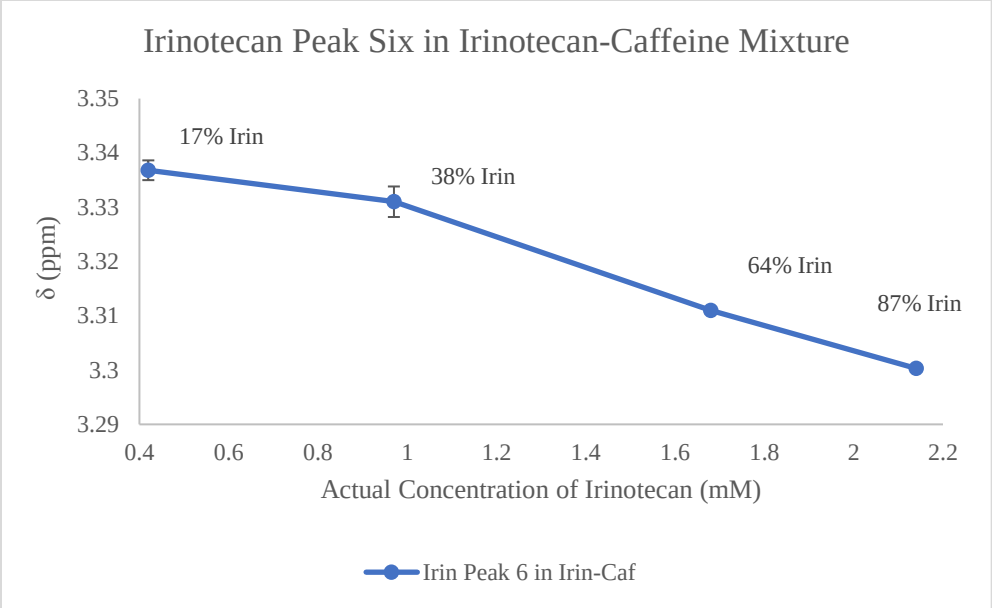

Graph 3.35 Average calculated proton peak positions for irinotecan peak six in the irinotecan-caffeine mixture with STDEV error bars. Refer to tables 3.41-3.44 for irinotecan peak trials one-three and the average proton peak positions.

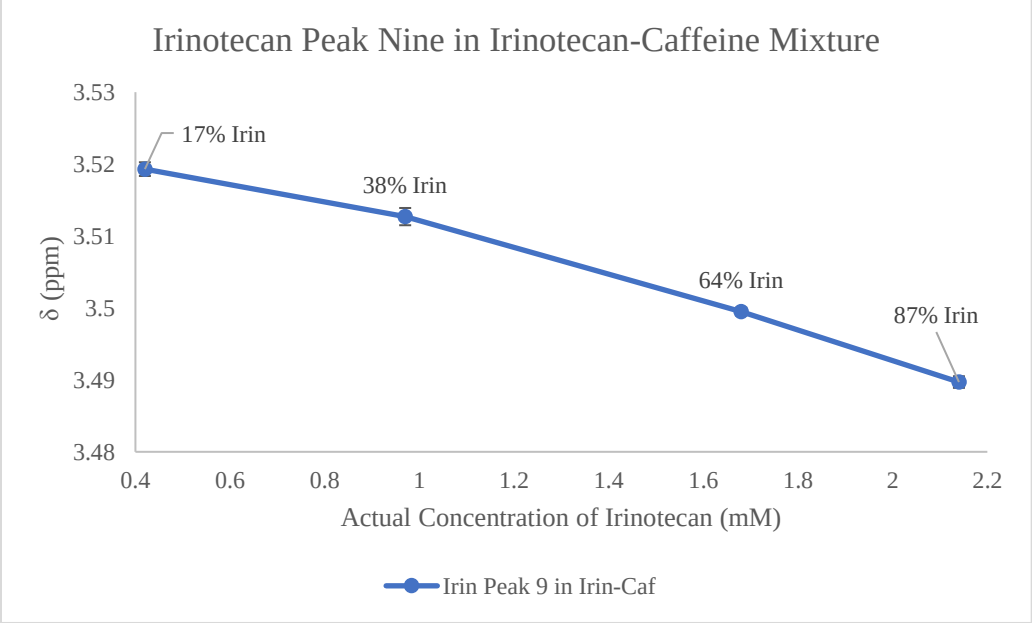

Graph 3.36 Average calculated proton peak positions for irinotecan peak nine in the irinotecan-caffeine mixture with STDEV error bars. Refer to tables 3.41-3.44 for irinotecan peak trials one-three and the average proton peak positions.

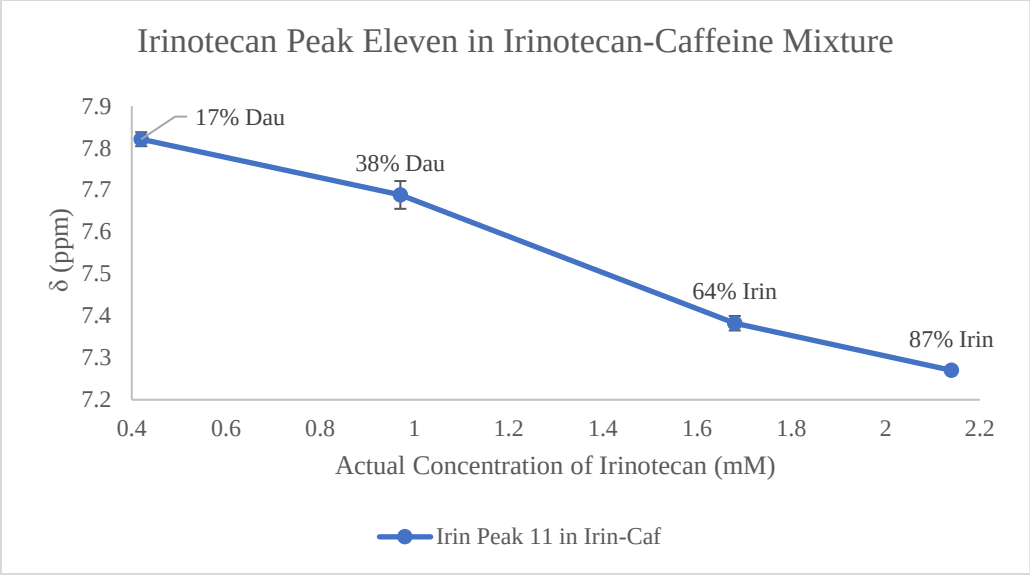

Graph 3.37 Average calculated proton peak positions for irinotecan peak eleven in the irinotecan-caffeine mixture with STDEV error bars. Refer to tables 3.41-3.44 for irinotecan peak trials one-three and the average proton peak positions.

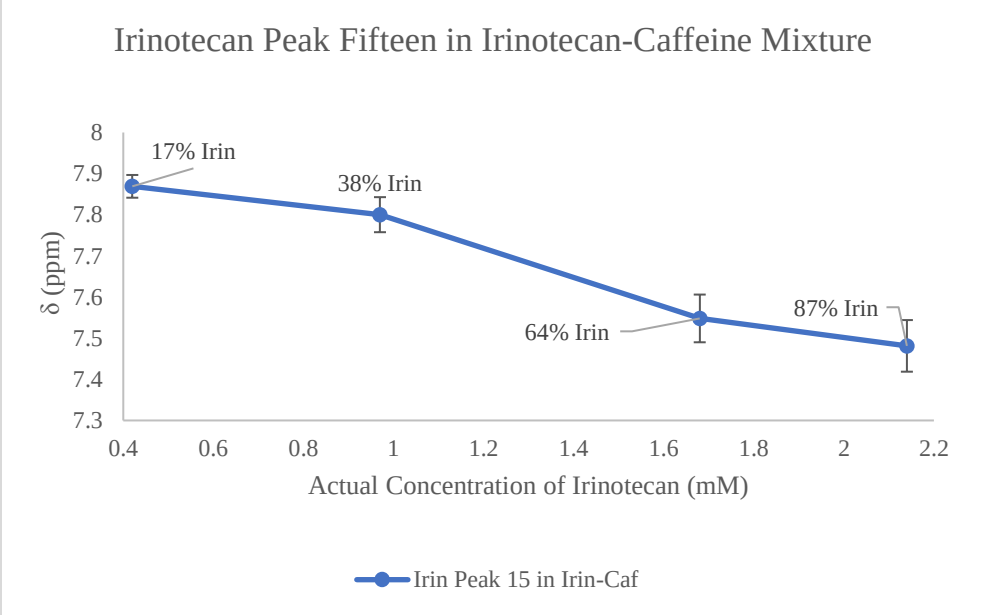

Graph 3.38 Average calculated proton peak positions for irinotecan peak fifteen in the irinotecan-caffeine mixture with STDEV error bars. Refer to tables 3.41-3.44 for irinotecan peak trials one-three and the average proton peak positions.

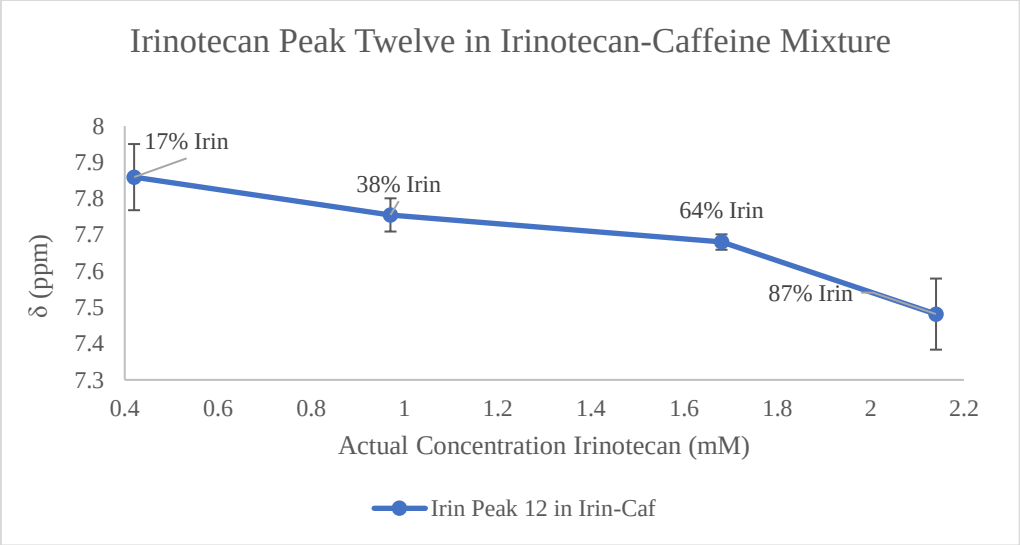

Graph 3.39 Average experimental proton peak positions for irinotecan peak twelve in the irinotecan-caffeine mixture with STDEV error bars. Refer to tables 3.41-3.44 for irinotecan peak trials one-three and the average proton peak positions.

3.4.6 Caffeine-Irinotecan Mixtures Diffusion Coefficients

The diffusion coefficients for irinotecan in each of the irinotecan-caffeine mixtures are determined using 3 mm NMR tubes. The 3 mm NMR tubes are used for DOSY because they reduce the effect of convection on the spectrum. Table 3.48 outlines the diffusion coefficient information for the irinotecan-caffeine mixture trials one-three, the average diffusion coefficients, and the STDEV between trials one-three. Graph 3.40 shows the average diffusion coefficients for irinotecan plotted versus the concentration of irinotecan with STDEV error bars. The diffusion coefficients are obtained using the GNAT software. The diffusion coefficients increase with decreasing concentration of irinotecan and increasing concentration of caffeine. The molecular weight of irinotecan and caffeine is 871.39 g mol^{-1}. Table 3.49 shows the aggregate weight from each concentration of irinotecan in the irinotecan-caffeine mixture predicted from the diffusion

coefficients using SEGWE. The predicted aggregate weight and the molecular weight of irinotecan and caffeine are compared to determine the number of aggregates that are formed at each concentration of irinotecan and caffeine mixture. The lower the diffusion coefficient, the higher the predicted aggregate weight and number of aggregates formed. When comparing the aggregate weights for the concentrations of the caffeine and irinotecan mixtures, the highest number of aggregates forms at 87% irinotecan and 13% caffeine, and the lowest number of aggregates forms at 17% irinotecan and 83% caffeine.

Table 3.48 Diffusion coefficients for irin in irinotecan-caffeine mixtures in 10^{-10} m^2 s^{-1} from 3 mm NMR tubes.

Concentrations	**Diffusion Coefficients (10^{-10} m^2/s)**				
	Trial One	**Trial Two**	**Trial Three**	**Average**	**STDEV**
87% Irin	3.11	3.11	3.13	3.12	0.01
64% Irin	3.45	3.38	3.37	3.40	0.04
38% Irin	4.35	4.35	4.35	4.36	0.02
17% Irin	6.84	6.83	6.83	6.82	0.03

Table 3.49 Aggregate weight (g mol^{-1}) and number for irin in irin-caf mix from SEGWE.

Concentrations	**Aggregate Weight (g mol^{-1})**	**Aggregate Number**
87% Irin	1170.42	1.34
64% Irin	942.33	1.08
38% Irin	511.39	0.59
17% Irin	181.32	0.21

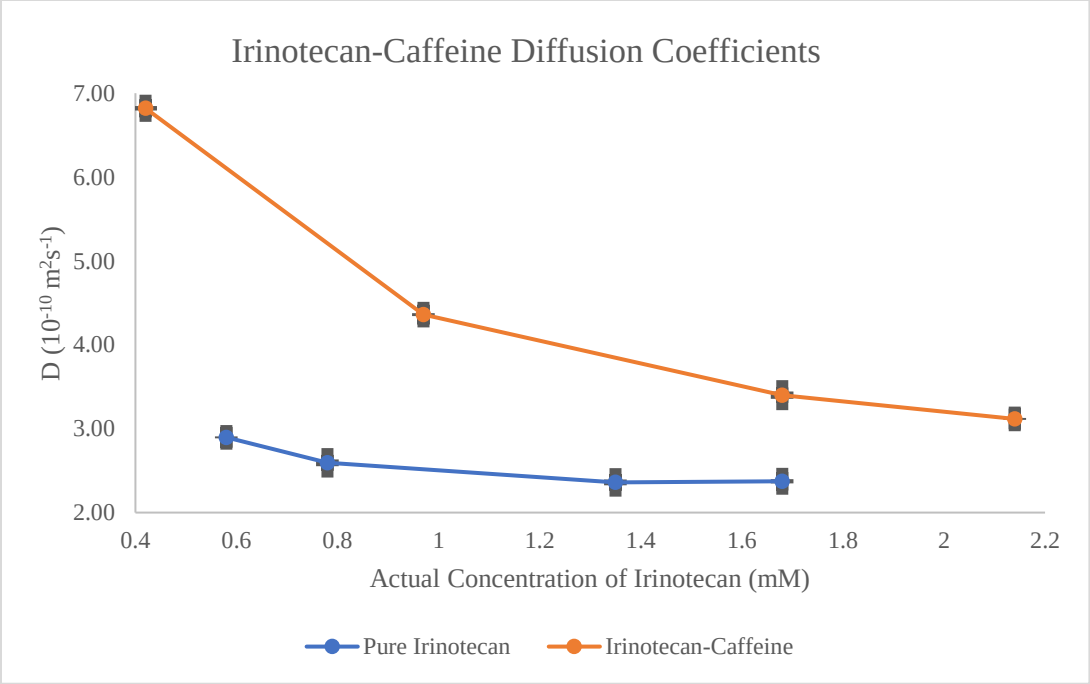

Graph 3.40 Average irinotecan diffusion coefficients in irinotecan-caffeine mix with STDEV error versus pure irinotecan diffusion coefficients.

Table 3.50 outlines the diffusion coefficient information for caffeine in the irinotecan-caffeine mixture for trials one-three, the average diffusion coefficients, and STDEV between trials one-three. Graph 3.41 shows the average diffusion coefficients for caffeine in the irinotecan-caffeine mixture plotted versus the concentration of caffeine in the irinotecan-caffeine mixture for trials one-three. The diffusion coefficients are obtained using GNAT software. The diffusion coefficients decrease with increasing concentrations of caffeine and decreasing concentrations of irinotecan. Table 3.51 shows the aggregate weight from each concentration of caffeine in the irinotecan-caffeine mixture predicted from the diffusion coefficients using SEGWE. When comparing the

aggregate weights for caffeine concentrations of the irinotecan-caffeine mixtures, the highest number of aggregates forms at 83% caffeine and 17% irinotecan, and the lowest number of aggregates forms at 13% caffeine and 87% irinotecan.

Table 3.50 Diffusion coefficients for caf in irinotecan-caffeine mixtures in 10^{-10} m^2 s^{-1} from 3 mm NMR tubes.

Concentrations	**Diffusion Coefficients (10^{-10} m^2/s)**				
	Trial One	**Trial Two**	**Trial Three**	**Average**	**STDEV**
13% Caf	7.22	7.21	7.18	7.20	0.02
36% Caf	4.35	4.32	4.33	4.33	0.02
62% Caf	3.55	3.51	3.56	3.54	0.03
83% Caf	3.40	3.41	3.37	3.39	0.02

Table 3.51 Aggregate weight (g mol^{-1}) and number for caf in irin-caf mix from SEGWE.

Concentrations	**Aggregate Weight (g mol^{-1})**	**Aggregate Number**
13% Caf	160.79	0.18
36% Caf	519.97	0.60
62% Caf	851.96	0.98
83% Caf	949.31	1.09

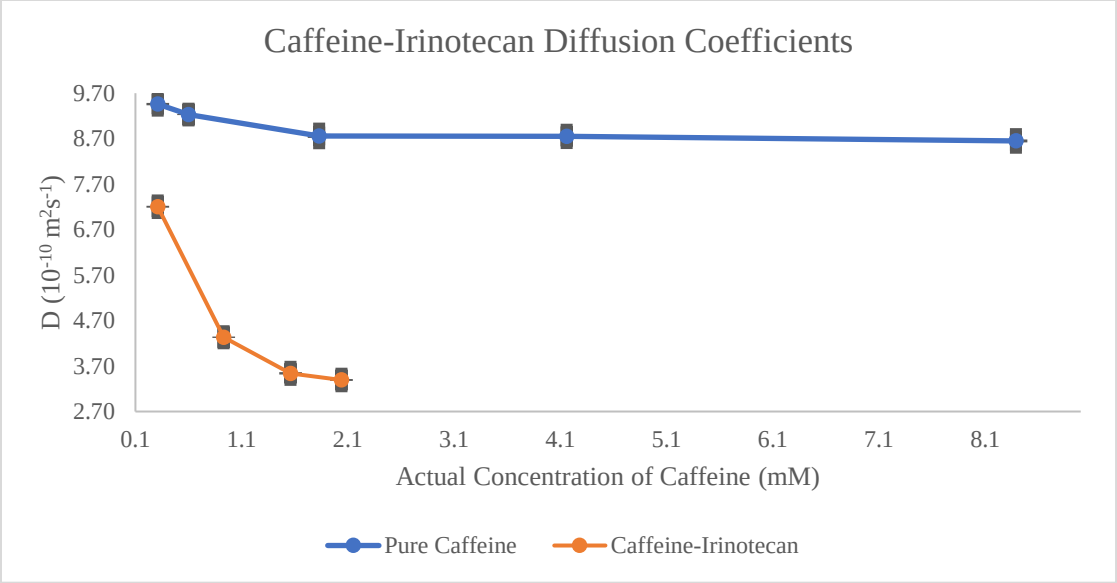

Graph 3.41 Average caffeine diffusion coefficients in irinotecan-caffeine mixtures with STDEV error bars versus pure caffeine diffusion coefficients.

3.5 Caffeine Peaks in Anticancer Drug Mixtures

The shifts in caffeine peak position in the anticancer drug and caffeine mixtures are because of the interactions between the drug and caffeine. In Table 3.52, the actual percentages and concentrations of caffeine in daunorubicin are reported. Tables 3.53-3.55 show the proton peak positions for caffeine in the daunorubicin mixture. The average proton peak positions for caffeine in the daunorubicin-caffeine mixtures are reported in Table 3.56 along with the STDEV, and the change in average proton peak position is reported in Table 3.57 along with STDEV.

In Table 3.58, the actual percentages and concentrations of caffeine in irinotecan are reported. All concentrations are confirmed using MestreNova. Tables 3.59-3.61 show the proton peak positions for caffeine in the irinotecan mixture. The average proton peak positions for caffeine in the irinotecan-caffeine mixtures are reported in Table 3.62 along

with the STDEV, and the change in average proton peak position is reported in Table 3.63 along with the STDEV. Refer to Tables 3.1-3.5 for information on the proton peak position of pure caffeine. The numbering and naming are the same as in previous caffeine and anticancer drug tables.

Table 3.52 Caffeine (Caf) percentages (%) and concentrations (mM) in daunorubicin

Percentage Caf (%)	**Concentration Caf (mM)**
90% Caf	2.20 mM Caf
65% Caf	1.62 mM Caf
30% Caf	0.75 mM Caf
5% Caf	0.15 mM Caf

Table 3.53 Caf proton positions in dau mix in parts per million (ppm) trial one.

Concentrations of Caf (%)	**Peak Positions (δ, ppm)**			
	1	**2**	**3**	**4**
90% Caf	3.3214	3.5020	4.0109	7.8393
65% Caf	3.2971	3.4766	3.9934	7.8350
30% Caf	3.2688	3.4465	3.9738	7.8068
5% Caf	3.4135	3.4133	3.9310	7.8090

Table 3.54 Caf proton positions in dau mix in parts per million (ppm) trial two.

Concentrations of Caf (%)	**Peak Positions (δ, ppm)**			
	1	**2**	**3**	**4**
90% Caf	3.3214	3.5022	4.0107	7.8391
65% Caf	3.2974	3.4767	3.9934	7.8370
30% Caf	3.2686	3.4466	3.9738	7.8068
5% Caf	3.4134	3.4134	3.9312	7.8080

Table 3.55 Caf proton positions in dau mix in parts per million (ppm) trial three.

Concentrations of Caf (%)	**Peak Positions (δ, ppm)**			
	1	**2**	**3**	**4**
90% Caf	3.3213	3.5021	4.0109	7.8392
65% Caf	3.2975	3.4767	3.9936	7.8360
30% Caf	3.2687	3.4469	3.9739	7.8069
5% Caf	3.4134	3.4135	3.9311	7.8080

Table 3.56 Caffeine proton positions in daunorubicin mix in parts per million (ppm).

Concentrations of Caf (%)	Peak Positions (δ, ppm)			
	1	**2**	**3**	**4**
90% Caf	3.3214±0.0001	3.5021±0.0001	4.0108±0.0001	7.8392±0.0001
65% Caf	3.2973±0.0002	3.4767±0.0001	3.9935±0.0001	7.8360±0.0010
30% Caf	3.2687±0.0001	3.4467±0.0002	3.9738±0.0001	7.8068±0.0001
5% Caf	3.4134±0.0001	3.4134±0.0001	3.9311±0.0001	7.8080±0.0006

Table 3.57 Changes in proton peak position for caffeine in dau-caf mixtures.

Concentrations of Caf (%)	Proton Peaks (Δδ, ppm)			
	1	**2**	**3**	**4**
90% Caf-5% Caf	0.0784±0.0001	0.0887±0.0002	0.0797±0.0010	0.0312±0.0001
90% Caf-30% Caf	0.0527±0.0001	0.0554±0.0001	0.0370±0.0006	0.0324±0.0006
90% Caf- 65% Caf	0.0241±0.0002	0.0254±0.0002	0.0173±0.0006	0.0032±0.0002

Table 3.58 Caffeine (Caf) percentages (%) and concentrations (mM) in irinotecan.

Percentage Caf (%)	Concentration Caf (mM)
83% Caf	2.04 mM Caf
62% Caf	1.56 mM Caf
36% Caf	0.93 mM Caf
13% Caf	0.31 mM Caf

Table 3.59 Caf proton positions in irin mix in parts per million (ppm) trial one.

Concentrations of Caf (%)	Peak Positions (δ, ppm)			
	1	**2**	**3**	**4**
83% Caf	3.3363	3.5889	3.9389	8.0050
62% Caf	3.3304	3.5659	3.9321	7.8630
36% Caf	3.3189	3.5560	3.9225	7.8562
13% Caf	3.3033	3.5533	3.9070	7.8255

Table 3.60 Caf proton positions in irin mix in parts per million (ppm) trial two.

Concentrations of Caf (%)	Peak Positions (δ, ppm)			
	1	2	3	4
83% Caf	3.3363	3.5887	3.9388	8.0040
62% Caf	3.3307	3.5659	3.9320	7.8631
36% Caf	3.3188	3.5561	3.9224	7.8563
13% Caf	3.3033	3.5531	3.9060	7.8257

Table 3.61 Caf proton positions in irin mix in parts per million (ppm) trial three.

Concentrations of Caf (%)	Peak Positions (δ, ppm)			
	1	2	3	4
83% Caf	3.3364	3.5888	3.9389	8.0040
62% Caf	3.3305	3.5658	3.9324	7.8631
36% Caf	3.3188	3.5562	3.9224	7.8562
13% Caf	3.3031	3.5532	3.9080	7.8256

Table 3.62 Caffeine average proton positions in irinotecan mix in parts per million (ppm).

Concentrations of Caf (%)	Peak Positions (δ, ppm)			
	1	2	3	4
83% Caf	3.3363±0.0002	3.5888±0.0002	3.9389±0.0003	8.0040±0.0003
62% Caf	3.3305±0.0004	3.5659±0.0002	3.9322±0.0001	7.8631±0.0003
36% Caf	3.3188±0.0000	3.5561±0.0003	3.9224±0.0002	7.8562±0.0001
13% Caf	3.3032±0.0002	3.5532±0.0002	3.9077±0.0002	7.8256±0.0001

Table 3.63 Changes in average proton peak position for caffeine in irin-caf mixtures.

Concentrations of Caf (%)	Proton Peaks (Δδ, ppm)			
	1	2	3	4
83% Caf-13% Caf	0.0331±0.0001	0.0356±0.0002	0.0312±0.0010	0.1784±0.0001
83% Caf-36% Caf	0.0175±0.0001	0.0327±0.0006	0.0165±0.0004	0.1478±0.0006
8% Caf 62% Caf	0.0058±0.0003	0.0229±0.0002	0.0067±0.0006	0.1409±0.0001

Graphs 3.42-3.45 represent each of the changes in peak position for the four protons in caffeine for both anticancer mixtures. The numbering and naming are the same as in previous caffeine and anticancer drug graphs.

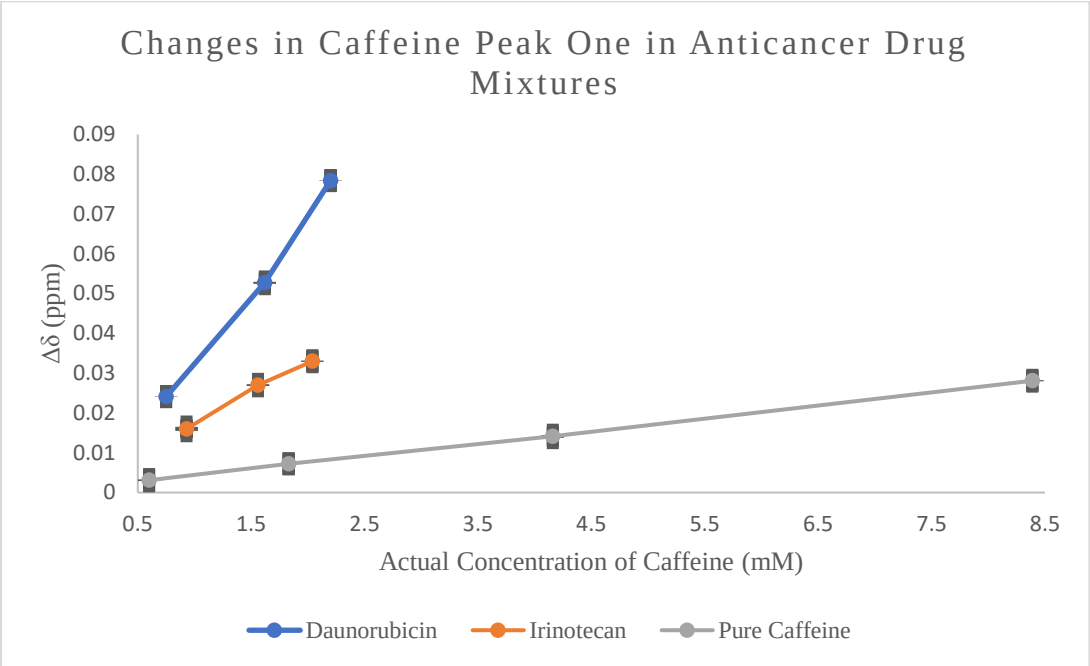

Graph 3.42 Caffeine peak one chemical shift changes in anticancer drugs and pure caf.

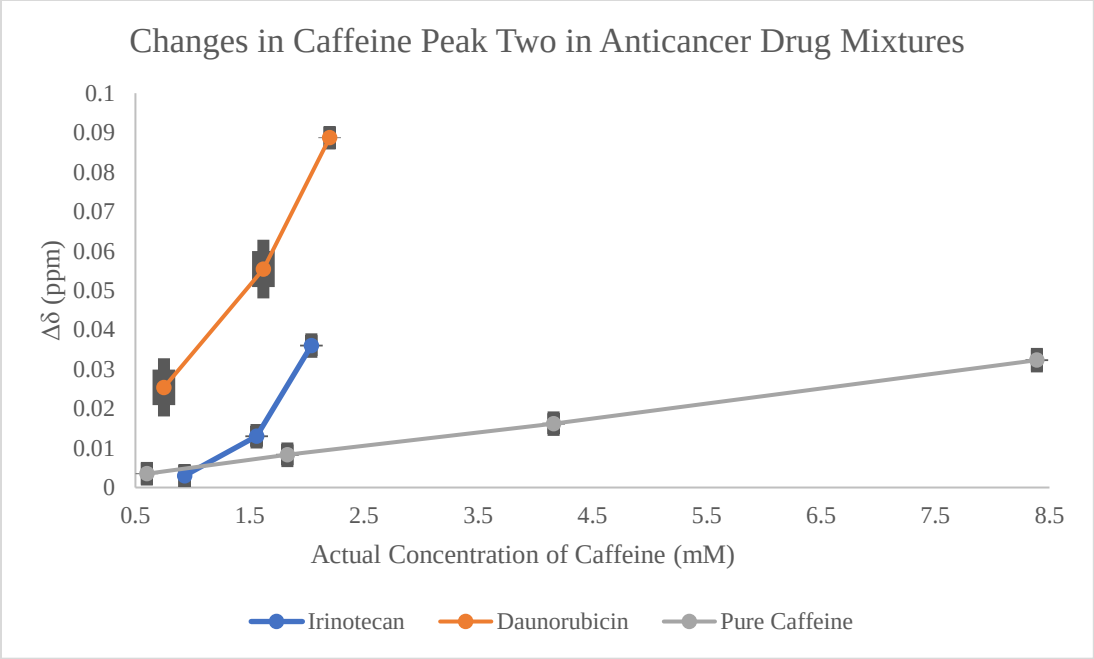

Graph 3.43 Caffeine peak two chemical shift changes in anticancer drugs and pure caf.

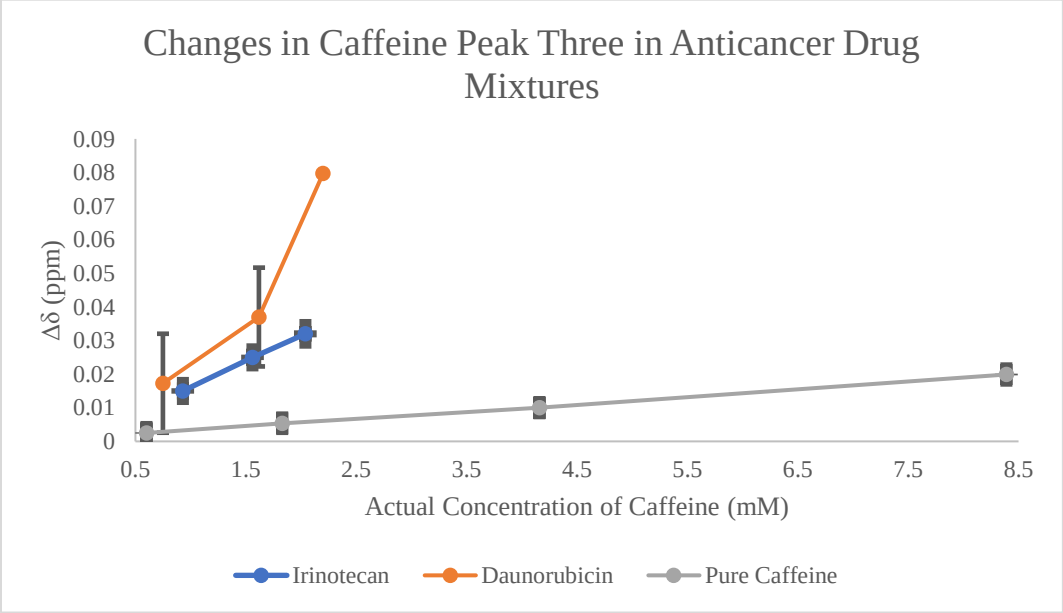

Graph 3.44 Caffeine peak three chemical shift changes in anticancer drugs and pure caf.

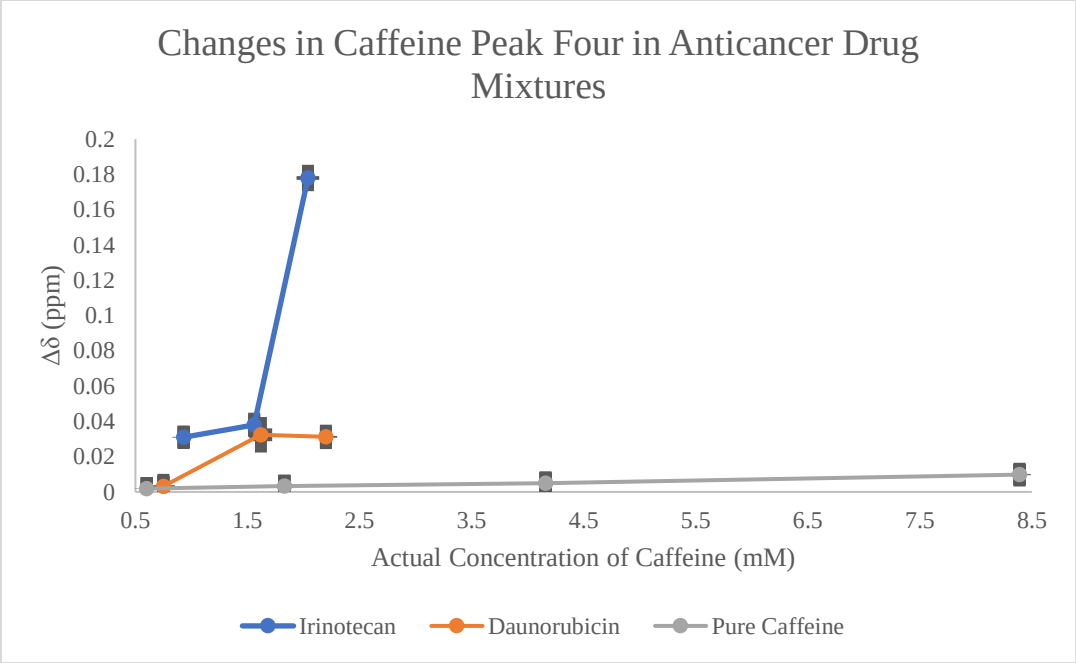

Graph 3.45 Caffeine peak four chemical shift changes in anticancer drugs and pure caf.

Chapter 4. Conclusion

4.1 Overview of Results

After analyzing the proton/PRESAT and DOSY NMR data, caffeine is determined to interact with both the anticancer drugs daunorubicin and irinotecan. The proton/PRESAT data allows for analysis of the chemical shift data. The chemical shift data is compared to the concentrations to determine the concentration effect on the chemical shift of the solution being analyzed. The K_a of the anticancer solutions are found using Solver and Excel to determine the extent of binding. The DOSY NMR data is used to determine the diffusion coefficients of the caffeine and anticancer drug solutions, as well as, the anticancer drug mixtures with caffeine. DOSY and SEGWE calculators are used to establish the relationship between the aggregate weight of the compounds with the diffusion coefficients of the compounds and how the relationship is connected to the binding of the caffeine and anticancer drug mixtures.

4.1.1 Caffeine Results

Tables 3.1-3.5 and Graphs 3.1 and 3.2 illustrate the relationship between the concentration of caffeine and the chemical shift of the protons. Overall, with decreasing concentration, the chemical shift values increase by shifting further downfield on the

NMR spectrum. As the concentrations of the samples decrease, the chemical shift values increase. The correlation between the concentration and chemical shift is true for both the non-aromatic protons and the aromatic protons of caffeine. The changes in chemical shift are more noticeable with the aromatic proton of caffeine when compared to the non-aromatic protons. The data from Graph 3.1 suggests dimerization is less likely to occur in the lowest two concentrations as compared to the higher concentrations. The relatively larger chemical shifts in the higher concentrations account for the more likely dimerization occurring in these higher concentrations. Graph 3.2 illustrates the changes in chemical shift for each concentration compared to the lowest caffeine concentration. The graph shows the largest changes in chemical shift data occur with higher concentrations, and the smallest changes in chemical shift data occur with lower concentrations. Caffeine peak three has a noticeable decrease in the middle of Graph 3.2, unlike the other three caffeine peaks. Caffeine peak three is the closest proton to the water peak which could lead to the distortion shown in Graph 3.2.

Tables 3.6 and 3.7 and Graphs 3.3-3.6 illustrate the K_a data for pure caffeine. The K_a for pure caffeine is between 1.01 mM^{-1} and 3.61 mM^{-1}. This differs with the K_a values of caffeine from similar experiments where the K_a for caffeine is 251 mM^{-1}.[43] The difference in K_a value could be due to differing concentrations used for pure caffeine in the analysis. Table 3.8 and Graph 3.7 outline the diffusion coefficients for the caffeine concentrations. After analyzing the diffusion coefficient data, the diffusion coefficients increase with decreasing concentration of caffeine. The average diffusion coefficients range from 8.65 x 10^{-10} m^2 s^{-1} to 9.46 x 10^{-10} m^2 s^{-1}. Compared to daunorubicin and

irinotecan, caffeine diffuses at a faster rate. The higher rate of diffusion for caffeine makes sense due to the smaller molecular weight of caffeine compared to daunorubicin and irinotecan.[40] Table 3.7 illustrates the aggregate weight and number determined from SEGWE using the diffusion coefficients of the different concentrations of caffeine. The highest aggregate weight (107.99 g mol^{-1}) corresponds to the highest number of aggregates formed (0.556) for caffeine. The highest aggregate weight occurs with 8.39 mM caffeine. The lowest aggregate weight (89.34 g mol^{-1}) gives the lowest number of aggregates formed (0.460), which corresponds to the 0.31 mM dilution from pure caffeine. The aggregate values for some of the concentrations are less than one, which seems unlikely since there can not be only a part of a molecule. The data from SEGWE only gives a theoretical estimate based on the determined aggregate weight of the molecule in question; this may account for not having whole numbers for the number of aggregates formed.

From the data, it is determined that the concentration of caffeine affects the chemical shift values of the proton peak positions. As the concentration decreases, the chemical shift value increases. Despite this trend, there is a noticeable issue with some of the data for pure caffeine. The K_a for pure caffeine is significantly lower than the K_a values from the literature. This is most probably due to the low concentration used for these experiments. In the future, a higher concentration range for the pure caffeine dilution series may lead to more literature accurate data. Working at a higher concentration may lead to differences not only in the K_a values but also in the chemical shift values and the diffusion coefficients.

4.1.2 Daunorubicin Results

Tables 3.10-3.12, as well as, Graphs 3.8 and 3.9 outline the chemical shift value for the different concentrations of daunorubicin. With the protons of pure daunorubicin, the chemical shift values increase with decreasing concentration.

Tables 3.15 and 3.16 and Graphs 3.10-3.14 illustrate the K_a data for pure daunorubicin. The K_a for pure daunorubicin is between 3.52 mM^{-1} and 16.81 mM^{-1}. Table 3.17 and Graph 3.15 illustrate the diffusion coefficients for daunorubicin. The diffusion coefficients range from 2.71 x 10^{-10} m^2 s^{-1} to 3.47 x 10^{-10} m^2 $s^{-}1$. For daunorubicin, the diffusion coefficients increase with decreasing concentrations. The one exception is the decrease in diffusion coefficients between the 0.49 mM and the 0.20 mM daunorubicin concentrations. Concentrations 0.49 mM and 0.20 mM concentrations may have been mislabeled, which led to the deviation in the trend. Daunorubicin has a larger diffusion coefficient than caffeine and thus diffuses at a slower rate than caffeine. The slower diffusion rate with increased molecular weight corresponds with results from Evans, et al.[40] Table 3.18 shows the aggregate weight (g mol^{-1}) and number for daunorubicin determined from SEGWE using the diffusion coefficients for each dilution of daunorubicin. The highest aggregate weight (1679.58 g mol^{-1}) represents the highest number of aggregates formed (2.98) for pure daunorubicin. The highest aggregate weight and number occur at the 1.95 mM dilution of daunorubicin. The lowest aggregate weight (895.48 g mol^{-1}) and number (1.59) correspond to 0.49 mM of the daunorubicin dilutions.

Like with pure caffeine, it is determined that the concentration of pure daunorubicin affects the chemical shift values of the proton peak positions. As the

concentration decreases, the chemical shift value increases. When comparing the proton chemical shift changes between pure caffeine and pure daunorubicin, pure daunorubicin has larger changes in the pure chemical shift values. This indicates that daunorubicin self-associates more readily than pure caffeine. This is supported by the aggregate formation data for pure daunorubicin, which indicates the formation of more aggregates when compared to pure caffeine.

4.1.3 Irinotecan Results

Tables 3.19-3.23 and Graphs 3.16 and 3.17 show the chemical shift value for the dilution series concentrations for irinotecan. The proton spectrum of irinotecan follows the same pattern as both caffeine and daunorubicin. For irinotecan, there is an increase in chemical shift with decreasing concentrations.

Tables 3.24 and 3.25 and Graphs 3.18-3.22 illustrate the K_a data for pure irinotecan. The K_a for pure irinotecan is determined to be between 1.49 mM^{-1} and 23.32 mM^{-1}. Table 3.26 and Graph 3.23 illustrate the diffusion coefficients for irinotecan. The diffusion coefficients for pure irinotecan are between 2.36×10^{-10} m^2 s^{-1} and 2.90×10^{-10} m^2 s^{-1}. Overall, the diffusion coefficients increase with decreasing concentration. The one exception is between the 1.68 mM and the 1.35 mM concentrations; between these two concentrations, there is a slight decrease in diffusion coefficients from 2.37×10^{-10} m^2 s^{-1} to 2.36×10^{-10} m^2 s^{-1}. Irinotecan diffuses faster than daunorubicin but slower than caffeine. Again, this follows the pattern established in previous studies that the molecular weight and the diffusion coefficients correlate. The molecular weight of

irinotecan is between the molecular weights of caffeine and daunorubicin, and irinotecan's diffusion rate is also between that of caffeine and daunorubicin. Table 3.27 illustrates the aggregate weight and number from irinotecan dilutions using the diffusion coefficients and SEGWE. The highest aggregate weight (2410.34 g mol^{-1}) and number (3.56) occurs with a 1.35 mM dilution of pure irinotecan. The lowest aggregate weight (1410.49 g mol^{-1}) and number (2.08) occurs with a 0.58 mM dilution of irinotecan.

Like with pure caffeine and pure daunorubicin, it is determined that the concentration of pure irinotecan affects the chemical shift values of the proton peak positions. As the concentration decreases, the chemical shift value increases. When comparing the proton chemical shift changes between pure caffeine, pure daunorubicin, and pure irinotecan, pure irinotecan has the largest changes in the proton chemical shift values. This indicates that irinotecan self-associates more readily than either pure daunorubicin or pure caffeine. This is again supported by the aggregate formation data for pure irinotecan, which indicates the formation of more aggregates when compared to either pure daunorubicin or pure caffeine.

4.1.4 Daunorubicin-Caffeine Mixture Results

Table 3.28 reports the expected percentages and concentrations for daunorubicin and caffeine versus the actual percentages and concentrations for daunorubicin and caffeine. Tables 3.29-3.33, as well as, Graphs 3.24 and 3.25 highlight the chemical shift value for the daunorubicin-caffeine mixture. The chemical shift for the non-aromatic and aromatic daunorubicin protons in the mixture increases as the concentration of the

daunorubicin decreases. When comparing the chemical shift values of pure daunorubicin to daunorubicin in the daunorubicin-caffeine mixture, the chemical shift values are higher in pure daunorubicin for the non-aromatic protons. The chemical shift values of the non-aromatic protons of caffeine are increasing, moving downfield on the NMR spectrum, with an increasing concentration of caffeine and a decreasing concentration of daunorubicin. The chemical shift values of the aromatic protons are also increasing with an increasing concentration of caffeine and a decreasing concentration of daunorubicin. Graphs 3.42-3.45 show the changes in caffeine proton chemical shift for daunorubicin-caffeine irinotecan-caffeine mixtures, and pure caffeine. For each of the caffeine peaks, the highest chemical shift changes occur in the daunorubicin-caffeine mixtures. The exception is with caffeine peak four, the aromatic proton. The aromatic proton of caffeine has the highest chemical shift change with irinotecan-caffeine mixtures. For each of the caffeine peaks, except for caffeine peak two, pure caffeine has smaller changes in chemical shift changes the both daunorubicin-caffeine mixtures and irinotecan-caffeine mixtures.

Tables 3.34 and 3.35 and Graphs 3.26-3.30 illustrate the K_a data for the daunorubicin-caffeine mixture. The K_a for the daunorubicin-caffeine is between 20.45 mM^{-1} and 67.55 mM^{-1}. This is significantly higher than the K_a range of pure daunorubicin (3.52 mM^{-1} - 16.81 mM^{-1}). The increase in K_a could be due to the binding of caffeine to daunorubicin.

Table 3.36 and Graph 3.31 illustrate the diffusion coefficients for daunorubicin in the daunorubicin-caffeine mixture. The diffusion coefficients for the daunorubicin-

caffeine mixture based on the concentration of daunorubicin ranges from 2.50 x 10^{-10} m^2 s^{-1} and 8.15 x 10^{-10} m^2 s^{-1}. After analyzing the data for daunorubicin in the daunorubicin-caffeine mixtures diffusion coefficients, there is an increase in the diffusion coefficient with a decrease in the concentration of daunorubicin and an increase in the concentration of caffeine. The highest diffusion coefficient occurs with 10% daunorubicin and 90% caffeine, and the lowest diffusion coefficient occurs with 95% daunorubicin and 5% caffeine. Table 3.37 shows the aggregate weight and number for daunorubicin-caffeine mixtures using the diffusion coefficients and SEGWE. The highest aggregate weight (2071.88 g mol^{-1}) and number (2.73) occurs at 95% daunorubicin, which corresponds to 2.89 mM of daunorubicin. On the other hand, the lowest aggregate weight (123.36 g mol^{-1}) and number (0.16) occurs at 10% daunorubicin, which corresponds to 0.25 mM of daunorubicin.

Table 3.38 and Graph 3.32 illustrate the diffusion coefficients for caffeine in the daunorubicin-caffeine mixture. The diffusion coefficients for the daunorubicin-caffeine mixture based on the concentration of caffeine ranges from 3.07 x 10^{-10} m^2 s^{-1} and 9.12 x 10^{-10} m^2 s^{-1}. After analyzing the data for caffeine in the daunorubicin-caffeine mixtures diffusion coefficients, there is a decrease in the diffusion coefficient with an increase in the concentration of caffeine and a decrease in the concentration of daunorubicin. The highest diffusion coefficient occurs with 5% caffeine and 95% daunorubicin, and the lowest diffusion coefficient occurs with 90% caffeine and 10% daunorubicin. Table 3.39 shows the aggregate weight and number of caffeine in the daunorubicin-caffeine mixtures using the diffusion coefficients and SEGWE. The

highest aggregate weight (1219.47 g mol^{-1}) and number (1.61) occurs at 5% caffeine and 95% daunorubicin. On the other hand, the lowest aggregate weight (96.51 g mol^{-1}) and number (0.13) occurs at 90% caffeine and 10% daunorubicin. The aggregate formation decreases with decreasing concentration of caffeine in daunorubicin-caffeine mixtures.

The concentration of the daunorubicin-caffeine mixture affects the proton peak chemical shift positions. As the concentration decreases, the chemical shift value increases. When comparing the proton chemical shift changes for the daunorubicin-caffeine to pure daunorubicin, the daunorubicin-caffeine mixture has the larger change in the proton chemical shift values. This indicates that the daunorubicin mixture associates more readily than pure daunorubicin. This supports the theory that adding caffeine to an aromatic anticancer drug changes the drug's binding ability.

4.1.5 Irinotecan-Caffeine Mixture Results

Table 3.40 shows the expected percentages and concentrations of irinotecan and caffeine versus the actual percentages and concentrations of irinotecan and caffeine Tables 3.41-3.45 and Graphs 3.33 and 3.34 illustrate the chemical shift values for irinotecan-caffeine mixtures. Overall, the pattern for the non-aromatic and aromatic irinotecan protons in the mixture increases as the concentration of irinotecan decreases. When comparing pure irinotecan chemical shift values to irinotecan in the irinotecan-caffeine mixtures, pure irinotecan has a higher chemical shift value for the non-aromatic protons. When comparing pure irinotecan chemical shift values to irinotecan in irinotecan-caffeine mixture, the pure irinotecan is not higher for the aromatic protons.

The chemical shift values of the non-aromatic protons of caffeine are increasing with an increasing concentration of caffeine and a decreasing concentration of irinotecan. The chemical shift values of the aromatic protons are also increasing with an increasing concentration of caffeine and a decreasing concentration of irinotecan. When analyzing Graphs 3.42-3.45 the greatest change in chemical shift values for each of the caffeine protons occurs in the daunorubicin-caffeine mixtures except for the aromatic caffeine proton four. In caffeine peak four, the irinotecan-caffeine mixture has higher changes in chemical shift than the daunorubicin-caffeine mixture. For each of the caffeine peaks, except for caffeine peak two, pure caffeine has smaller changes in chemical shift changes the both daunorubicin-caffeine mixtures and irinotecan-caffeine mixtures.

Tables 3.46 and 3.47 and Graphs 3.35-3.39 illustrate the K_a data for the irinotecan-caffeine mixture. The K_a for the irinotecan-caffeine is between 5.04 mM^{-1} and 52.86 mM^{-1}. This is higher than the K_a range for pure irinotecan (1.49 mM^{-1} and 23.32 mM^{-1}). The increase in K_a could be due to the binding of caffeine to irinotecan. Table 3.48 and Graph 3.40 illustrate the diffusion coefficients for irinotecan in the irinotecan-caffeine mixture. The diffusion coefficients for irinotecan in the irinotecan-caffeine mixture is between 3.12×10^{-10} m^2 s^{-1} and 6.82×10^{-10} m^2 s^{-1}. The highest diffusion coefficient for irinotecan in the irinotecan-caffeine mixture occurs at 17% irinotecan, and the lowest diffusion coefficient for irinotecan in the irinotecan-caffeine mixture occurs at 87% irinotecan. After analyzing the data from the irinotecan-caffeine mixture diffusion coefficients, there is an increase in the diffusion coefficient with a decrease in the concentration of irinotecan and an increase in the concentration of caffeine. The addition

of caffeine to irinotecan slows the rate of diffusion making the mixture slower than caffeine or irinotecan alone. Table 3.49 shows the aggregate weight (g mol^{-1}) and number formed in the irinotecan-caffeine mixtures using the diffusion coefficients and SEGWE. The highest aggregate weight (1170.42 g mol^{-1}) and number (1.34) correspond to 87% irinotecan in the irinotecan-caffeine mixture. The lowest aggregate weight (181.32 g mol^{-1}) and number (0.21) occurs with 17% irinotecan in the irinotecan-caffeine mixture.

Table 3.50 and Graph 3.41 illustrate the diffusion coefficients for caffeine in the irinotecan-caffeine mixture. The diffusion coefficients for caffeine in the irinotecan-caffeine mixture are between 3.39 x 10^{-10} m^2 s^{-1} and 7.20 x 10^{-10} m^2 s^{-1}. After analyzing the data for caffeine in the irinotecan-caffeine mixtures diffusion coefficients, there is an increase in the diffusion coefficient with a decrease in concentration of caffeine and an increase in the concentration of irinotecan. The highest diffusion coefficient occurs with 13% caffeine and 87% daunorubicin, and the lowest diffusion coefficient occurs with 83% caffeine and 17% daunorubicin. Table 3.51 shows the aggregate weight and number of caffeine in the irinotecan-caffeine mixtures using the diffusion coefficients and SEGWE. The highest aggregate weight (949.31 g mol^{-1}) and number (1.09) occurs at 83% caffeine and 17% irinotecan. On the other hand, the lowest aggregate weight (160.79 g mol^{-1}) and number (0.18) occurs at 13% caffeine and 87% irinotecan. The aggregate formation decreases with decreasing concentration of caffeine in the irinotecan-caffeine mixtures.

The concentration of irin-caf mix affects proton peak chemical shift positions. As

the concentration decreases, the chemical shift value increases. When comparing the proton chemical shift changes for the irinotecan-caffeine to pure irinotecan, the irinotecan-caffeine mixture has the larger change in the proton chemical shift values. This indicates that the irinotecan mixture associates more readily than pure irinotecan. This supports the theory that adding caffeine to an aromatic anticancer drug changes the drug's binding ability.

4.2 Future Studies

Another valuable piece of information about caffeine, daunorubicin, and irinotecan binding is relaxation times, T_1. Spin-lattice relaxation can also be referred to as either longitudinal relaxation or T_1 relaxation. Longitudinal relaxation is a time constant. This time constant describes when approximately 63% of the magnetization applied to the sample has recovered to equilibrium.[58] Longitudinal relaxation is instrumental in determining intermolecular and intramolecular interactions that take place in the sample analyzed.[58] Longitudinal relaxation is largely dependent on the external magnetic field strength.[58] The T_1 relaxation times can be useful in further examining the stacking that can occur through π bonds in aromatic compounds. If the relaxation times for caffeine and the two anticancer drugs of interest are determined, the binding of caffeine and the anticancer drugs can be better understood. NOSEY, nuclear overhauser effect spectroscopy, would also help study binding of caffeine and anticancer drugs. NOSEY can aid in identifying the actual site of binding as compared to T_1 relaxation times. This study can also be expanded to include other aromatic anticancer drugs to

determine if the caffeine affects either the binding and the efficacy of other anticancer drugs.

As previously mentioned, the greatest limitation of this analysis is the low concentration range. The low concentration range seems to have the greatest effect on pure caffeine. Since pure caffeine may need to be in a higher concentration range, the analysis could be performed at a higher concentration to see if that changes the outcome of the analysis. Even though it appears that pure caffeine is most affected by the low concentration range, the concentration of the anticancer drugs and the anticancer drug caffeine mixtures could be changed as well to see if the outcome of the analysis changes.

References

(1) Ferlay, J.; Ervik, M.; Lam, F.; Colombet, M.; Mery, L.; Pineros, M. Global Cancer Observatory: Cancer Today https://gco.iarc.fr/today/home.

(2) What Is Cancer? https://www.cancer.gov/about-cancer/understanding/what-is-cancer#definition (accessed Sep 1, 2023).

(3) Division of Cancer Prevention and Control, C. for D. C. and P. Cancer Treatments https://www.cdc.gov/cancer/survivors/patients/treatments.htm.

(4) Chemotherapy to Treat Cancer https://www.cancer.gov/about-cancer/treatment/types/chemotherapy.

(5) Types of Chemotherapy Drugs https://training.seer.cancer.gov/treatment/chemotherapy/types.html.

(6) Xu, Y.; Li, Q.; Ma, H. Y.; Sun, T.; Xiang, R. L.; Di, F. Therapeutic Effect and Side Effects of Bevacizumab Combined with Irinotecan in the Treatment of Paediatric Intracranial Tumours: Meta-Analysis and Systematic Review. *J. Clin. Pharm. Ther.* **2020**, *45* (6), 1363–1371. https://doi.org/10.1111/jcpt.13228.

(7) Nature Education. Cells Can Replicate Their DNA Precisely https://www.nature.com/scitable/topicpage/cells-can-replicate-their-dna-precisely-6524830/#:~:text=How is DNA replicated%3F,specific location called the origin.

(8) Bell, S. P.; Dutta, A. DNA Replication in Eukaryotic Cells. *Annual Review of Biochemistry*. 2002, pp 333–374. https://doi.org/10.1146/annurev.biochem.71.110601.135425.

(9) Nitiss, J. L.; Soans, E.; Rogojina, A.; Seth, A.; Mishina, M. Topoisomerase Assays. *Curr. Protoc. Pharmacol.* **2012**, No. SUPPL.57. https://doi.org/10.1002/0471141755.ph0303s57.

(10) Baker, N. M.; Rajan, R.; Mondragń, A. Structural Studies of Type I Topoisomerases. *Nucleic Acids Research*. 2009, pp 693–701. https://doi.org/10.1093/nar/gkn1009.

(11) Checa-Chavarria, E.; Rivero-Buceta, E.; Sanchez Martos, M. A.; Martinez Navarrete, G.; Soto-Sánchez, C.; Botella, P.; Fernández, E. Development of a Prodrug of Camptothecin for Enhanced Treatment of Glioblastoma Multiforme. *Mol. Pharm.* **2021**, *18* (4), 1558–1572. https://doi.org/10.1021/acs.molpharmaceut.0c00968.

(12) Fujita, K. I.; Kubota, Y.; Ishida, H.; Sasaki, Y. Irinotecan, a Key Chemotherapeutic Drug for Metastatic Colorectal Cancer. *World Journal of Gastroenterology*. WJG Press November 21, 2015, pp 12234–12248. https://doi.org/10.3748/wjg.v21.i43.12234.

(13) Pommier, Y. Camptothecins and Topoisomerase I: A Foot in the Door. Targeting the Genome Beyond Topoisomerase I with Camptothecins and Novel Anticancer Drugs: Importance of DNA Replication, Repair, and Cell Cycle Checkpoints. *Natl. Libr. Med.* **2004**, *4* (5), 429–434.

(14) Pophali, P.; Litzow, M. What Is the Best Daunorubicin Dose and Schedule for Acute Myeloid Leukemia Induction? *Current Treatment Options in Oncology*. Springer New York LLC January 1, 2017. https://doi.org/10.1007/s11864-017-0446-4.
(15) National Center for Biotechnology Information. PubChem Compound Summary for CID 30323, Daunorubicin https://pubchem.ncbi.nlm.nih.gov/compound/Daunorubicin.
(16) Johnson-Arbor, K.; Dubey, R. Doxorubicin https://www.ncbi.nlm.nih.gov/books/NBK459232/.
(17) Gallois, L.; Fiallo, M.; Garnier-Suillerot, A. *Comparison of the Interaction of Doxorubicin, Daunorubicin, Idarubicin and Idarubicinol with Large Unilamellar Vesicles Circular Dichroism Study*; 1998; Vol. 1370.
(18) Řeha, D.; Kabeláč, M.; Ryjáček, F.; Sponer, J.; Šponer, J. E.; Elstner, M.; Suhai, S.; Hobza, P. Intercalators. 1. Nature of Stacking Interactions between Intercalators (Ethidium, Daunomycin, Ellipticine, and 4′,6-Diaminide-2-Phenylindole) and DNA Base Pairs. Ab Initio Quantum Chemical, Density Functional Theory, and Empirical Potential Study. *J. Am. Chem. Soc.* **2002**, *124* (13), 3366–3376. https://doi.org/10.1021/ja011490d.
(19) Tacar, O.; Sriamornsak, P.; Dass, C. R. Doxorubicin: An Update on Anticancer Molecular Action, Toxicity, and Novel Drug Delivery Systems. *J. Pharm. Pharmacol.* **2012**.
(20) Evans, J.; Richards, J. R.; Battisti, A. S. Caffeine https://www.ncbi.nlm.nih.gov/books/NBK519490/.
(21) Cui, W. Q.; Wang, S. T.; Pan, D.; Chang, B.; Sang, L. X. Caffeine and Its Main Targets of Colorectal Cancer. *World Journal of Gastrointestinal Oncology*. Baishideng Publishing Group Co February 15, 2020, pp 149–172. https://doi.org/10.4251/wjgo.v12.i2.149.
(22) Drewnowski, A.; Rehm, C. D. Sources of Caffeine in Diets of US Children and Adults: Trends by Beverage Type and Purchase Location. *Nutrients* **2016**, *8* (3). https://doi.org/10.3390/nu8030154.
(23) Gottwalt, B.; Tadi, P. Methylxanthines https://www.ncbi.nlm.nih.gov/books/NBK559165/.
(24) D'Agata, E. M. C.; Mount, D. B.; Thayer, V.; Schaffner, W. Hetero-Association of Caffeine and Aromatic Drugs and Their Competitive Binding with a DNA Oligomer. *Eur. Biophys. J.* **2001**, *30* (5), 354–366. https://doi.org/10.1007/s002490100150.
(25) Palchaudhuri, R.; Hergenrother, P. J. DNA as a Target for Anticancer Compounds: Methods to Determine the Mode of Binding and the Mechanism of Action. *Current Opinion in Biotechnology*. December 2007, pp 497–503. https://doi.org/10.1016/j.copbio.2007.09.006.
(26) Hill, G. M.; Moriarity, D. M.; Setzer, W. N. Attenuation of Cytotoxic Natural Product DNA Intercalating Agents by Caffeine. *Sci. Pharm.* **2011**, *79* (4), 729–747. https://doi.org/10.3797/scipharm.1107-19.

(27) Bharti, S. K.; Roy, R. Quantitative 1H NMR Spectroscopy. *TrAC - Trends in Analytical Chemistry*. May 2012, pp 5–26. https://doi.org/10.1016/j.trac.2012.02.007.
(28) Clark, J.; Schaller, C. P. Introduction to Proton NMR https://chem.libretexts.org/Courses/University_of_Illinois_Springfield/Introduction_to_Organic_Spectroscopy/5%3A_Proton_Nuclear_Magnetic_Resonance_Spectroscopy_(NMR)/5.08%3A_Structural_Assignment/Introduction_to_Proton_NMR.
(29) Aue, W. P.; Bartholdi, E.; Ernst, R. R. Two-Dimensional Spectroscopy. Application to Nuclear Magnetic Resonance. *J. Chem. Phys.* **1976**, *64* (5), 2229–2246. https://doi.org/10.1063/1.432450.
(30) 2D NMR Introduction https://chem.libretexts.org/Bookshelves/Physical_and_Theoretical_Chemistry_Textbook_Maps/Supplemental_Modules_(Physical_and_Theoretical_Chemistry)/Spectroscopy/Magnetic_Resonance_Spectroscopies/Nuclear_Magnetic_Resonance/2D_NMR/2D_NMR_Introduction.
(31) Zaza, K. Pi-Stacking Interactions between Caffeine and Berberine in Aqueous Solution Studied by Nuclear Magnetic Resonance Spectroscopy , University of Alabama in Huntsville, Huntsville, 2020.
(32) Li, D.; Keresztes, I.; Hopson, R.; Williard, P. G. Characterization of Reactive Intermediates by Multinudear Diffusion-Ordered NMR Soectroscoy (DOSY). *Acc. Chem. Res.* **2009**, *42* (2), 270–280. https://doi.org/10.1021/ar800127e.
(33) NMR Theories and Techniques.
(34) Amin, N.; Claridge, T. Diffusion NMR and DOSY.
(35) Li, D.; Kagan, G.; Hopson, R.; Williard, P. G. Formula Weight Prediction by Internal Reference Diffusion-Ordered NMR Spectroscopy (DOSY). *J. Am. Chem. Soc.* **2009**, *131* (15), 5627–5634. https://doi.org/10.1021/ja810154u.
(36) Diffusion NMR http://chem.ch.huji.ac.il/nmr/techniques/other/diff/diff.html.
(37) Diffusion Ordered Spectroscopy (DOSY).
(38) Senra, T. D. A.; Khoukh, A.; Desbrieres, J. Interactions between Quaternized Chitosan and Surfactant Studied by Diffusion NMR and Conductivity. *Carbohydr. Polym.* **2017**, *156*, 182–192.
(39) SEGWE Calculator: Diffusion Coefficient and Molecular Weight Estimation https://nmr.chemistry.manchester.ac.uk/?q=node/432.
(40) Evans, R.; Deng, Z.; Rogerson, A. K.; McLachlan, A. S.; Richards, J. J.; Nilsson, M.; Morris, G. A. Quantitative Interpretation of Diffusion-Ordered NMR Spectra: Can We Rationalize Small Molecule Diffusion Coefficients. *Angew. Chemie Int. Ed.* **2013**, *52* (11), 3199–3202.
(41) Soult, A. Chemical Equilibrium .
(42) Redmon, W. Interactions of Caffeine with Aromatic Anticancer Drugs in Aqueous Solutions Studied by Nuclear Magnetic Resonance Spectroscopy, University of Alabama in Huntsville, Huntsville, 2017.
(43) Swan, I.; Reid, M.; Howe, P. W. A.; Connell, M. A.; Nilsson, M.; Moore, M. A.; Morris, G. A. Sample Convection in Liquid-State NMR: Why It Is Always with Us, and What We Can Do about It. *J. Magn. Reson.* **2015**, *252*, 120–129. https://doi.org/10.1016/j.jmr.2014.12.006.

(44) Kiraly, P.; Swan, I.; Nilsson, M.; Morris, G. A. Improving Accuracy in DOSY and Diffusion Measurements Using Triaxial Field Gradients. *J. Magn. Reson.* **2016**, *270*, 24–30. https://doi.org/10.1016/j.jmr.2016.06.011.
(45) Le Guennec, A.; Tayyari, F.; Edison, A. S. Alternatives to Nuclear Overhauser Enhancement Spectroscopy Presat and Carr-Purcell-Meiboom-Gill Presat for NMR-Based Metabolomics. *Analytical Chemistry*. American Chemical Society September 5, 2017, pp 8582–8588. https://doi.org/10.1021/acs.analchem.7b02354.
(46) Kruse, N. Dosy10june1591813642782. **2020**.
(47) Hannigan, M. *McNeil Group NMR Guide Nuclear Magnetic Resonance Spectroscopy*; 2019.
(48) Concentration Analysis by NMR in Automation https://mestrelab.com/software/mnova-gears-concentration/ (accessed Nov 9, 2023).
(49) Hargrove, M.; Brown, J. R.; Bellucco-Chatham, A. Standard Deviation Formula and Uses vs. Variance.
(50) Vogel, G. C.; Searby, L. A. Lewis Aicd-Base Interactions of Zinc Alpha, Beta, Gama, Delta- Tetraphenylporphine with Several Neutral Donors. *J. Amer. Chem. Soc* **1973**, *12* (4), 936–939.
(51) Seal, B. K.; Mukherjeet, A. K. *A Computerised Least Square Method for Determination of Stability Constants of 1 : 1 Molecular Complexes & Chemical Shift of Pure Complexes from Nuclear Magnetic Resonance Data*; 1986; Vol. 25.
(52) Wachter, H. N.; Fried, V. Wachter-Fried-1974-Use-of-the-Rose-Drago-Method-for-Evaluation-of-Complex-Formation-Constants. *J. Chem. Educ.* **1974**, *51* (12), 798–799.
(53) Fielding, L. Determination of Association Constants (Ka) from Solution NMR Data. *Tetrahedron* **2000**, *56* (34), 6151–6170.
(54) Model Evaluation-Regression https://www.saedsayad.com/model_evaluation_r.htm.
(55) Microsoft. Define and Solve a Problem by using Solver.
(56) Piorecka, K.; Stanczyk, W.; Florczak, M. NMR Analysis of Antitumor Drugs: Doxorubicin, Daunorubicin and Their Functionalized Derivatives. *Tetrahedron Lett.* **2016**, *58* (2). https://doi.org/10.1016/j.tetlet.2016.11.118.
(57) D'Amelio, N.; Aroulmoji, V.; Toraldo, A.; Sundaraganesan, N.; Anbarasan, P. M. Aggregation Properties and Structural Studies of Anticancer Drug Irinotecan in DMSO Solution Based on NMR Measurements. *J. Mol. Struct.* **2012**, *1013*, 26–35. https://doi.org/10.1016/j.molstruc.2012.01.012.
(58) Kaseman, D. Relaxation https://chem.libretexts.org/Bookshelves/Physical_and_Theoretical_Chemistry_Textbook_Maps/Supplemental_Modules_(Physical_and_Theoretical_Chemistry)/Spectroscopy/Magnetic_Resonance_Spectroscopies/Nuclear_Magnetic_Resonance/NMR_-_Theory/Relaxation.